THE UNIVERSITY OF MICHIGAN

INDUSTRY PROGRAM OF THE COLLEGE OF ENGINEERING

AN EXPERIMENTAL STUDY OF STRESSES IN THE END BLOCKS OF POST-TENSIONED PRESTRESSED CONCRETE BEAMS

Ti Huang

A dissertation submitted in partial fulfillment
of the requirements for the degree of
Doctor of Philosophy in the
University of Michigan
1959

September, 1959

IP-381

Doctoral Committee:

Professor Leo M. Legatski, Chairman
Assistant Professor Glen V. Berg
Professor Wilfred Kaplan
Professor Lawrence C. Maugh

ACKNOWLEDGEMENT

The author wishes to express his deep gratitude toward Professor Leo M. Legatski, under whose direction and personal supervision this investigation was undertaken. The author is also grateful to the other members of his special committee, Professors Glen V. Berg, Wilfred Kaplan and Lawrence C. Maugh, for their continuous encouragements and valuable suggestions; and to Professor Bruce G. Johnston for his help in the numerical solution.

The experimental study of this investigation was made in the Structural Laboratory of the Civil Engineering Department of the University of Michigan; and was financed by that Department. The prestressing cables used in the model beam were donated by John A. Roebling's Sons Corporation of Trenton, New Jersey. Mr. George Geisendorfer of the Structural Laboratory rendered much help in the making and the testing of the model beam. A portion of the numerical computation work was done in the Statistical and Computation Laboratory of the University of Michigan. The rough draft of this dissertation was typed by Miss Reta Teachout. The final typing and reproduction were done by the College of Engineering Industry Program of the University of Michigan. To all persons who helped in the preparation of this dissertation, the author wishes to express his sincere thankfulness.

TABLE OF CONTENTS (CONT'D)

TABLE OF CONTENTS (CONT'D)

LIST OF TABLES

LIST OF FIGURES

LIST OF FIGURES

LIST OF FIGURES

NOMENCLATURE

Dimensions

a	Half length of loading plate in simplified beam
A	Cross sectional area of concrete (gross)
b	Width of end block; also length of each bearing plate in simplified beam
B	Static moment about centroidal axis of the portion of sectional area above the point used for shear stress computation = $\int_{y}^{\bar{y}_t} t y dy$
c	Half depth of simplified beam
d	Depth of beam
h	Grid size of fine network used in numerical solution
I	Moment of inertia of A about its horizontal centroidal axis
k_t, k_b	Top and bottom kern distances, respectively
ℓ	Half length of simplified beam
r	Radius of gyration of concrete section A
t	Thickness of section
$\bar{y}_t$, $\bar{y}_b$	Distance from centroidal axis of top and bottom fiber, respectively

Forces and Moments

F	Body force
M	Bending moment at the juncture
P	Resultant horizontal force at the juncture; also prestress
q	Vertical pressure per unit length from curved cables
Q	Vertical load at mid-span

R	Vertical reaction of the beam (also see below).
S	Vertical total shear force at the juncture
w	Unit weight
w_a	Applied load
W	Concentrated load per unit width at mid-span of simplified beam; also total weight of end block

Stresses, Strains and Others

C,D	Parameters used in computation of principal stresses
E	Modulus of elasticity of concrete
k,K	Parameters used in computation of stresses in a cantilever beam
p	Internal normal pressure at the juncture
p_1, p_2	Major and minor principal stress, respectively
R	Biharmonic residual of ϕ used in relaxation computation (also see above)
R_V, R_H, R_D	Apparent strain as read by the vertical, horizontal and diagonal gage of a rosette, respectively
s	Internal shearing stress at the juncture
Z	Potential of body forces
ϵ	Normal strain
η	Ratio indicating prestress losses
ν	Poisson's ratio for concrete
σ	Normal stress
τ	Shear stress
ϕ	Angle between major principal direction and x-axis, measured counterclockwise from x-axis; also $\frac{1}{h^2}\Phi$

NOMENCLATURE (CONT'D)

Φ	Airy's stress function
ψ	Auxiliary stress function

Subscripts

x,y,z	Pertaining to the coordinating directions x, y, and z, respectively
D,L	Pertaining to dead and live load, respectively
T,M,B	Pertaining to top, middle and bottom cable, respectively

Coordinate System

Origin	Middle point of the bottom edge of the exterior end of the end block
Ox	Horizontal longitudinal axis, pointing the mid-span of beam
Oy	Vertical axis, pointing upward
Oz	Transverse axis, pointing right when viewed facing the end of beam

Sign Convention

Normal and principal stresses	Positive sign signifies tension
Shearing stress	Positive sign signifies traction in positive direction on positive face of the section
Normal strain	Positive sign signifies elongation

CHAPTER I

INTRODUCTION

Statement of Problem

In general, prestressed concrete beams are made in modified I-shape, or box-shape, consisting of relatively thin flanges and webs. The main reason for using these shapes is an economical one, that as much material as possible should be placed far away from the centroidal axis. Near the ends of post-tensioned beams, however, solid rectangular blocks are usually used. These "end blocks" serve two purposes: (1) to make more area available at the ends for anchoring the prestressing cables; and (2) to spread out the highly concentrated forces from the end anchorages gradually over the entire beam section.

Figure 1.1 shows a free body diagram of a typical end block. The forces acting on this end block include the following:

1. The prestressing forces from the anchoring devices of cables, P_1, P_2, etc. The number, locations and directions of these forces all may vary. In general, they act on the exterior end of the end block.
2. The reaction of the beam from its support, R.
3. The vertical load over the block, including both dead and live load, w_a.
4. The weight of the end block, W.

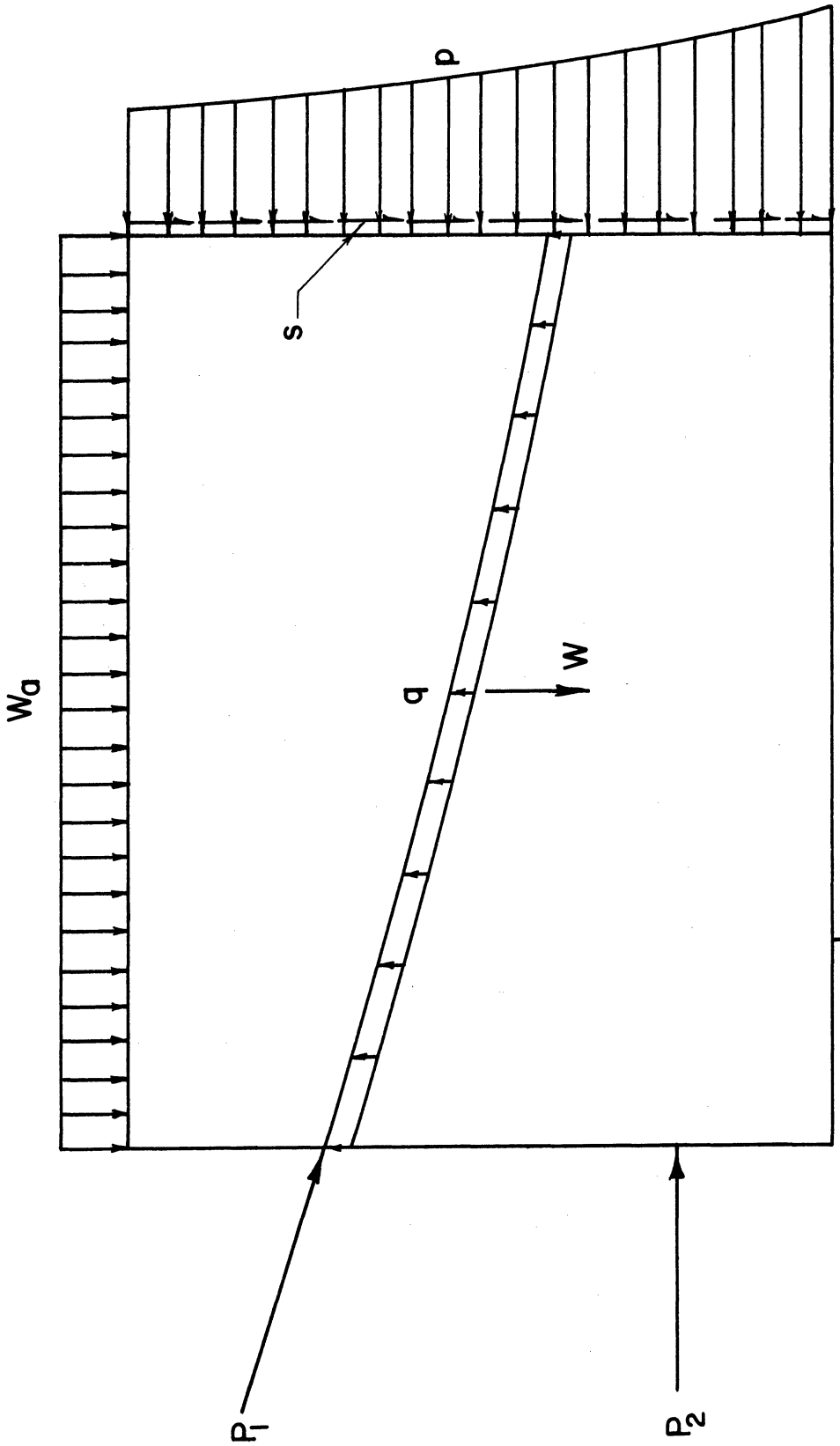

Figure 1.1. Typical End Block.

5. The vertical pressure from the prestressing cables, q, associated with any change of direction of the cable. For cables draped into a parabola, this pressure may be considered uniformly distributed and vertically upward.
6. The internal normal pressure, p, over the interior end of the end block.
7. The internal shearing stresses, s, over the interior end of the end block. The distributions of forces p and s are not exactly known; but their resultants can be represented by the normal force, P, the bending moment about the centroidal axis M, and the vertical shear, S.

It should be mentioned that Figure 1.1 is a two-dimensional representation of a three dimensional body. Actually, P_1, P_2, etc., act through bearing plates which are as a rule narrower than the block itself; q is concentrated in the lateral direction; and the internal stresses p and s are distributed over the beam section, which is much narrower than the end block at its web (or webs). These clearly show the three-dimensional nature of the end block problem.

The existing methods for analyzing end blocks almost unanimously treat the problem as two-dimensional. The forces in vertical direction, such as w_a, W, q and R, are often neglected. Even the vertical components of P are sometimes not considered.

In this investigation, the actual distribution of stresses inside an end block was studied both experimentally and analytically.

The experiment was carried out on a full-sized concrete model. The analytical investigation was made in two dimensions by means of a numerical process. The results were then compared to establish qualitatively the stress distribution in the third (lateral) direction.

Historical Review

Although the post-tensioning method for prestressing concrete structural members has been used by engineers for more than thirty years, literature concerning the end block stresses has been remarkably scarce.

In 1946, Professor Magnel[18] made probably the first publication dealing with this problem. He considered the end block as a deep beam, loaded by the prestress forces at the external end, and supported by the body of beam at the internal end. He further assumed that, on any horizontal section of the end block, the normal stress σ_y varies according to a quadratic parabola, and consequently, the shear stress τ_{xy} varies according to a cubic parabola. For the third component of stress, σ_x, Magnel assumed linear distribution on vertical sections, and 45° angles of dispersion of the pressure from end forces. Three years later, Magnel revised his method[19,20], changing the distribution of σ_y over any horizontal section into a cubic parabolic curve, and hence that of τ_{xy} into a fourth degree parabolic curve. The distribution of σ_x remained unchanged. Of all the forces acting on the end block, Magnel considered only the prestress P and the internal normal stress p. The stress s was included as an

additional shear to be superimposed later. Billig[3] and Walley[30] followed this approach in their books. Walley made one improvement in considering a vertical force on any horizontal section to insure static equilibrium. Evans and Bennett[11] also presented Magnel's method in this version. Walley also used the rectangular section of the end block, instead of the section of the beam, for the computation of p and s. This later procedure, in the opinion of the author, was quite erroneous.

Chaikes presented a slightly different method in 1951.[5] The earlier Magnel proposal for distributions of σ_y and τ_{xy} over horizontal sections was adopted. But the distribution of σ_x was found from consideration of interior equilibrium to be a fourth degree parabola along the x-direction. Besides the horizontal forces on the block, the vertical components of prestress forces and the load w_a on the block were also given consideration.

Guyon presented a completely different method for analyzing end block stresses in his book.[16] The basis of his approach was his theoretical analysis of rectangular prismatic bodies subject to end loadings,[15] supported by earlier work by Bleich,[4] and by Tesár's photo elastic study.[28] An idealized problem of an infinitely long prism subject to constant loadings on top and bottom faces at every cross section was first solved approximately by means of Fourier series. Corrective terms were then added for complete satisfaction of the boundary conditions. Both normal and tangential forces in either symmetrical or anti-symmetrical distribution with respect to

the longitudinal middle plane of the prism were considered. In essence, this approach was the same as that Filon used in his treatise concerning beam bending,[12] except for the proportions of the dimensions of the members. After the theoretical solution was obtained, however, Guyon considered it impractical to apply the results directly, and proposed to use successive square blocks with symmetrical loading for the determination of the maximum tensile stress σ_y. Evans and Bennett[11] adopted Guyon's theory, but suggested that influence lines for σ_y may be used to advantage. Lin[17] also recommended Guyon's method.

Pirson[21] and Sievers[23,24] both used the stress trajectories as the means for determining the maximum tensile stress in end blocks. It was established that the magnitude of tensile principal stress is closely related to the curvature of the trajectory of the compressive principal stress. Pirson's trajectories were composed of straight line segments, while those used by Sievers were smooth curves, which conceivably would yield better results. Sievers[24] also presented an approximate three-dimensional analysis by considering a varying effective width of the block.

Pirson and Sievers considered only the forces P and p. Guyon's method included also the vertical component of P. But the vertical shear stress s was neglected in all of these methods. The forces acting on the top and bottom faces were also omitted.

Most experimental work concerning this problem has been done photoelastically. Tesař's work,[28] although not originally intended for this end block problem, nevertheless furnished valuable information

for Guyon in the development of his method. More recently, Christodoulides[4-7] has made both two-dimensional and three-dimensional photoelastic investigations of end block stresses, and has found some discrepancy between the experimental results and the results yielded by Guyon's method. Sievers[23] also made some photoelastic investigations to support his method. With the exception of Christodoulides' three-dimensional investigation, these experiments were all made on rectangular blocks uniformly supported at the bottom and centrally loaded at the top.

Of the very few experimental studies made with concrete specimens, one was recently reported by Ban, Muguruma and Ugaki.[2] They conducted both two-dimensional and three-dimensional investigations on rectangular columns centrally prestressed. Their results also deviated from those obtained from Guyon's method, but in general agreed with Siever's method.

Probably the only experimental investigation which also included the effect of the vertical forces was conducted at the U. S. Naval Civil Engineering Research and Evaluation Laboratory at Port Hueneme, California.[27] Surface gage rosettes were used on an end block of a prestressed beam with an I-section at the middle portion. Almost all the forces enumerated at the beginning of this chapter were involved, except q and w_a, due to the systems of prestressing and loading employed. It was unfortunate that no interior gages were used so that more information would be available. It was found, nevertheless,

that the magnitudes and directions of the principal tensile stresses along the mid-height of the end block were not changed appreciably by the application of live load. This seems to indicate the predominant character of the prestressing force in this problem.

In an attempt to avoid higher mathematics, Ramaswamy and Goel[22] used the lattice analogy method to solve a problem of a square end block with one normal load at the middle of its top face. They, too, found larger bursting zone and higher tensile stress than indicated by Guyon's method. On the other hand, the maximum tensile stress in spalling zones found in this way was small.

CHAPTER II

EXPERIMENTAL INVESTIGATION

Design of the Model Beam

The model beam, as shown in Figure 2.1, was designed as a simple beam, with a span of fifty feet center to center of reactions, supporting a uniformly distributed load, and with the central forty-two feet removed. The end bearings were six inches long. During testing, a concentrated load equal to the total load (dead and live) on the removed portion was applied at the center of the model. By virtue of St. Venant's principle, if the distances between this load and the end blocks under study are "large", the effect of this replacement should be negligible. Thus, a beam of only 9'-6" long was needed for the testing of the end blocks of the designed fifty-foot beam.

The body of the beam was 22" deep, 12" wide at top, 8" at bottom, and 3" thick at the web. The end blocks were 22" x 12" rectangular. The two end blocks were made of different lengths, 22" and 33" respectively, in order that the effect of the length of end blocks could be studied. The distances from the central load to the interior ends of the end blocks were 35" and 24" respectively, and were considered large enough for the application of St. Venant's principle.

The properties of the beam section are as following:

$A = 144.5$ sq. in

$\bar{y}_b = 11.29$ in. $\qquad \bar{y}_t = 10.71$ in.

$I = 6,752.6$ in.^{4} $\qquad r^2 = 58.97$ in.^{2}

$k_b = 5.506$ in. $\qquad k_t = 5.224$ in.

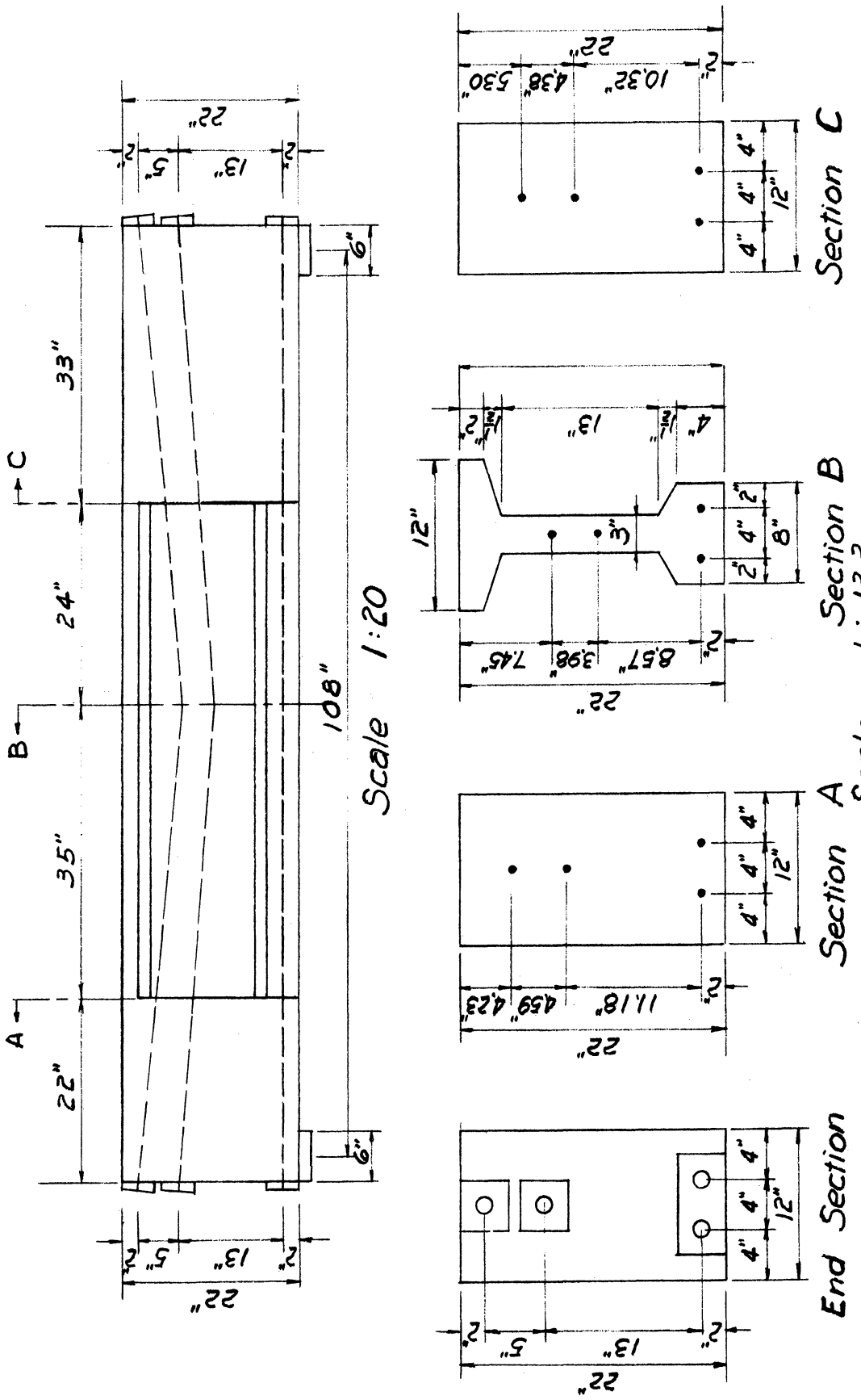

Figure 2.1. Model Beam

Four 0.600" diameter seven wire prestressing strands with type SDS-35 anchorage fittings were used in the beam. The two bottom ones were laid straight, while the other two were draped in parabolic shapes. In the fifty-foot prototype, the middle cable would come down to the level of the bottom cables at the center of the beam; and the top cable would be 2" higher. According to the manufacturer, these strands had the following properties:

Area	0.215 sq. in.
Ultimate Strength	46,000 lbs.
Design Load	26,000 lbs.
Modulus of Elasticity	25,000,000 psi

The locations of the cables are shown in Figure 2.1.

The concrete used in the model was designed to have a 28-day compressive strength of 6,000 psi, a 3-day strength of 4,000 psi, and a slump of 3 in. The maximum size of aggregate was limited to 3/4", due to the presence of strain gage capsules in the end blocks. The mix finally adopted was composed of the following constituents per cubic yard:

Portland cement (Type I)	705 lbs.
Sand (dry weight)	1420 lbs.
Gravel (dry weight)	1800 lbs.
Water	250 lbs.
Pozzolith	1.87 lbs.

Several standard 12" x 6" (height x diameter) cylinders were poured with the model beam. Subsequent testing of these cylinders at

an age of two to four months gave the following average properties of concrete:

Density	153.8 lbs. per cubic foot
Compressive Strength	6,130 psi
Modulus of Elasticity	4,870,000 psi
Poisson's Ratio	0.178

The allowable stresses used in the design were as following:

Concrete:	At transfer:	Compression:	0.55 x 4,000= 2,200 psi
		Tension	0.05 x 4,000 = 200 psi
	After losses:	Compression	0.40 x 6,000 = 2,400 psi
		Tension	0
Steel:	Initial stress:		140,000 psi
	Final stress:		120,000 psi
	Ratio indicating losses, η		0.85

Based on these stresses, the allowable total load on the beam was found to be 390 pounds per linear foot, and the allowable live load was 270.8 pounds per linear foot.

The cables were placed inside paper tubes so that no bond would exist between concrete and cables. The tubes had an inside diameter of 1.3 in. Near the ends, 2.2 in. tubes of 13 in. length were used to accommodate the anchorage fittings. The tubes were fixed in position by means of several 1/4" diameter rods placed transversely through the side forms.

Installation of Strain Gages

Strains in the end blocks were measured by means of SR-4 strain gages. A-1 gages were used on the surface; and for the interior, A-7 gages and AR-1 gage rosettes were used. Altogether, there were 110 A-7 gages and 18 AR-1 gage rosettes cast inside the concrete, and 22 A-1 gages on the surface. The names and the locations of these gages are shown in Figure 2.2 and Figure 2.3.

The interior gages were installed as "capsules". Figure 2.4 gives a schematic illustration of a single gage capsule. Two A-7 gages were mounted on the opposite faces, at the center, of a thin celluloid plate 0.030" thick, 3/8" wide and 1-1/2" long. On the longitudinal axis of the plate and about $\frac{3}{16}$" from the ends, two 1/8" x 3/16" holes were punched and 5/8" long brass bars inserted. Four small pieces of celluloid, 3/8" square and 0.030" thick, were also added at the ends. These brass bars served a dual purpose. First, small holes were drilled near each end of them so that wires could be threaded through for locating the capsule before pouring of concrete. Second, after the concreting, these bars would engage the neighboring concrete so that the capsule would deform with it. Since the SR-4 cement is also a solvent of the celluloid used for the capsule, there was a tendency for the capsule to warp or curl while drying. It was found that this tendency could be minimized by mounting the second gage at the earliest practical time. Still some distortion seemed unavoidable. In order that the distortion would not affect the readings significantly, the two gages were wired in series. Two lead wires, of #20 AWG size,

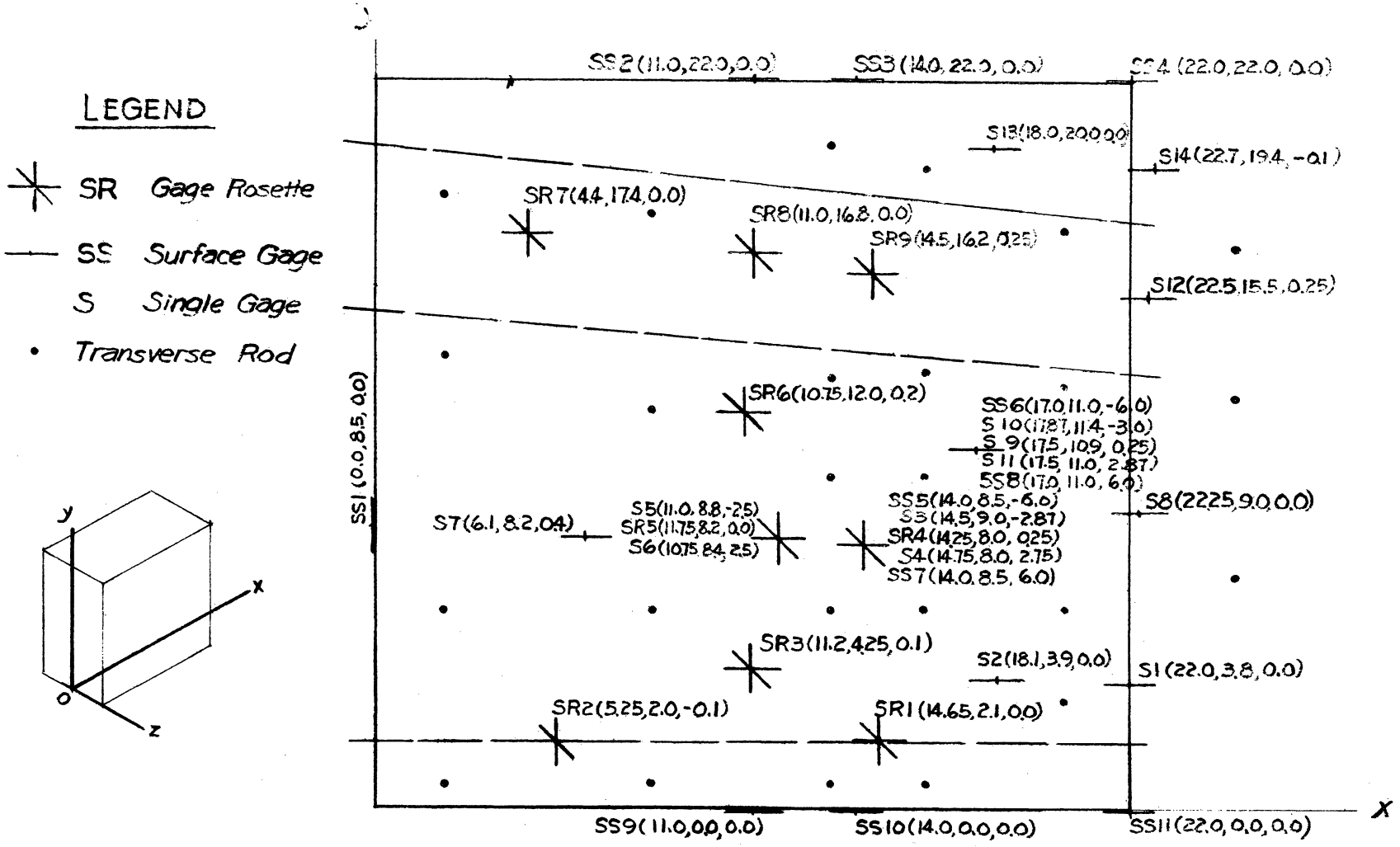

Figure 2.2. Locations of Strain Gages, Short End.

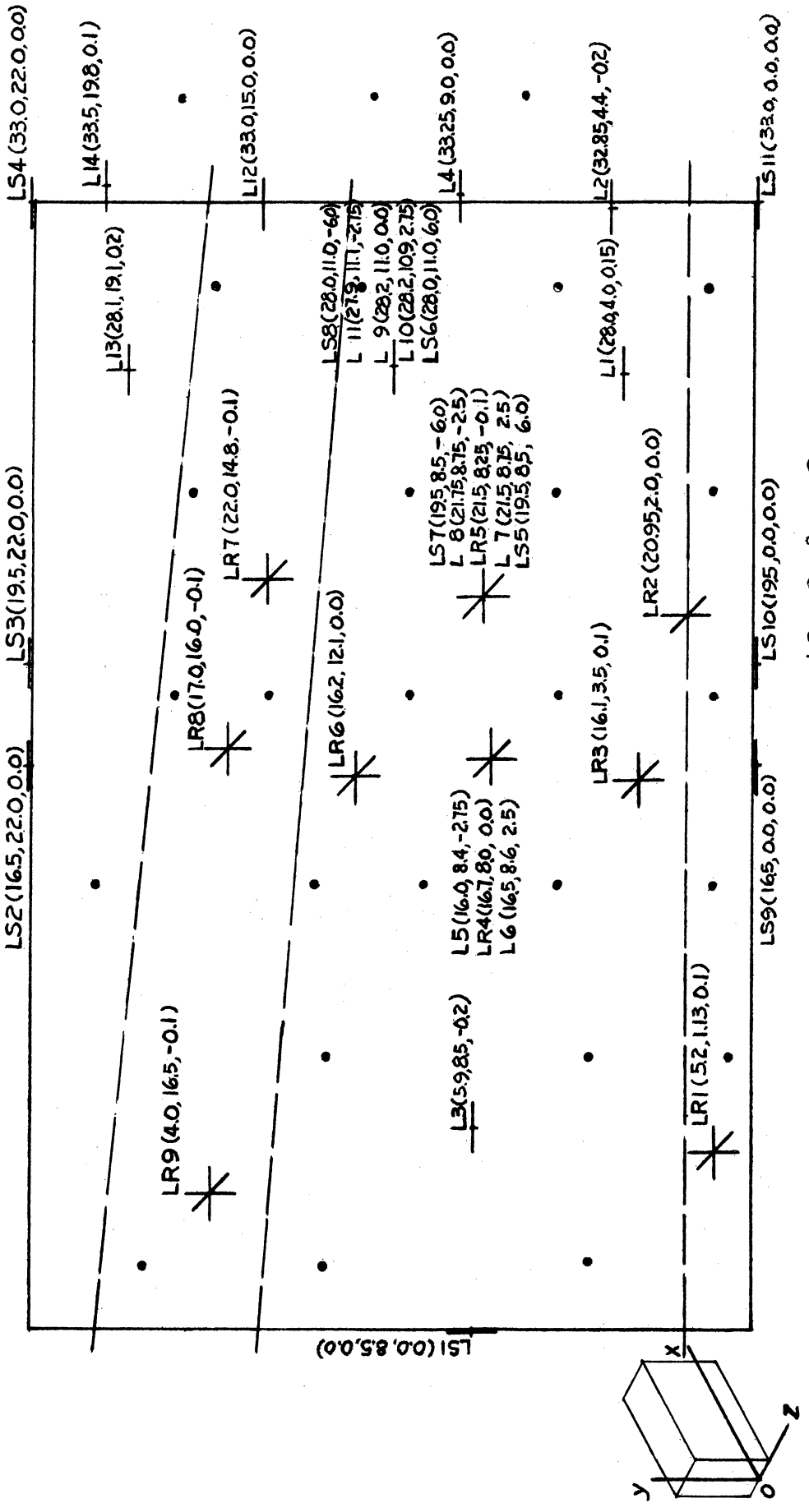

Figure 2.3. Locations of Strain Gages, Long End.

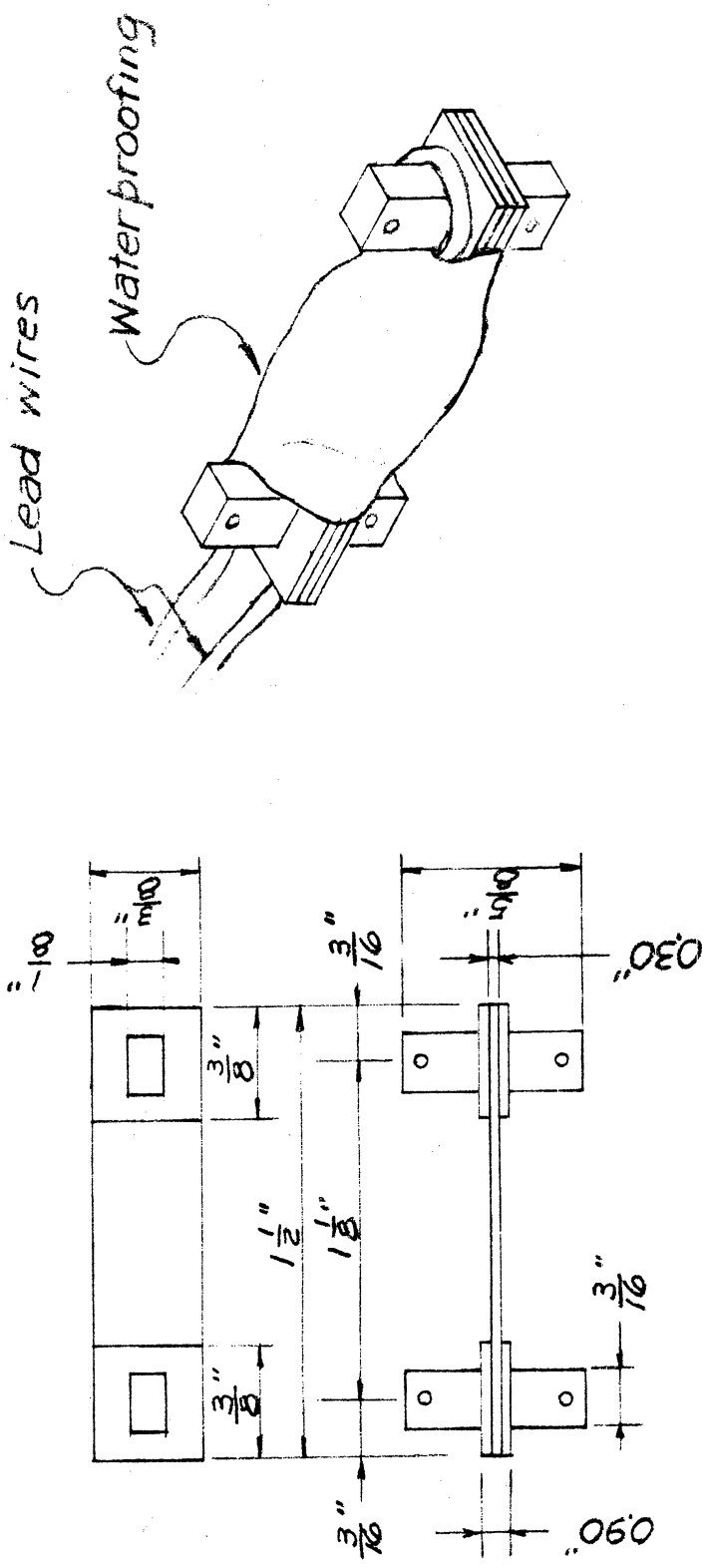

Figure 2.4. Single Gage Capsule.

stranded conductor with vinyl insulation were then soldered to the gages. After the wiring, the capsule was waterproofed with EC-711 rubber cement (product of Minnesota Mining and Manufacturing Company). The cement was applied around the central portion of the capsule, leaving the brass bars clear. Due to the liquid form of the cement, the application had to be made in several layers, and a heating lamp was also needed for accelerating the setting of rubber cement. During heating, the capsules were turned over frequently so that the two faces would be heated evenly.

The rosette capsules were made using similar procedures. The celluloid plates for these were 2-1/2" square, and six brass bars were used for each rosette, two on each gage line. In the wiring, only four lead wires were needed, as one wire could be used as a common ground line for all three gages. The warping problem was more severe for these capsules than those with single gage, and more care was necessary for satisfactory results. Due to a shortage of supply of AR-1 rosettes in the Structural Laboratory at the time this study was made, the rosettes in the long end block were made up by assembling three single gage capsules. Extreme care was taken in establishing the 45° angles between gage lines, but the result was not very successful. Consequently, some doubt must be given to the information obtained from these made-up rosettes.

For the placing of the capsules in the beam form, a number of quarter inch diameter rods were placed transversely through holes drilled in the side forms. All rods were threaded at both ends so that

nuts could be used to maintain the inside width of the forms at 12". On each rod were drilled three small holes, one at the center and the others 4" away. No. 26 bare copper wires were used for hanging the capsules. In general, double wires were used, and after both ends of the wires were fixed, minor adjustments of its length could be made simply by turning a nail between the two wires. To obtain sufficient accuracy of gage locations, eight wires were needed for each capsule. They held the capsule firmly in position, and were believed strong enough to withstand any possible pressure during the placing of concrete. It should easily be seen that with all the capsules in place, the inside of the end block forms contained quite a network of wires, rods and tubes, and the small size of aggregate used was an absolute necessity. Figure 2.5 shows the inside of the forms before placing concrete. The locations of the transverse rods are shown in Figure 2.2 and Figure 2.3.

It must be mentioned that the presence of transverse rods in the end block should not substantially affect the stress picture, primarily because of their direction. All gages were oriented parallel to the longitudinal vertical plane, and normal to the transverse direction. The rosettes were placed in such a way that the diagonal gages pointed upward toward the ends of the beam.

The compensating gages were cast inside two 1 ft. x 1 ft. x 1 ft. blocks, one for each end. The size of these dummy blocks was chosen so that the active and compensating gages would have similar thicknesses of concrete coverage.

Casting of Model Beam

The beam was cast on October 9, 1957. During the casting of the model beam, the vibrator was not used inside the end block to avoid undue pressure that might break the copper wires holding gage capsules in place. Instead, rodding was used internally and the vibrator used externally. The entire pouring, including the test cylinders and the dummy blocks, was completed in about an hour.

The model was covered with wet burlap after six hours, and was kept wet for a week. After that the form was stripped, and the surface gages were mounted.

Tensioning of Cables

Tensioning of cables was done by means of two thirty-ton Simplex jacks, operated in parallel by one single oil pump. The amount of prestress force in the cable was controlled by two A-12 strain gages mounted on the pull bar of each jack. These gages were first calibrated in the Tinius-Olsen Universal Testing Machine in the Structural Laboratory up to 36,000 pounds tension (as compared to a maximum tensioning force required in each cable of 30,750 pounds). The calibration resulted in a perfectly straight load-strain curve with a factor of 0.0428 microinches per inch per pound, and a modulus of elasticity of the pull bars of 29,800,000 pounds per square inch. The parts of the tensioning apparatus are shown in Figure 2.6, and Figure 2.7 gives an assembled view.

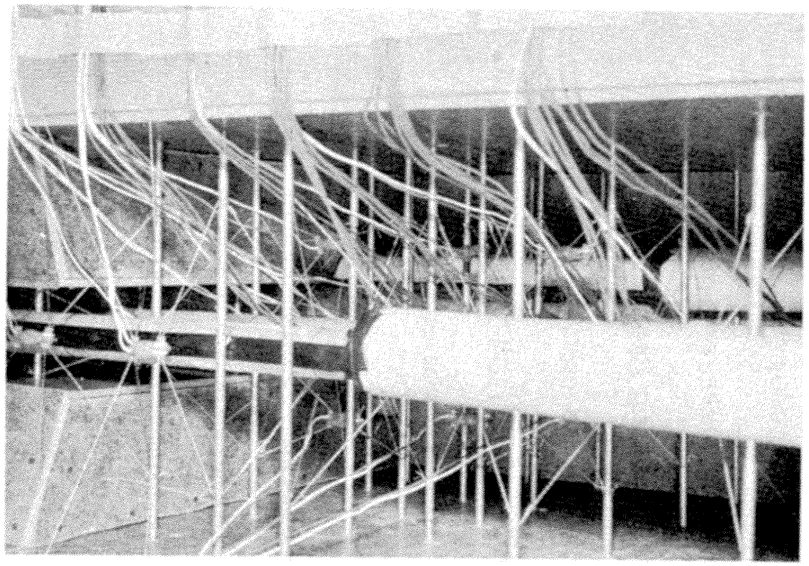

Figure 2.5. End Block Form Before Placing Concrete.

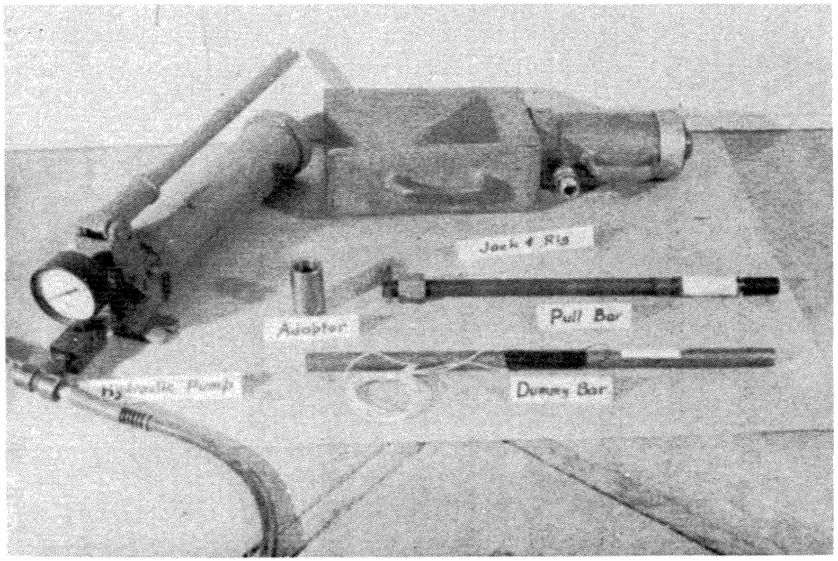

Figure 2.6. Parts of Tensioning Apparatus.

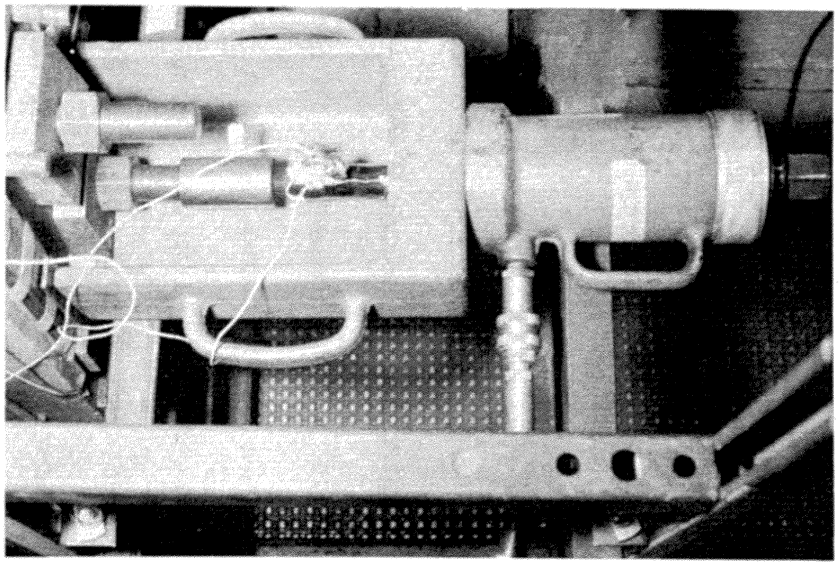

Figure 2.7. Tensioning Apparatus Attached to Middle Cable.

After the tension in the pull bar reached the desired value, the anchoring nuts at the ends of the cable were turned by hand until snug with the steel bearing plates. Then the jacking force was released and the pull bars disengaged from the cable. Subsequent checkings had indicated that this method of prestress control was quite accurate.

The bearing plates were cut from a piece of hard steel. Combined bearing plates 4" x 8" were used for the bottom cables. Those for the upper cables were 4" square and bevelled to the desired angle. The holes for the cables were 1-3/8" in diameter. All plates were 1" thick at the holes.

Two steel frames were built to support the jack and rig assemblies. Horizontal members were placed at different levels so that the jack and rig, when supported by these members, would be in the right position and inclination for each cable. As the two bent cables were rather close together at the ends, the supporting members for the high position were made removable.

In order that the jack, when working in an inclined position, might bear evenly on the concrete, a frame of masonite hard board was hung from the top of beam. Several thin steel strips were taped to the frame at different locations to make up the difference due to inclination (about half an inch for the top cable and seven-sixteenths of an inch for the middle cable). Both this frame and the steel frame mentioned in the previous paragraph can be seen in Figure 2.8.

A few difficulties were met during the tensioning of cables. The rig as provided by the jack manufacturers did not have the pull bar acting at the centroid of its bearing area, but about one third the way out toward the open side. This did not cause any serious problem with the middle cable stretching. However, since the top cable was only 2" from the top surface at the end, the toes of the rig actually projected out, and the situation was aggravated. The pressure under the toes became so high that the masonite frames were broken and had to be replaced several times. Small pieces of concrete at the top edge were also chipped out. Also, there was actually a tendency for the rigs to come off the supporting frames and flip up. Fortunately, it did not happen and no serious damage was done to the beam.

The two bottom cables were stretched simultaneously, one from each end. Due to the closeness of these two cables to each other and to the bottom of the beam, and because of the combined bearing plates used, the rigs could not be placed "face up" as for the two upper cables. Instead, they were placed standing up on one side, facing the longitudinal axial plane of the beam. A considerable portion of the "bearing face" of the rig was thus below the beam. Two L-shaped half-inch steel plates were used to help distribute the pressure, and were fairly effective. However, there were a few instances that the rigs did turn about the bearing toe, and the screw threads on the anchorage fitting were damaged because of moving against the bearing plate. At a latter stage of the experiment, there was also one lower corner broken because of excessive pressure.

These difficulties could all be avoided by modifying the design of the beam, locating the cables further in from the concrete surfaces. The shape of the rig also could be improved.

Testing of Model Beam

The beam was tested in the Tinius-Olsen Universal Testing Machine in the Structural Laboratory. Figure 2.8 shows the beam in the machine as viewed from near the short end. Figure 2.9 shows the electric wiring system, the strain indicator, the jacking pump, etc. The beam can also be seen behind the working table. The two dummy blocks were placed near the respective ends of the beam.

The procedures of testing were as follows:

1. With no prestress in the cables, no load on the beam, and with the beam supported at six points approximately two feet apart, take the "initial zero" reading on all gages.
2. Stretch the cables. In order to prevent any tensile fiber stress to develop in the concrete, the cables were stretched in the following order:
   a. Stretch the middle cable.
   b. Stretch the bottom cables to about two thirds of the force desired, accuracy was not required at this stage.
   c. Stretch the top cable.

d. Stretch the bottom cables to the desired prestress.

e. Check the force in the middle cable, and restretch it to the desired level. The effect of the top cable force on the lower ones, and vice versa, was so small that no corrections were necessary.

3. Remove the intermediate supports of the beam, leaving it simply supported at the two ends. Apply concentrated load of 4,890 pounds at the middle. Take readings. The value of 4,890 was reached as the weight of the "removed portion" of the 50-foot prototype. This corresponds to the "P.L. + D.L." condition.

4. Increase the concentrated load to include live load on the middle portion. Take the "P.L. + D.L. + L.L." readings.

5. Remove the concentrated load, set up the intermediate supports, release the prestresses and take the "final zero" readings. The order for releasing the prestress in cables was the reverse of that of stretching, except that Step No. e in stretching was not needed here, and the releasing was actually started at Step No. d, i.e., reducing the bottom cable forces by about one third.

These five steps constitute one cycle of testing.

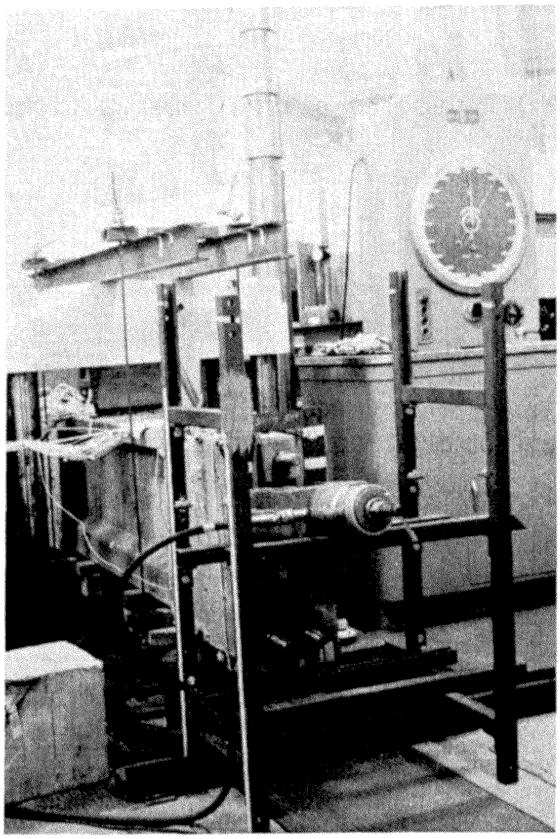

Figure 2.8. Model Beam in Testing Machine - Viewed from Near the Short End.

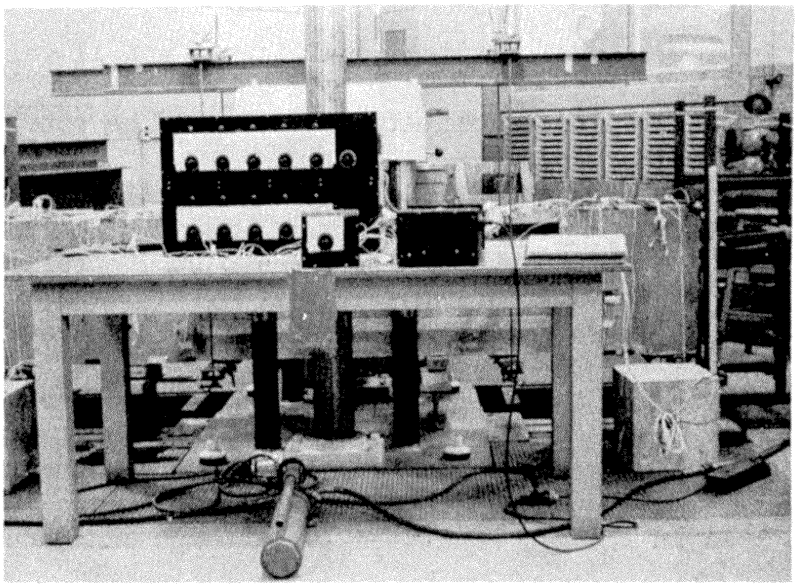

Figure 2.9. Testing Setup, Showing the Switching and Measuring Units.

Table 2.1 gives the several combinations of prestress and live load used in this investigation.

TABLE 2.1

LOADING CONDITIONS INVESTIGATED

No.	Cycles	Prestress		Concentrated Load	
		P_T & P_B	P_M	Q_D	Q_L
I	4	16,000#	15,170#	4,890#	6,000#
II	4	24,000	22,750	4,890	9,000
III	5	30,750	29,150	4,890	11,100
IV	3	30,750	32,120	4,890	11,100
V	4	30,750	30,750	4,890	11,100

The lower level loading conditions I and II were used to insure that some results of the experiment would be obtained in case the beam should fail under the "full load" condition V. The conditions III, IV and V were different only by the amount of prestress in the middle cable P_M. In conditions I, II and III, the stretchings were carried out by taking the Steps a through d, and no correction in P_M was made. The elastic shortening of the beam under the prestress forces caused the loss in P_M. In condition IV, attempt was made to counter this loss by initially overstressing the middle cable, resulted in a higher stress therein. In condition V, the stretching was done according to the procedures outlined above.

Emphasis was placed upon the results of loading condition V, as this corresponded to the actual loading condition of the prototype.

Immediately after the stripping of forms of the beam, an ohmmeter was used to check the interior gages. They all registered correct resistances. However, one month later, when the first trial run was performed, it was found that the gage S2 had broken inside the concrete. After the first cycle of testing, the gages LR8-H and LR4-D were both broken inside the concrete. The gage LR6-H was lost the same way near the end of the testing. The exact reason for these failures inside the concrete was not known, but faulty waterproofing was probably one major factor.

During the trial run, it was also found that all three gages of the rosette SR3 showed marked drop in electric resistance. Resistances of 15, 14 and 22 ohms were needed in series with the vertical, horizontal and diagonal gages, respectively, to get them balanced on the indicator. The response of the ammeter in the indicator to the adjustments was also very sluggish with these gages. After the first few cycles of testing, however, it was found that, in order to get a reading from SR3-D, the previously necessary resistance must now be removed. This peculiar behavior seems to indicate some damage to the rosette, and hence the unreliability of the information yielded by it.

A "drifting" phenomenon was noticed on all interior gages throughout the testing. The strain reading for any pair of active and compensating gages varied with time. If both gages were turned on at the same time, the variation was not excessive, but rather

irregular. If one compensating gage was used for several active gages, then except for the first active gage, the strain reading would always tend to increase with time, although at an ever decreasing rate. It was noted that, in order to get a stable strain reading, about ten minutes were needed for each gage. Such a long waiting period would certainly extend the time needed for each cycle of testing to such an extent that other adverse factors would show their effect. It was finally decided to wait one minute for each gage, and the result proved fairly successful. This drifting was attributed to the heat created by the current passing through the very fine wires of the strain gages. The use of celluloid plate as the base of the capsules apparently was also a factor. No such effect was noted with the surface gages which were cemented directly on the concrete surface.

With one minute needed to take a reading of each gage, and five steps to complete one stretching, or releasing of prestresses, the total time consumed for each cycle of testing was rather long. took two days to complete the first cycle. By better coordination of the work, and gaining experience, however, it was soon possible to complete one cycle in ten hours.

The testing first started on December 30, 1957. With a few interruptions due to conflicts in scheduling of the use of the testing machine, the last (20th) cycle of readings was taken on February 24, 1958.

Computation of Strains and Stresses

In general, for the interior gages, the "final zero" readings were different from the "initial zero" readings. These changes in zero readings were of the same order of magnitude as the strains measured due to loading. For example, in cycle number 4 using loading condition I, the strain gage S3 gave the following readings:

Initial zero	0 - 14 - 1359	Jan. 22, 1958-9:02 AM
P.L. + D.L.	0 - 14 - 1347	1:26 PM
P.L. + D.L. + L.L.	0 - 14 - 1354	3:07 PM
Final zero	0 - 14 - 1378	5:34 PM.

It is obvious that the actual strain due to loading could not be obtained accurately with the "zero readings" changing so much. It was first attempted to assume that the zero reading varies at a uniform rate, and the effective "zero" for each loading condition might be obtained by interpolation between the two zero readings. Thus, the strain due to P.L. + D.L. would be

$$(1347 - 1359) - (1378 - 1359) \times \frac{264}{512} = - 12\text{-}10$$

$$= - 22 \text{ micro-inches/in.},$$

and the strain due to P.L. + D.L. + L.L. would be

$$(1354 - 1359) - (1378 - 1359) \times \frac{365}{512} = - 5\text{-}14$$

$$= - 19 \text{ micro-inches/in.}$$

However, it was soon noticed that in the next cycle, the respective zero readings were:

Initial zero	0 - 14 - 1375	Jan. 24, 1958	10:40 AM
Final zero	0 - 14 - 1400	Jan. 25, 1958	5:22 PM.

In both cycles, the final zero was higher than the initial zero, while the initial zero of cycle 5 was lower than the final zero of cycle 4. Indeed, if the zero readings were plotted against time, a zigzag curve like Figure 2.10 would result. It seems apparent that more than one factor was causing the changing of strain readings. The continuing chemical reaction in concrete should be one important factor, but this should cause a rather uniform variation. It seems reasonable to assume that if the beam was lying idle, the zero readings would have changed according to this effect. The difference of the final reading from the initial one was attributed mainly to the residual strain in the celluloid capsule upon the release of load. Based upon this assumption, the interpolation of zero readings should be made between the successive initial zeroes. Thus, the strain due to P.L. + D.L. at gage S3 in cycle 4 would be

$$(1347 - 1359) - (1375 - 1359) \times \frac{4.40}{49.63} = -12\text{-}1$$

$$= -13 \text{ micro-inches/in.},$$

and the strain due to P.L. + D.L. + L.L. would be

$$(1354 - 1359) - (1375 - 1359) \times \frac{6.08}{49.63} = -5\text{-}2$$

$$= -7 \text{ micro-inches/in.}$$

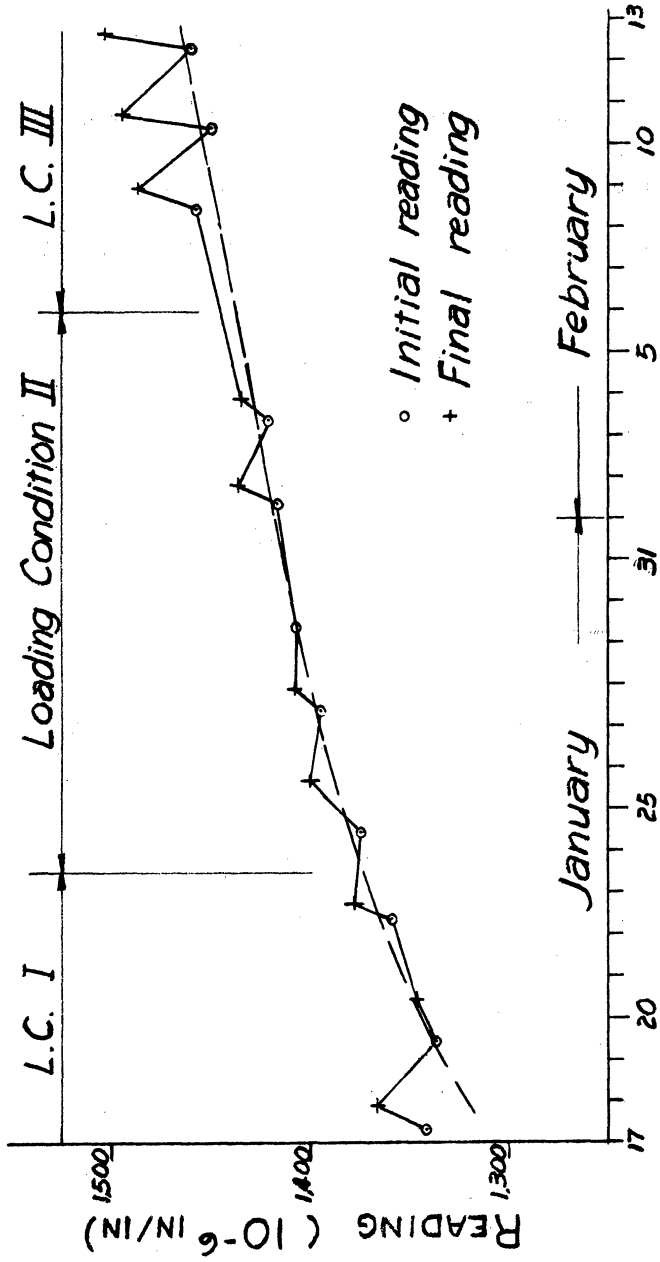

Figure 2.10. Zero Reading vs. Time Typical Interior Gage.

This latter method was adopted in general for computation of actual strains. For the surface gages, the changes in zero readings were very small in comparison with the strains due to loading, so the first method was used.

After the strains were obtained at each point, stresses were computed. Those for single gages were computed simply by multiplying the strain by the modulus of elasticity of concrete. For the rosettes, the computations were a little more complicated, as following;

$$\epsilon_V = R_V - \frac{1}{210} R_H$$

$$\epsilon_H = R_H - \frac{1}{210} R_V$$

$$\epsilon_D = 1.02\ R_D - \frac{1}{210} (R_H + R_V)$$

$$\sigma_x = \frac{E}{1-\nu^2} (\epsilon_H + \nu\ \epsilon_V)$$

$$\sigma_y = \frac{E}{1-\nu^2} (\epsilon_V + \nu\ \epsilon_H)$$

$$\tau_{xy} = - \frac{E}{2(1+\nu)} (2\ \epsilon_D - \epsilon_V - \epsilon_H)$$

$$C = \frac{1}{2} (\epsilon_H + \epsilon_V)$$

$$D = \sqrt{\frac{(\epsilon_H - \epsilon_D)^2 + (\epsilon_V - \epsilon_D)^2}{2}}$$

$$p_1 = E\left(\frac{C}{1-\nu} + \frac{D}{1+\nu}\right)$$

$$p_2 = E\left(\frac{C}{1-\nu} - \frac{D}{1+\nu}\right)$$

$$\text{Tan } 2\phi = - \frac{2\epsilon_D - \epsilon_H - \epsilon_V}{\epsilon_H - \epsilon_V}$$

The first three formulae were given by Baldwin-Lima-Hamilton Corporation (manufacturer of SR-4 strain gages) for the adjustments of rosette readings. The rest are the standard formulae for two-dimensional strain problems. The minus signs for τ_{xy} and Tan 2ϕ were inserted because the D direction used in the test was the "negative" diagonal, making a 135° angle with the positive x direction. The computations for rosette gages were made on the IBM 650 Electronic Digital Computer in the Statistical and Computing Laboratory of the University.

Results of Testing

The end block stresses under various loading conditions obtained from the experiment are shown in Figures 2.11 through 2.30.

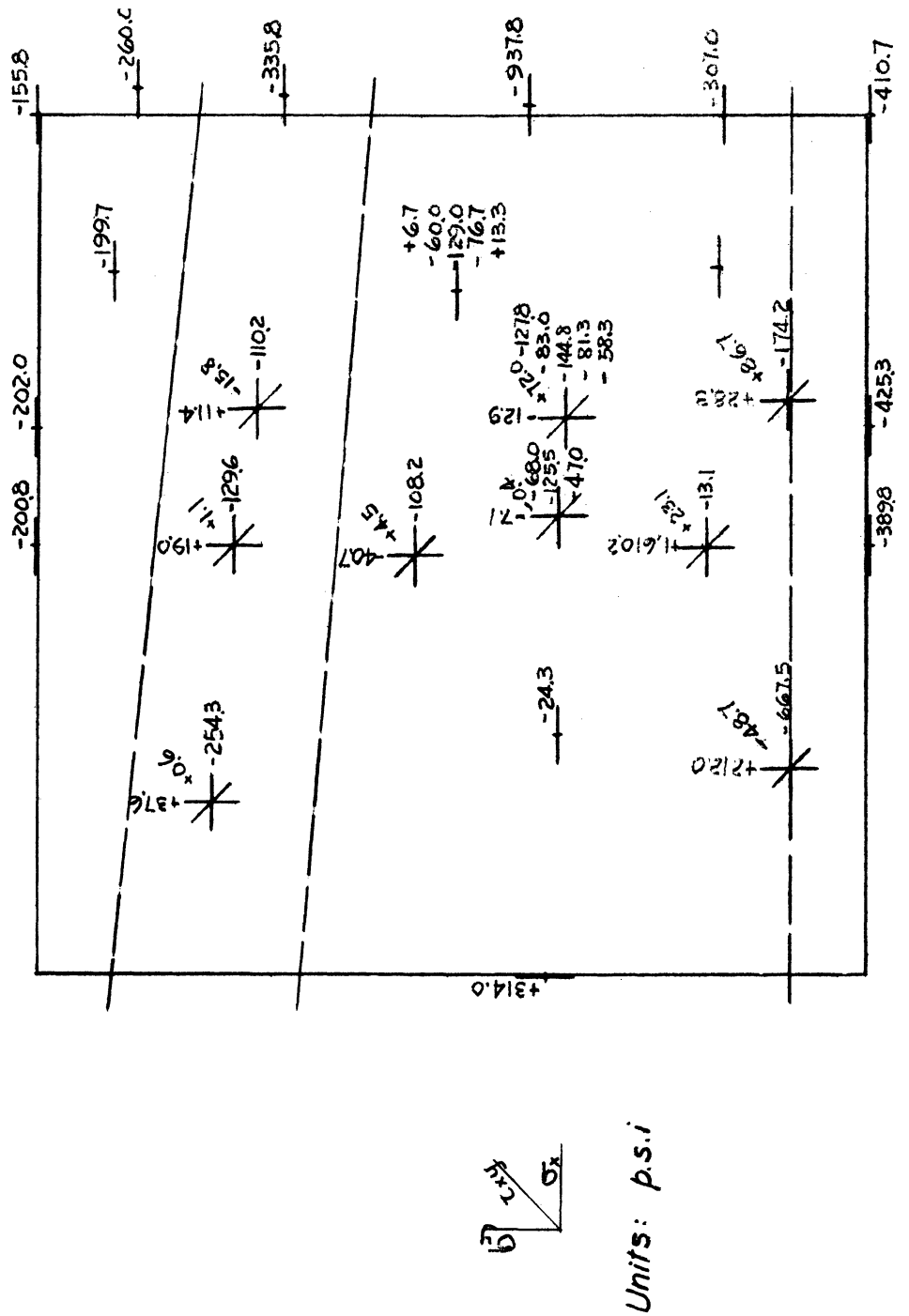

Figure 2.11. Stresses, Short End, Experimental, Loading Condition I, P.L. + D.L.

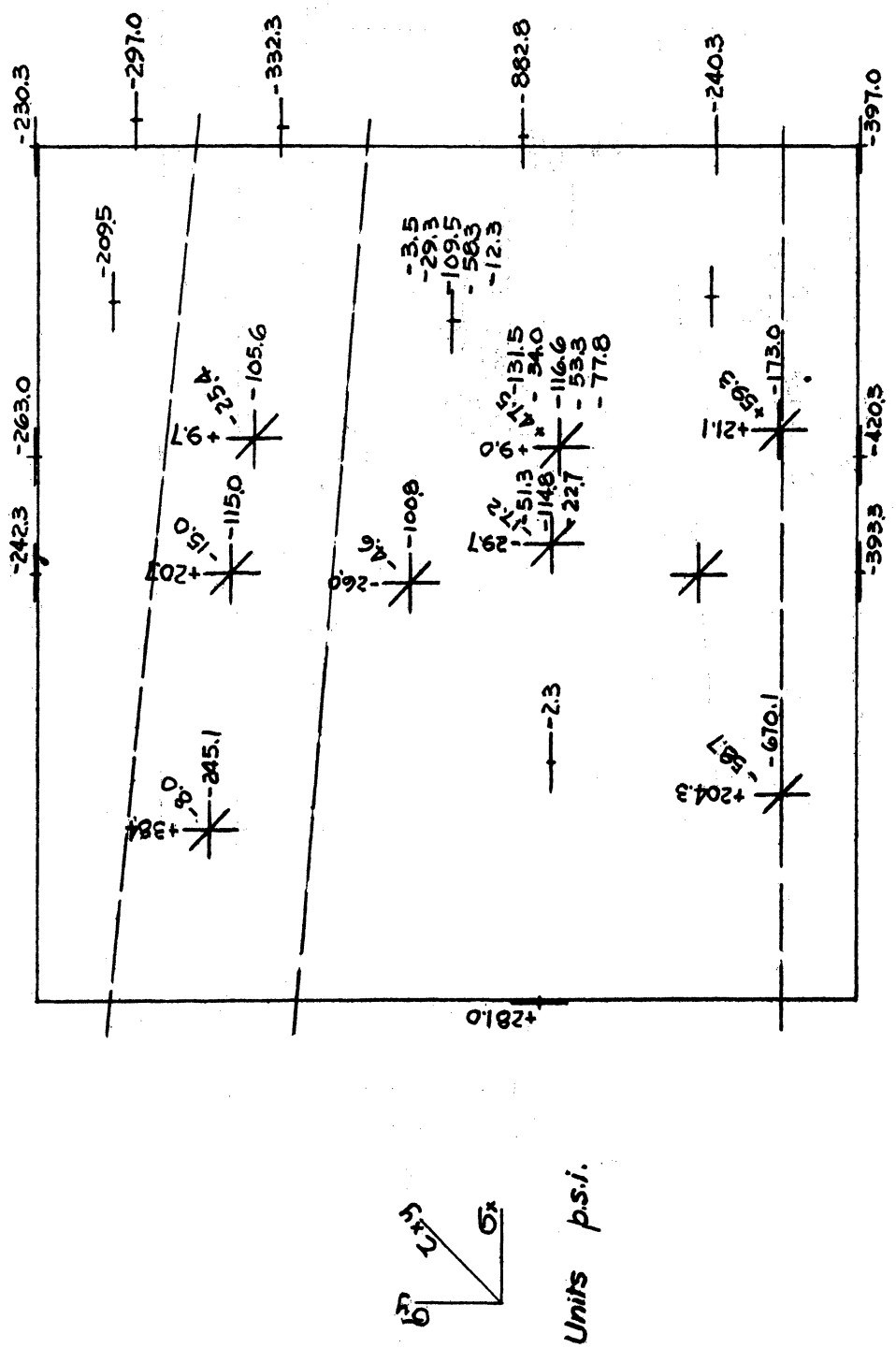

Figure 2.12. Stresses, Short End, Experimental, Loading Condition I, P.L. + D.L. + L.L.

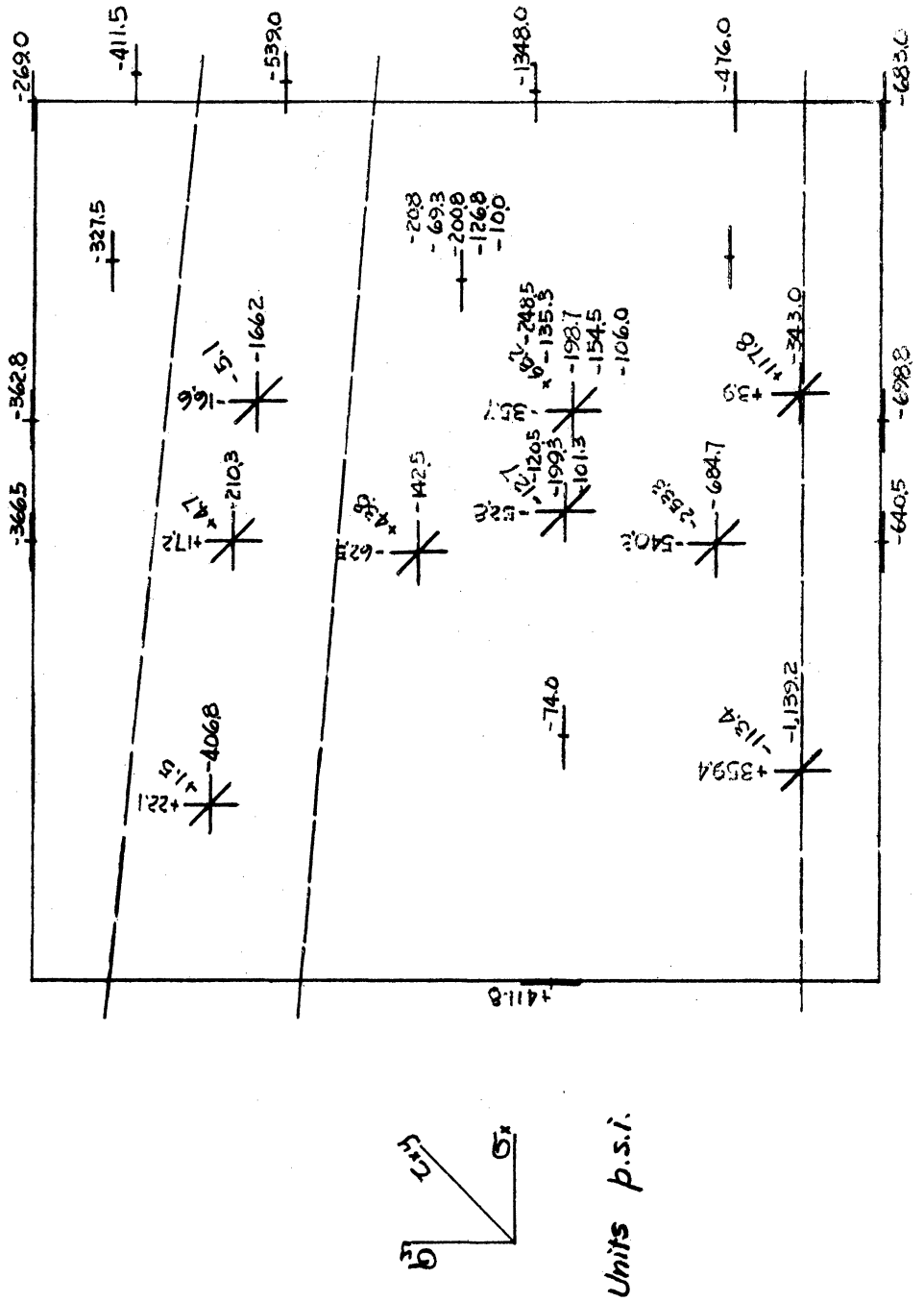

Figure 2.13. Stresses, Short End, Experimental, Loading Condition II, P.L. + D.L.

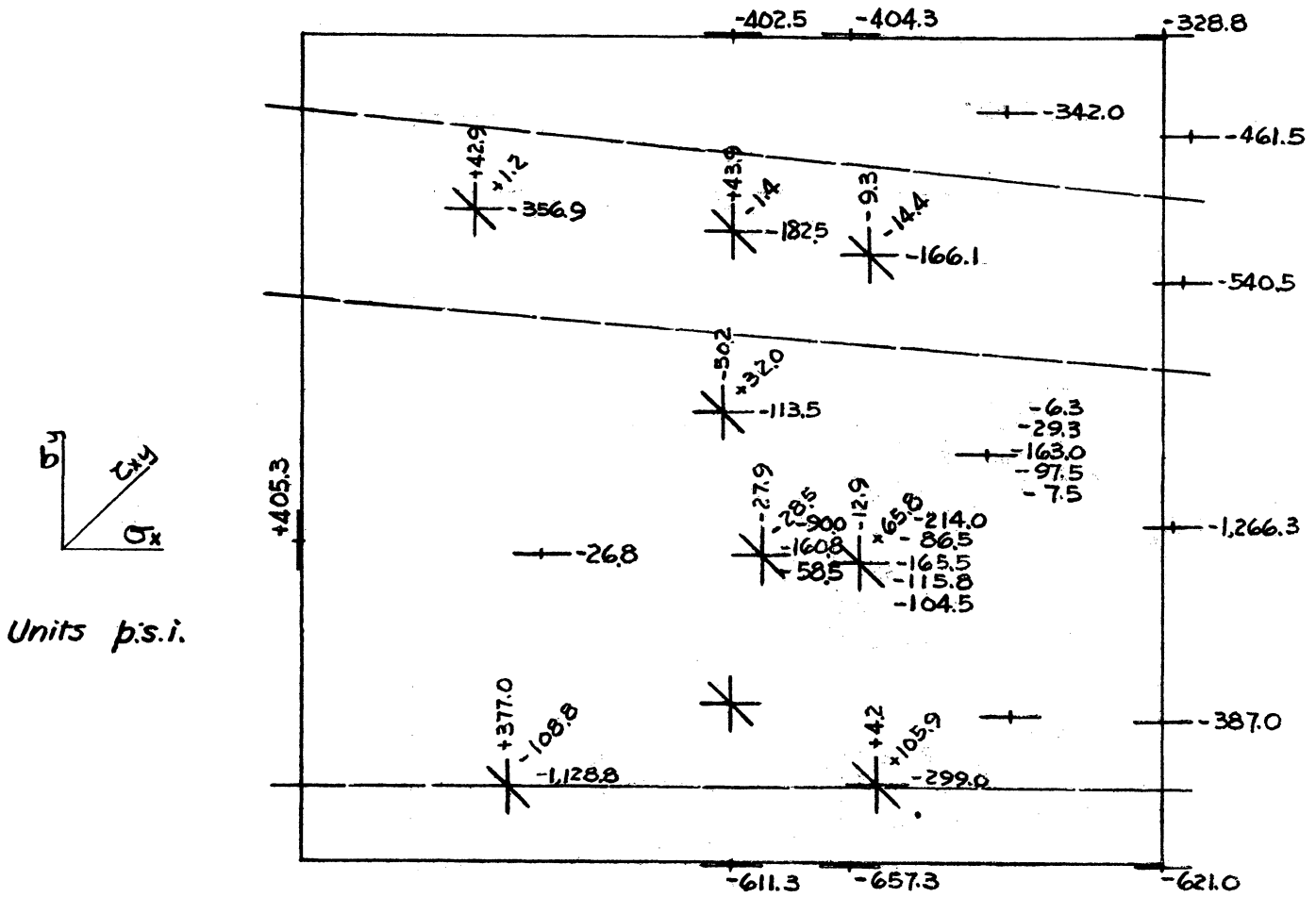

Figure 2.14. Stresses, Short End, Experimental, Loading Condition II, P.L. + D.L. + L.L.

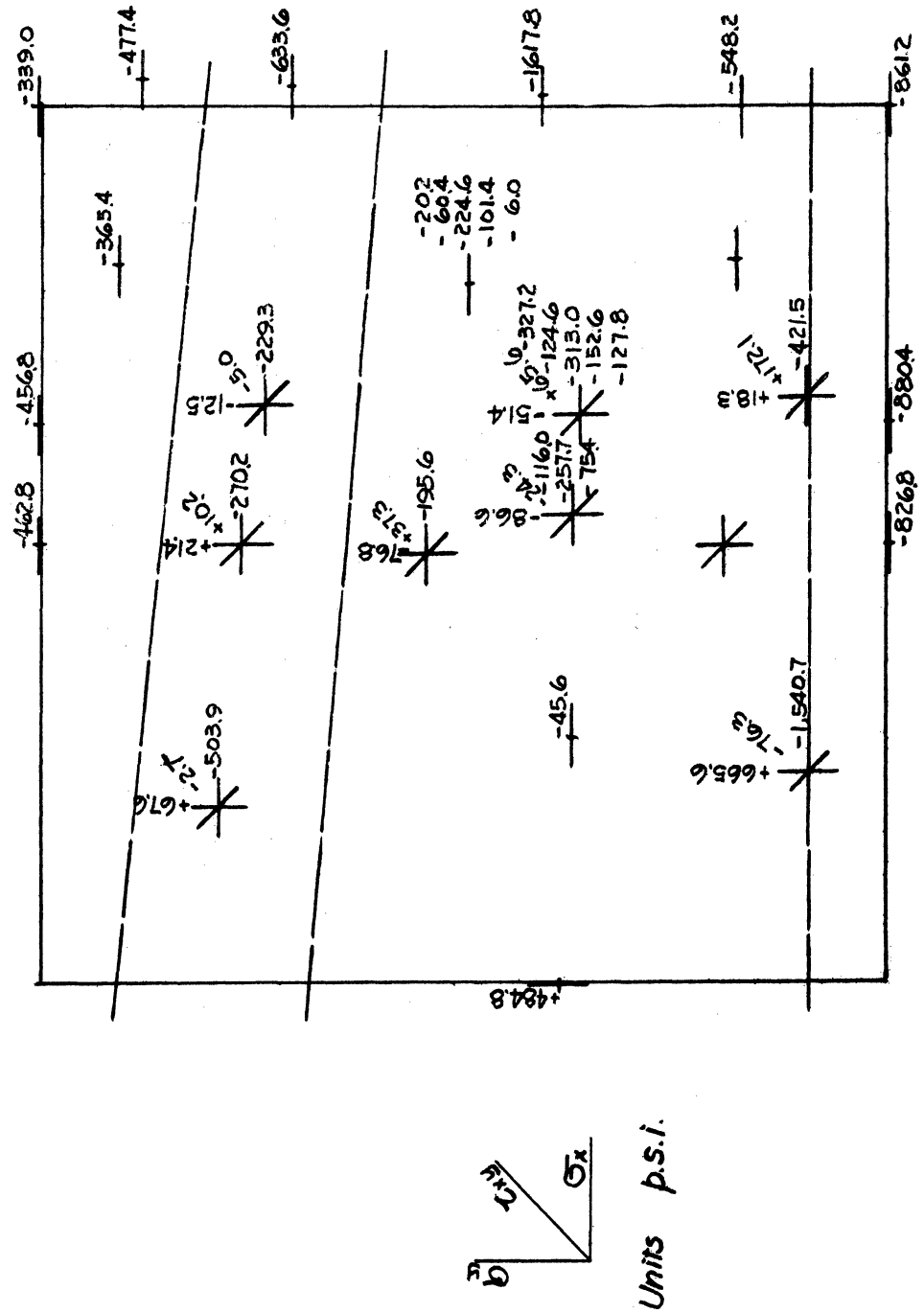

Figure 2.15. Stresses, Short End, Experimental, Loading Condition III, P.L. + D.L.

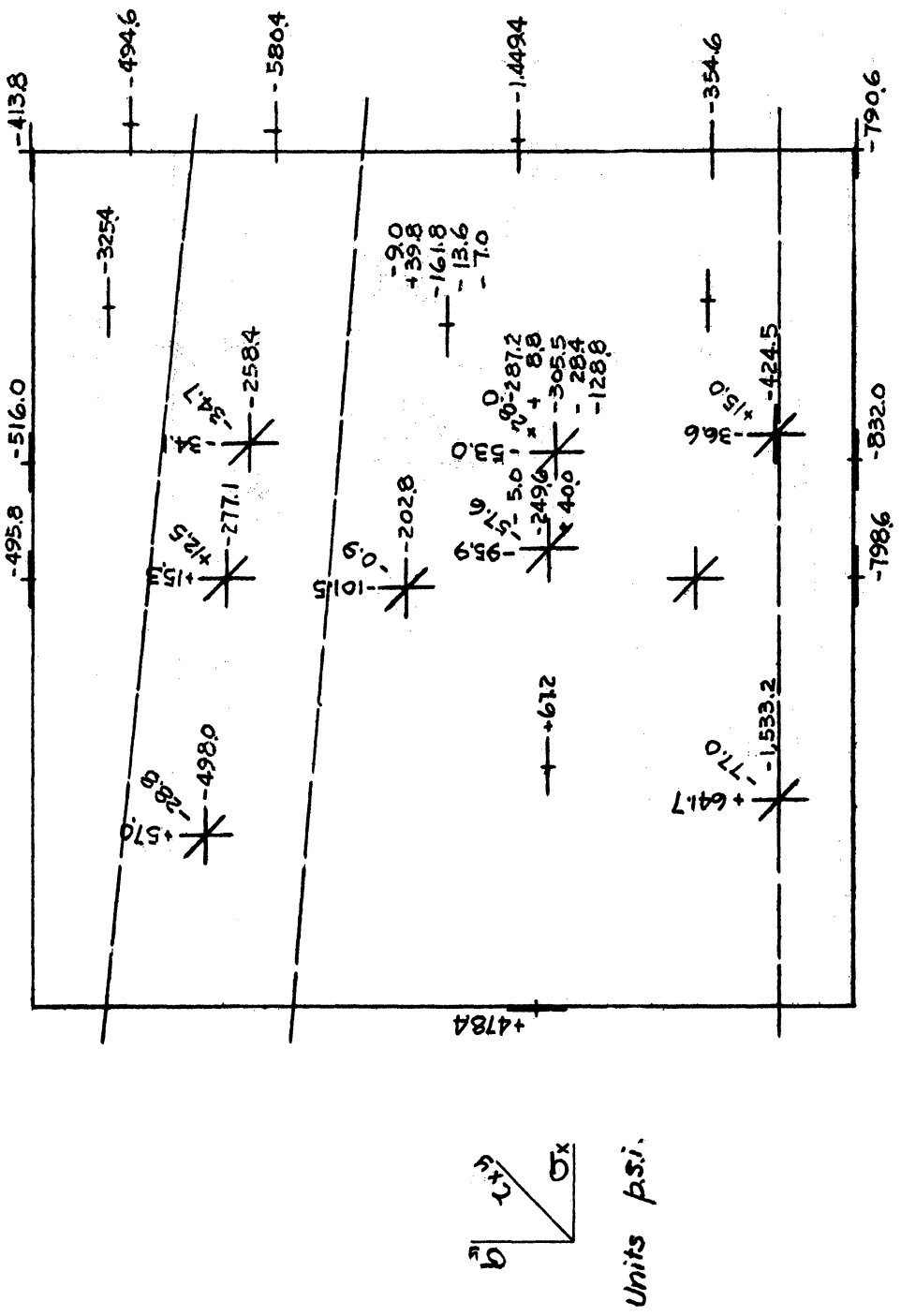

Figure 2.16. Stresses, Short End, Experimental, Loading Condition III, P.L. + D.L. + L.L.

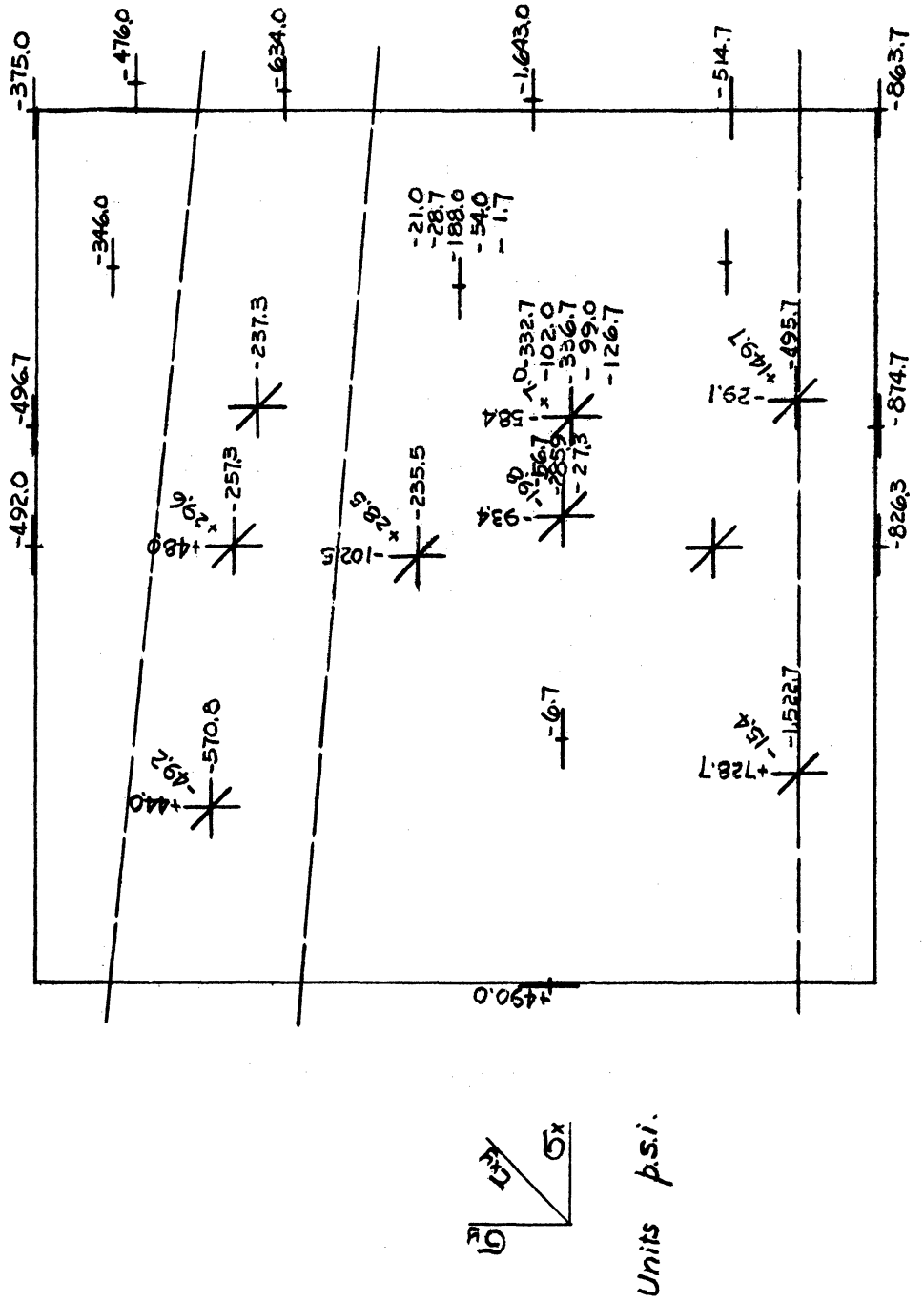

Figure 2.17. Stresses, Short End, Experimental, Loading Condition IV, P.L. + D.L.

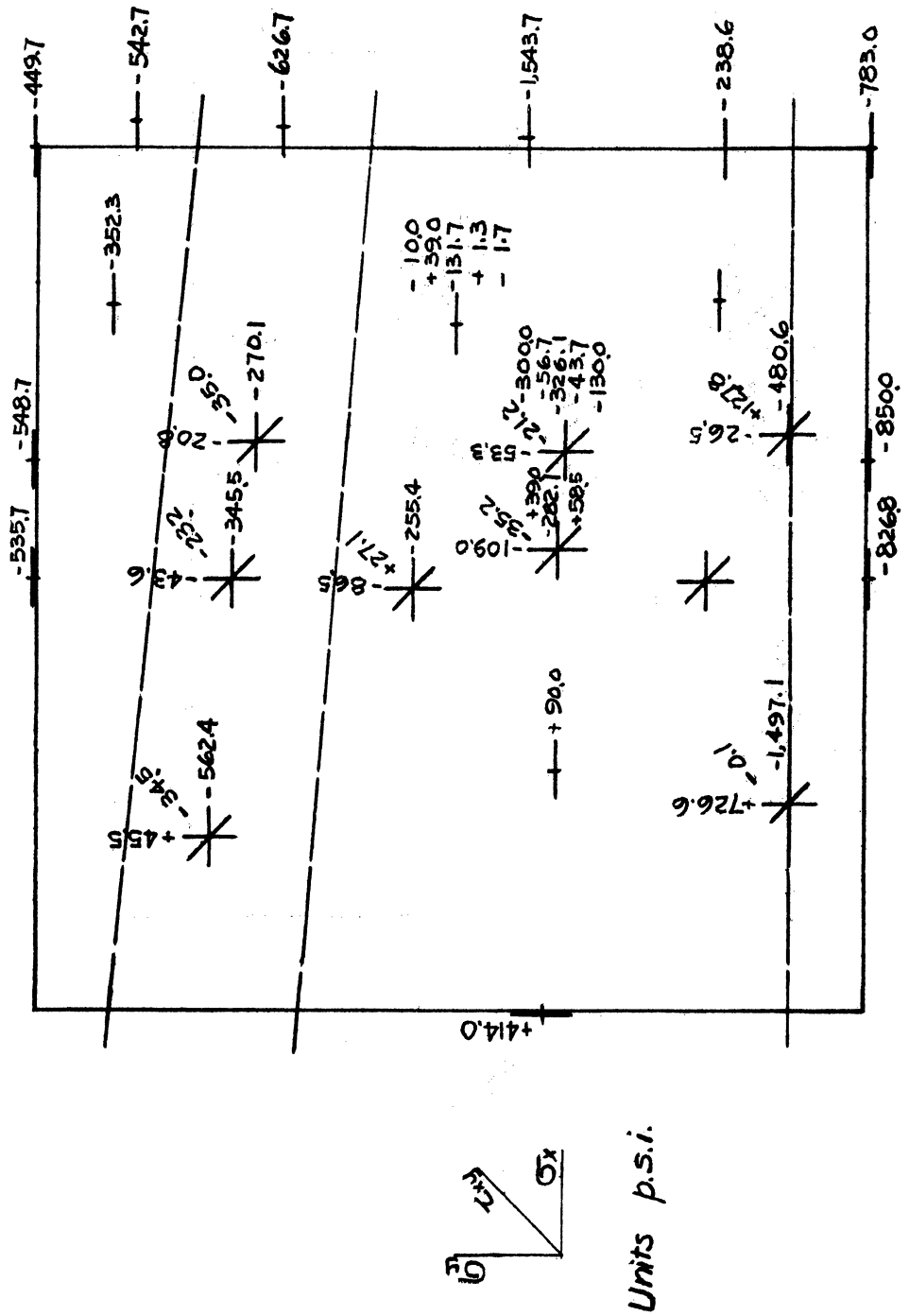

Figure 2.18. Stresses, Short End, Experimental, Loading Condition IV, P.L. + D.L. + L.L.

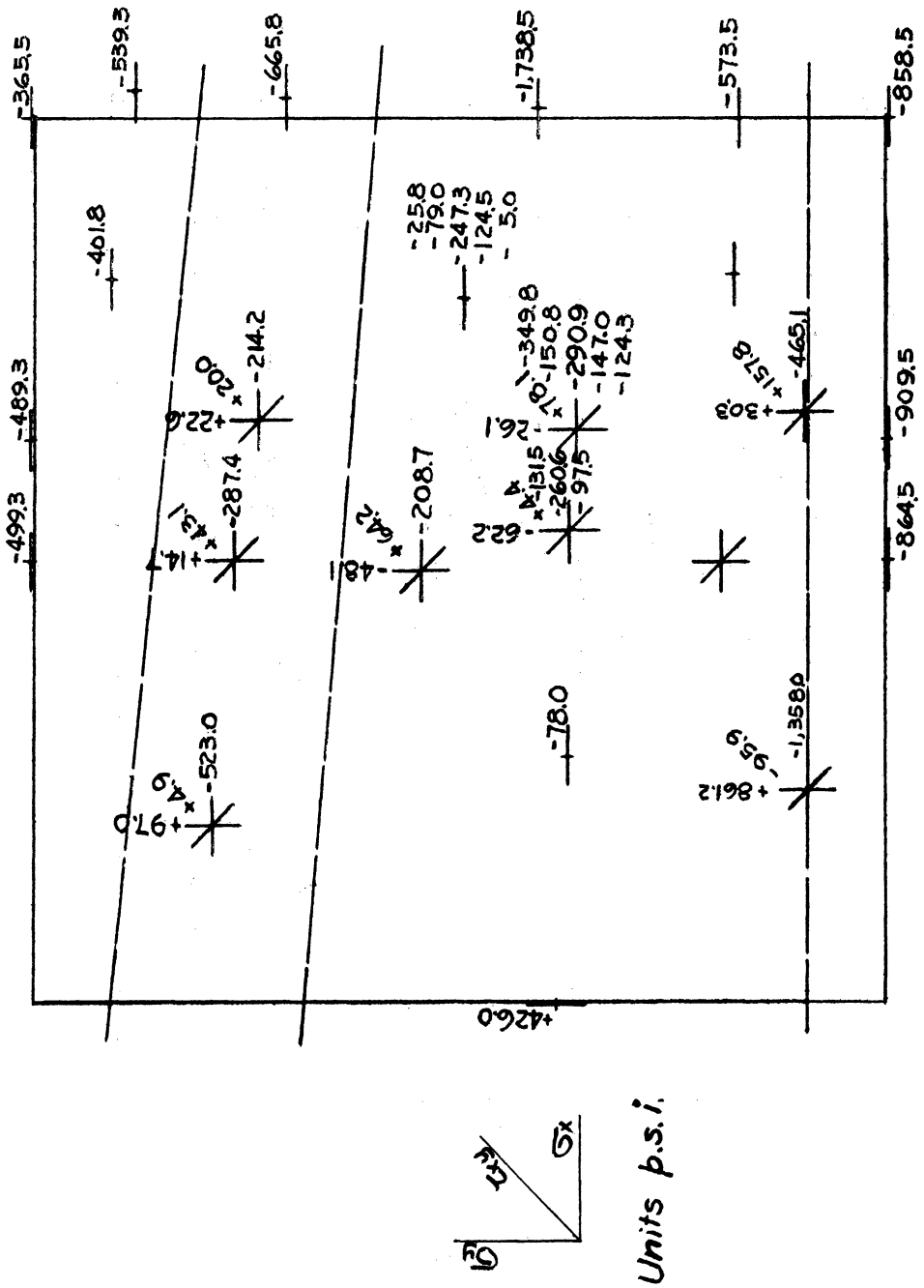

Figure 2.19. Stresses, Short End, Experimental, Loading Condition V, P.L. + D.L.

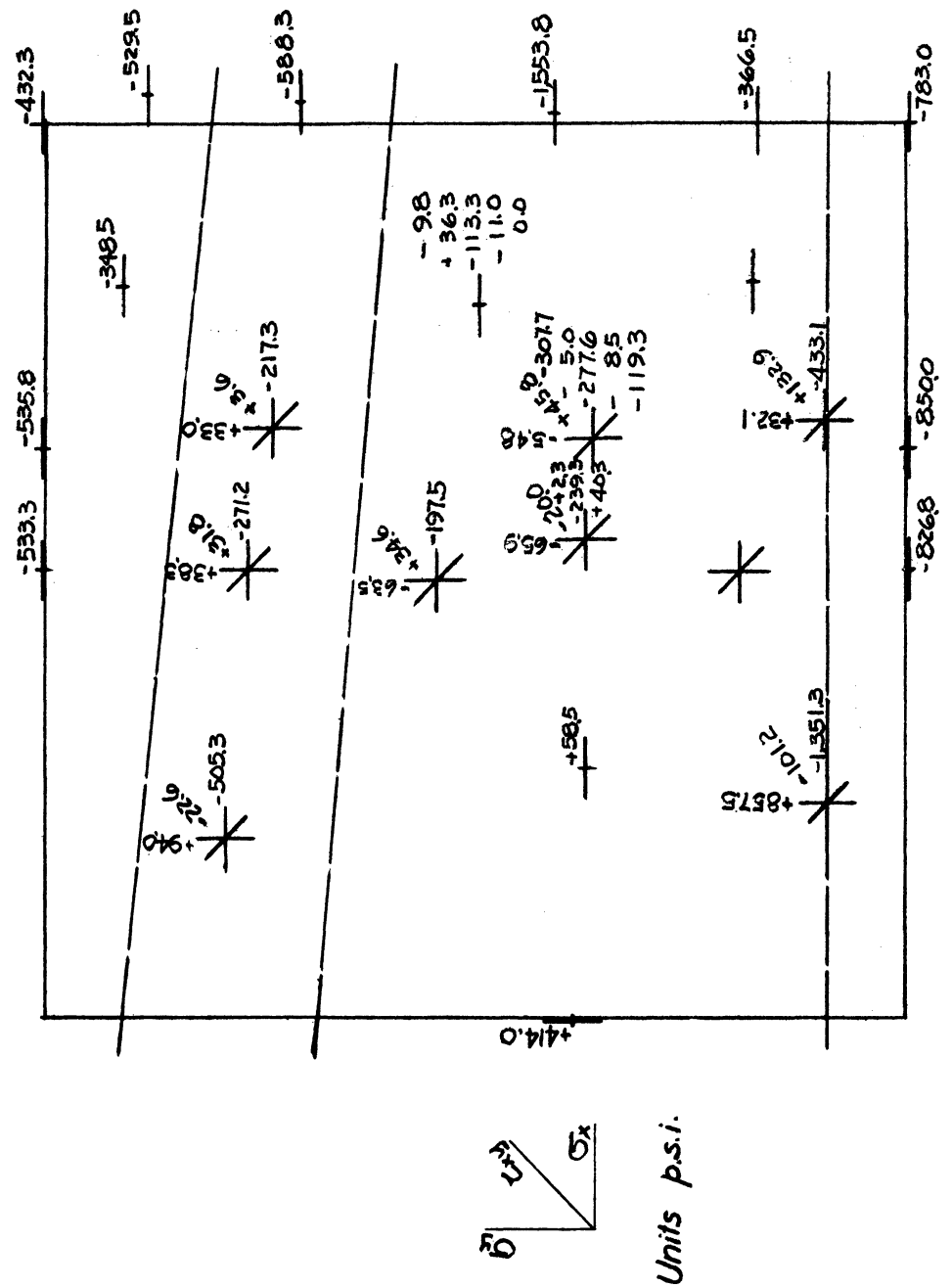

Figure 2.20. Stresses, Short End, Experimental, Loading Condition V, P.L. + D.L. + L.L.

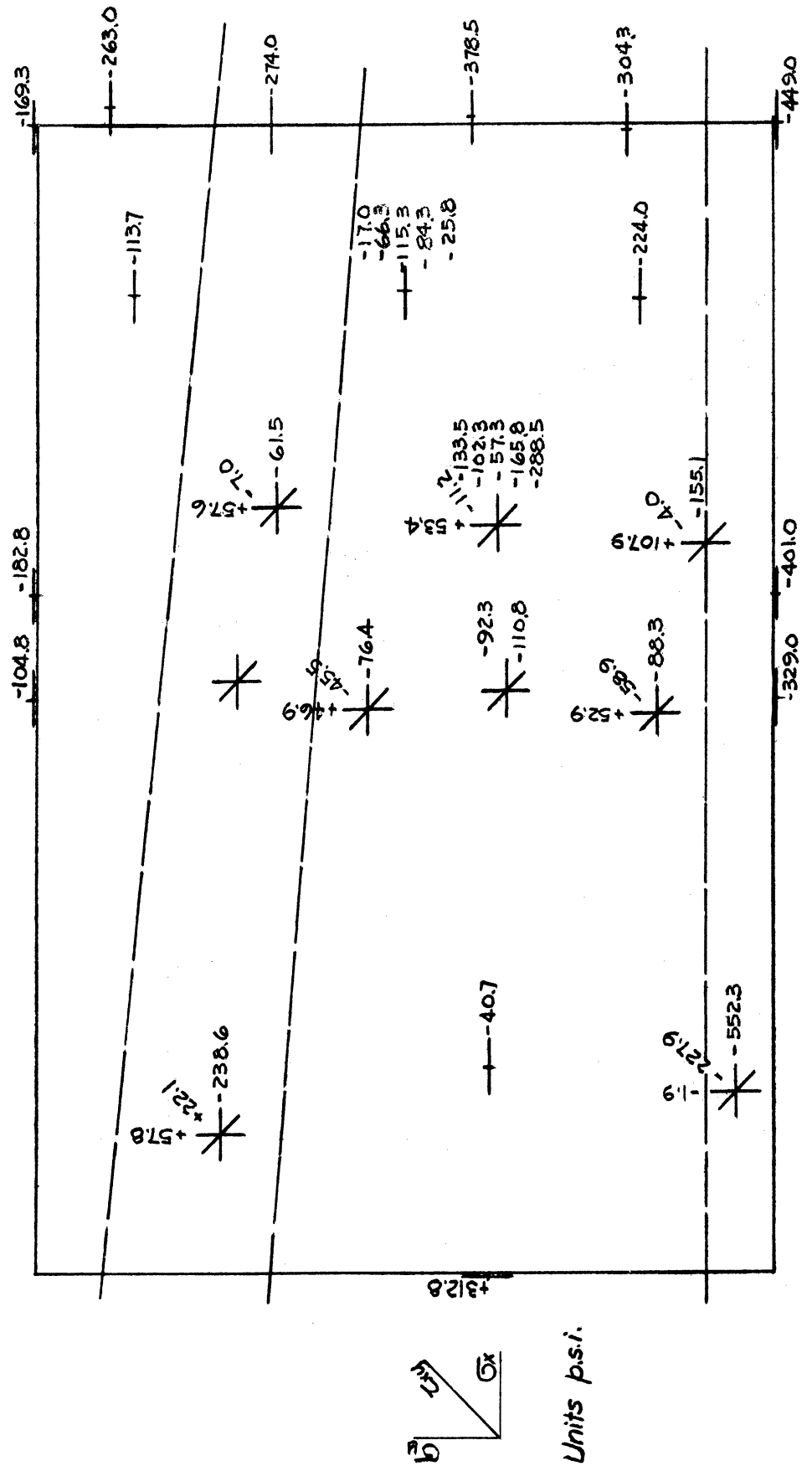

Figure 2.21. Stresses, Long End, Experimental, Loading Condition I, P.L. + D.L.

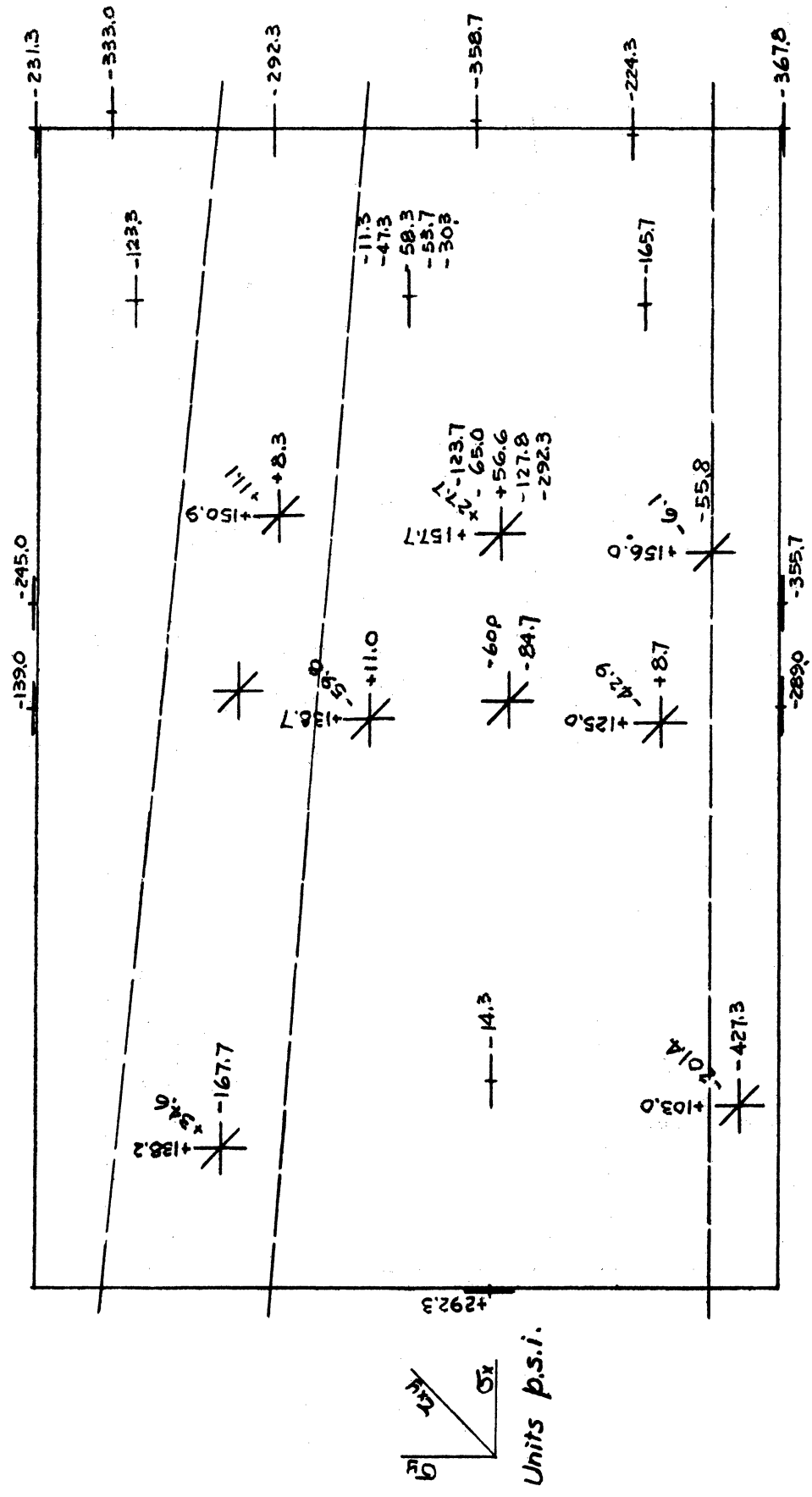

Figure 2.22. Stresses, Long End, Experimental, Loading Condition I, P.L. + D.L. + L.L.

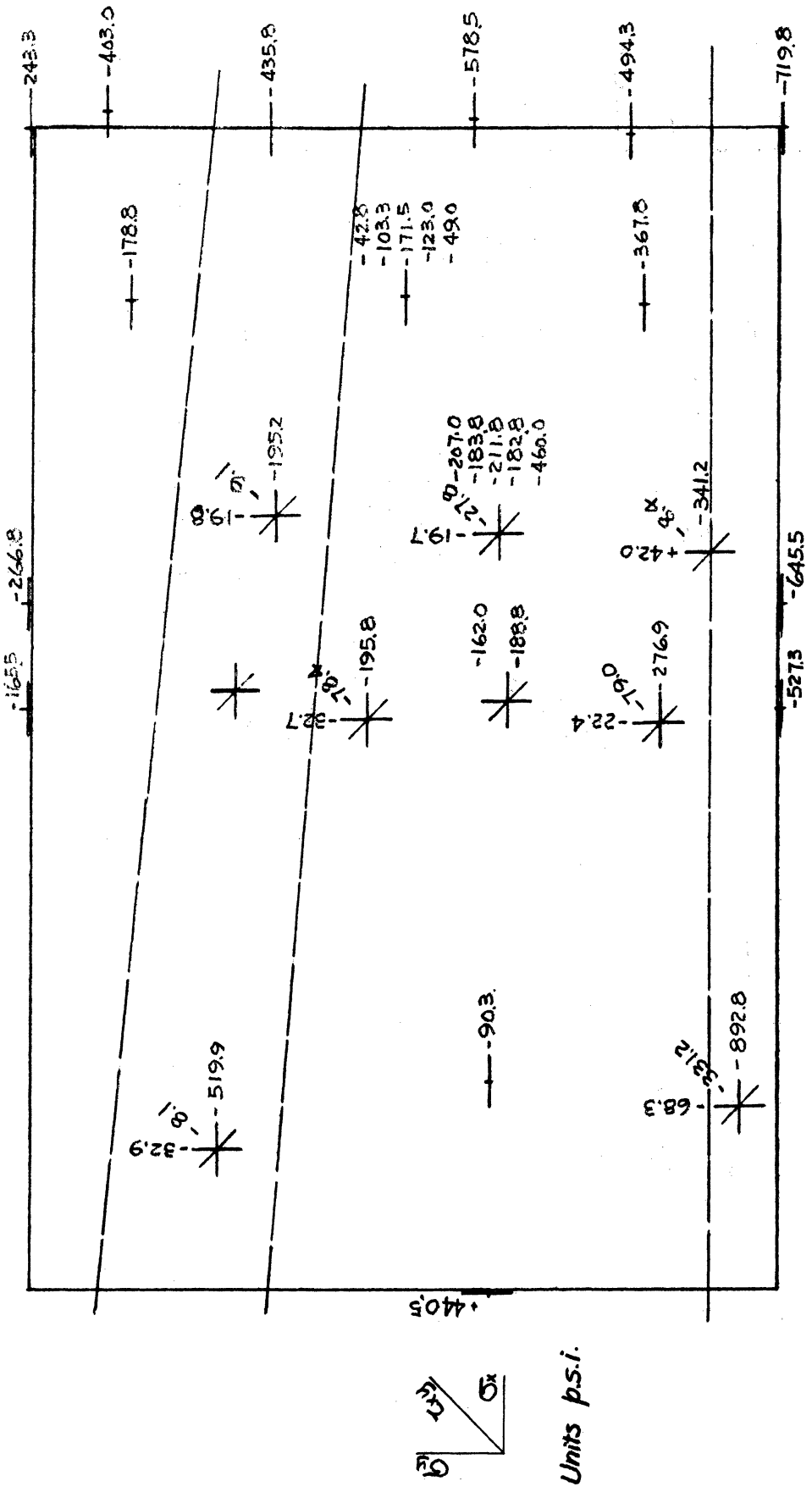

Figure 2.23. Stresses, Long End, Experimental, Loading Condition II, P.L. + D.L.

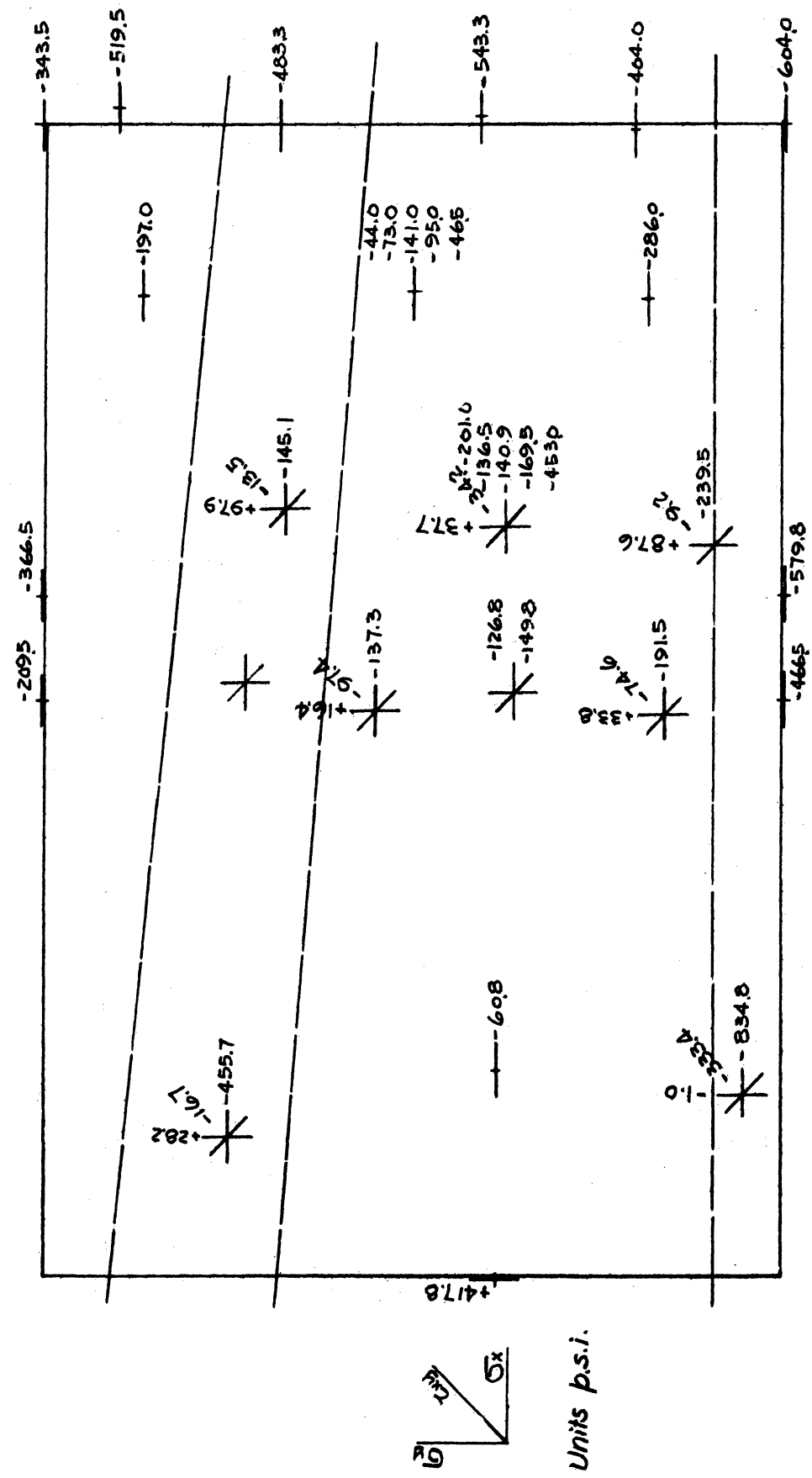

Figure 2.24. Stresses, Long End, Experimental, Loading Condition II, P.L. + D.L. + L.L.

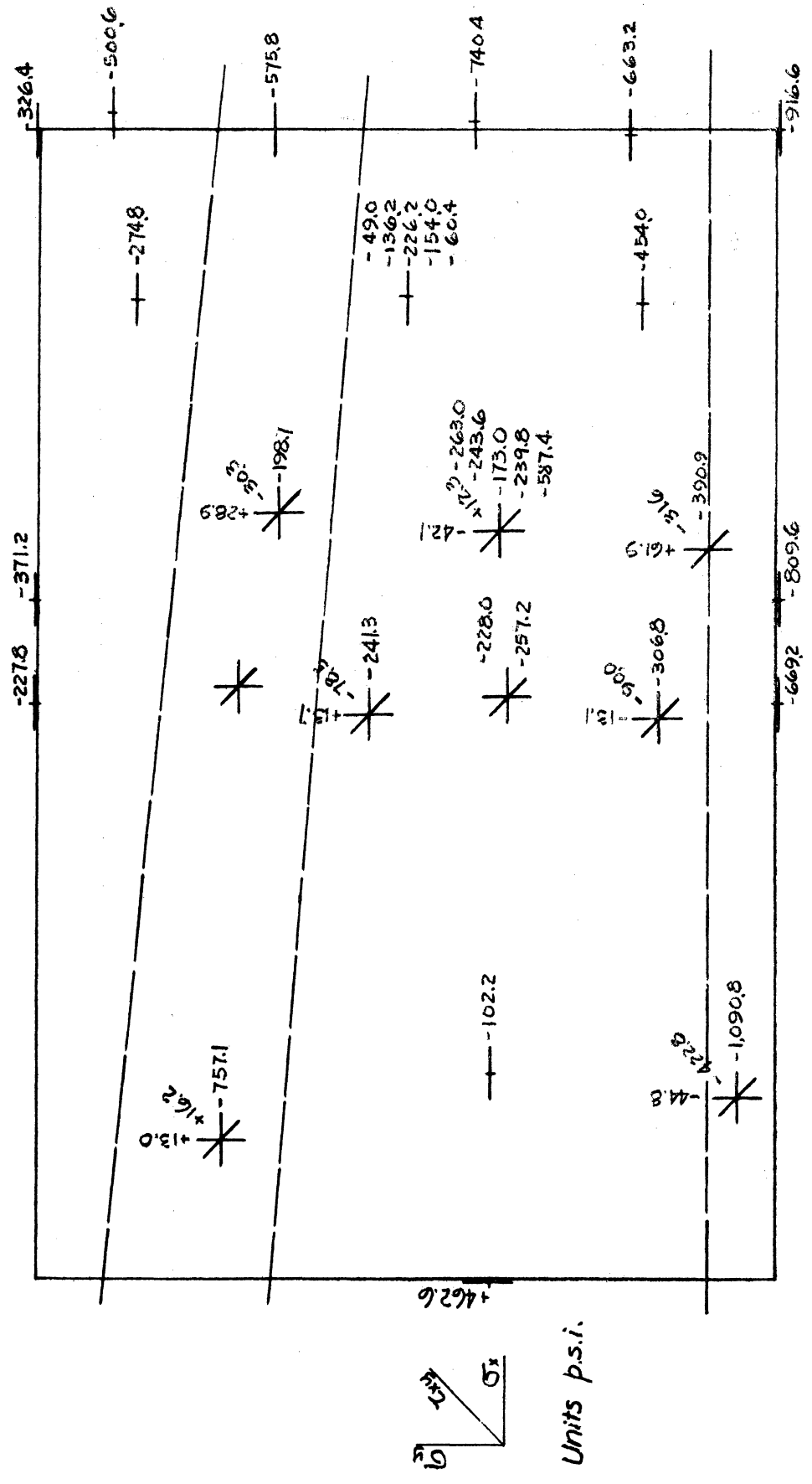

Figure 2.25. Stresses, Long End, Experimental, Loading Condition III, P.L. + D.L.

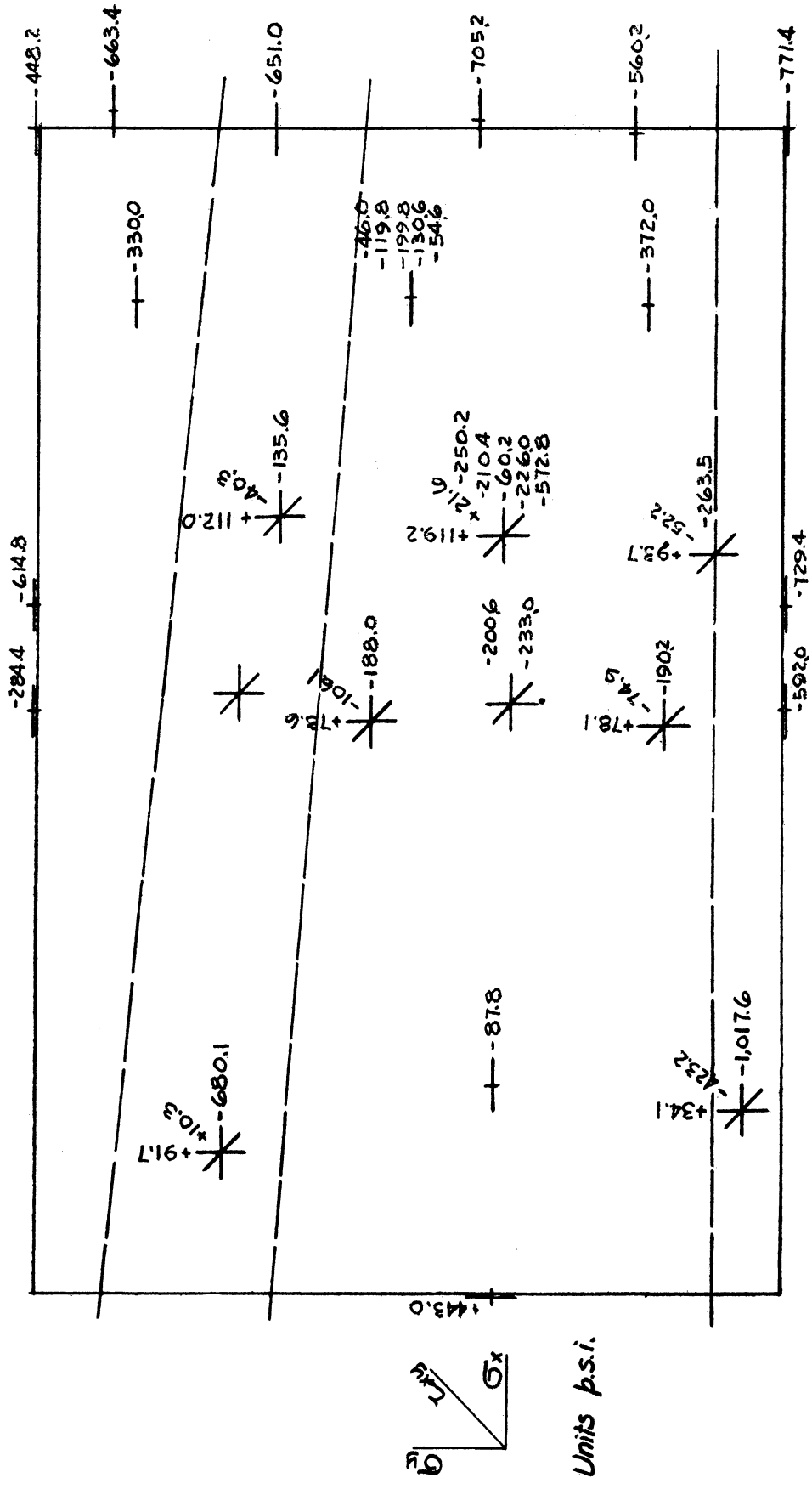

Figure 2.26. Stresses, Long End, Experimental, Loading Condition III, P.L. + D.L. + L.L.

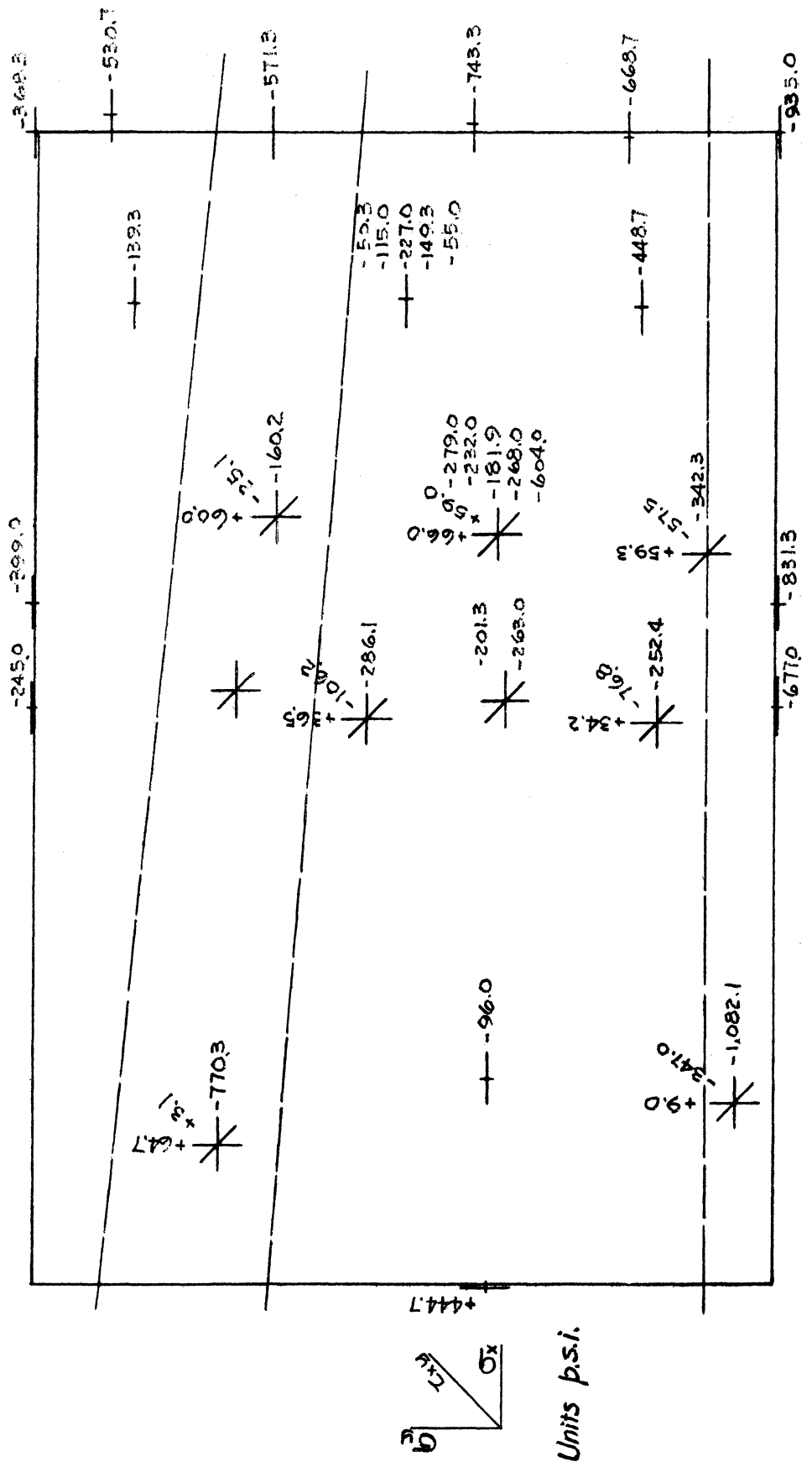

Figure 2.27. Stresses, Long End, Experimental, Loading Condition IV, P.L. + D.L.

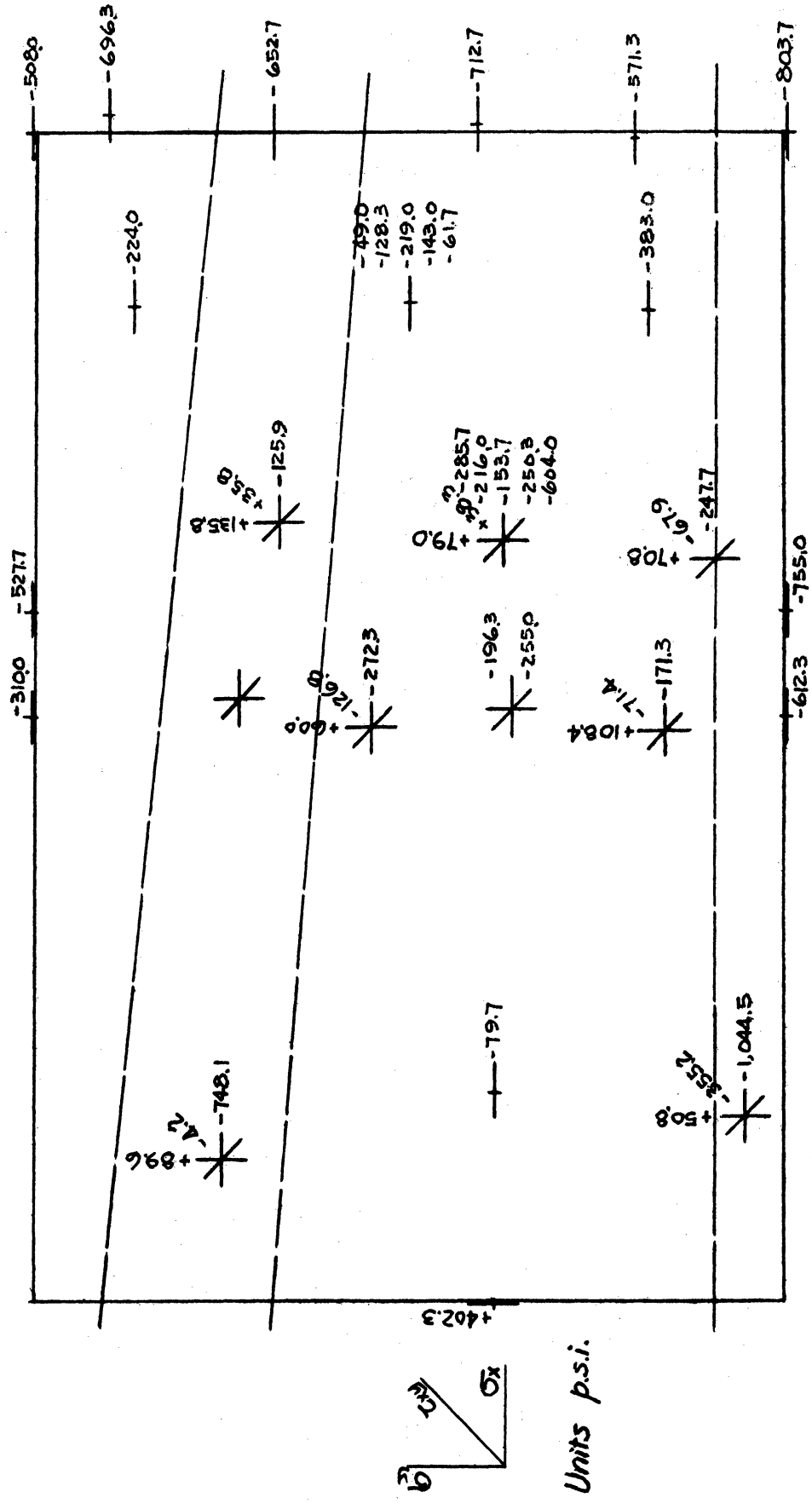

Figure 2.28. Stresses, Long End, Experimental, Loading Condition IV, P.L. + D.L. + L.L.

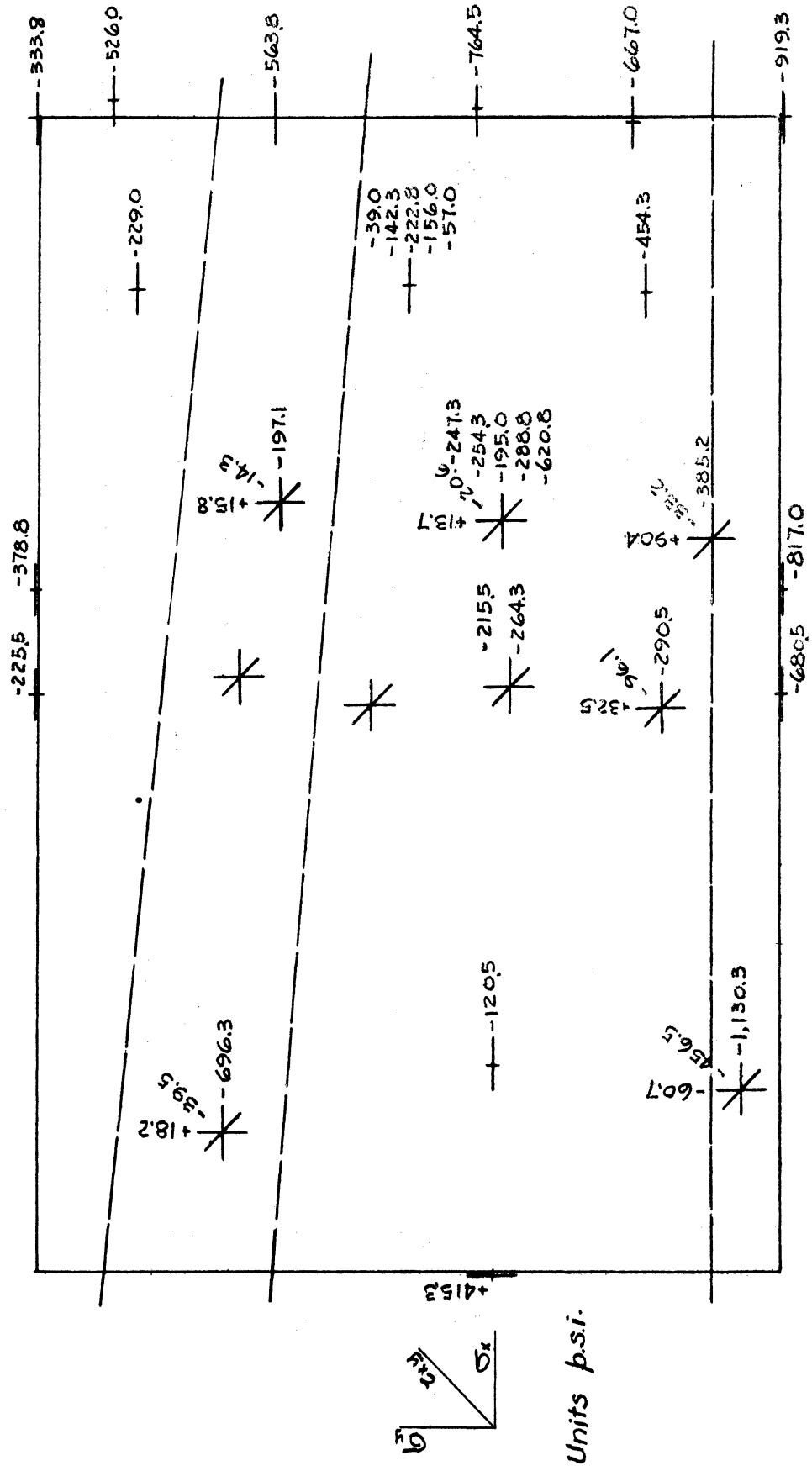

Figure 2.29. Stresses, Long End, Experimental, Loading Condition V, P.L. + D.L.

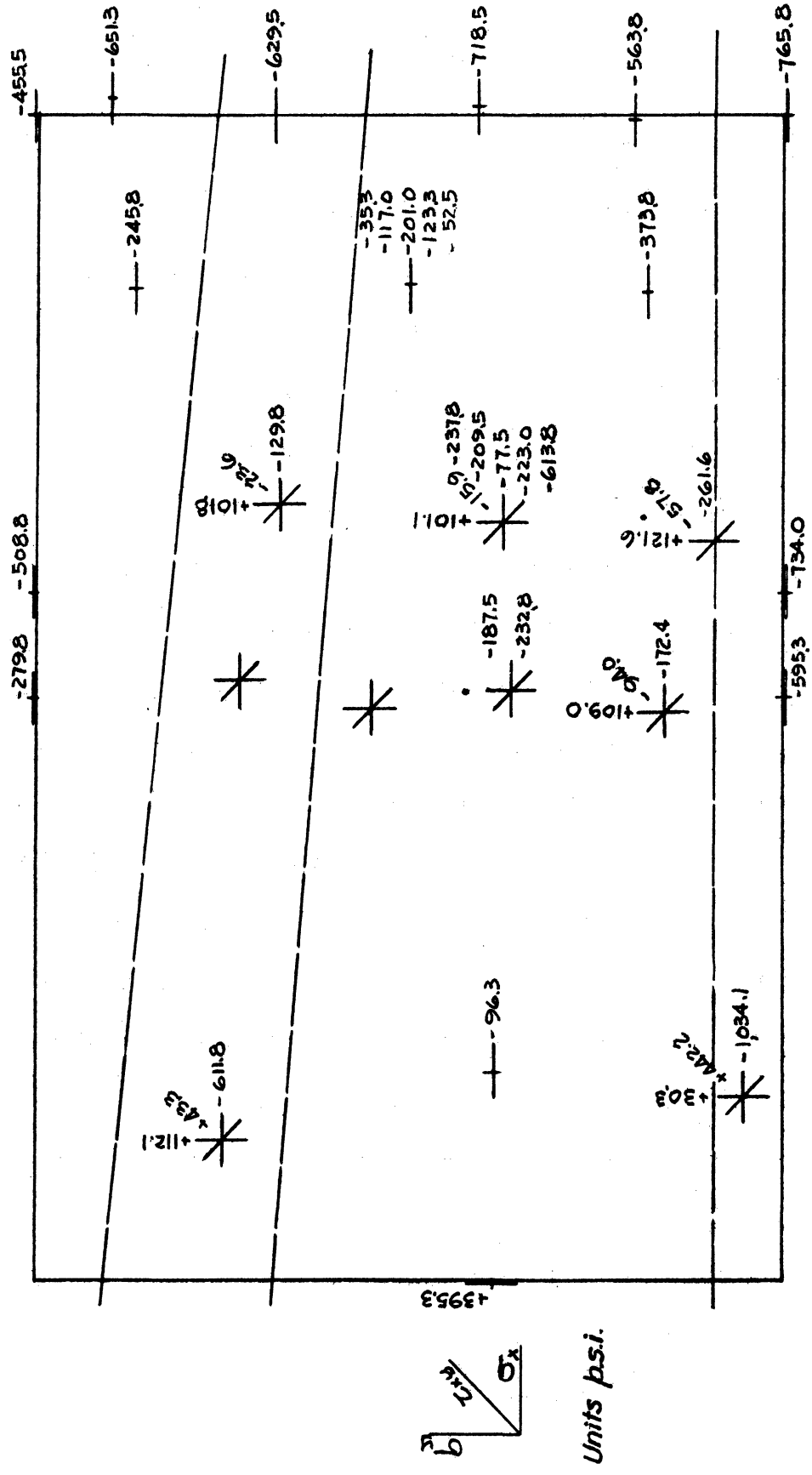

Figure 2.30. Stresses, Long End, Experimental, Loading Condition V, P.L. + D.L. + L.L.

CHAPTER III

ANALYTICAL INVESTIGATION

Three Dimensional Problem

Basically, the problems of end blocks are three dimensional, due to the relative smallness of the bearing plates at the end, and the variation of width of the beam body and the differences of these widths from that of the end block. Consider the variation of the distribution of longitudinal stress, σ_x, over successive transverse sections, for example. At the end surface ($x = 0$), σ_x is necessarily zero everywhere except under the anchorage bearing plates. As the section moves inward, it is obvious that the pressure will be distributed over wider area, with the tendency of achieving uniform, or at most linearly varying distribution. However, at the other end of this distribution zone, where the rectangular end block joins the I-shaped beam body (this plane will hereafter be called "the juncture section" or simply "the juncture"), the pressure must be restricted inside the boundary of the smaller section, i.e., the I-section. Thus, the longitudinal pressure spreads out from under the bearing plates, but "reconcentrates" toward the juncture section. Similarly, the vertical normal stress σ_y is concentrated at the bottom surface, zero at top, and is transmitted by shear τ_{xy} into the beam body. The transverse normal stress σ_z is zero over both side faces, and at some maximum value at the central plane ($z = 0$). It is seen that all six components of stress are present at arbitrary interior points, and the problem is truly three-dimensional.

Although enough equations are available for a theoretical solution of three-dimensional stress-strain problems, the extreme complexity, nevertheless, renders it impracticable to solve them, except for a few very special cases. In order to avoid the complexity of three-dimensional problems, simplifications were attempted.

Two Dimensional Problem

On the two side surfaces of the end block ($z = \pm \frac{1}{2} b$), the three stress components σ_z, τ_{yz}, and τ_{xz} are all zero. In view of the fact that the width of an end block is almost always its smallest dimension, it seems reasonable to assume that these three stress components will remain small, relative to the other three, throughout the end block, and hence may be considered as zero throughout without introducing serious error. Thus

$$\sigma_z = \tau_{yz} = \tau_{xz} = 0,$$

and the problem is reduced to two dimensional as plane stress. The problem can be further simplified by neglecting the variations of stress components with respect to z,* i.e., assuming

$$\frac{\partial \sigma_x}{\partial z} = \frac{\partial \sigma_y}{\partial z} = \frac{\partial \tau_{xy}}{\partial z} = 0.$$

*This assumption is actually equivalent of assuming that the normal strain in z direction, ϵ_z, is a linear function of x and y, which is in general not the case. However, the error thus introduced is not serious, cf. S. Timoshenko and J. N. Goodier, Theory of Elasticity, 2nd Edition, pp. 241-244.

So far as the author is aware, all of the existing methods of end block analysis are based on these assumptions. In this study, the end block will first be analyzed two dimensionally. The results will then be compared with the experimental data for a qualitative study of the distribution in the z-direction.

Solution of Plane Stress Problem

In the plane stress problem, with the assumption that all stress components are independent of z, the equations that must be satisfied are:

Equilibrium equations

$$\frac{\partial \sigma_x}{\partial x} + \frac{\partial \tau_{xy}}{\partial y} + F_x = 0 \qquad (1)$$

$$\frac{\partial \tau_{xy}}{\partial x} + \frac{\partial \sigma_y}{\partial y} + F_y = 0 \qquad (2)$$

Compatibility equation

$$\left(\frac{\partial^2}{\partial x^2} + \frac{\partial^2}{\partial y^2}\right)(\sigma_x + \sigma_y) + (1 + \nu)\left(\frac{\partial F_x}{\partial x} + \frac{\partial F_y}{\partial y}\right) = 0 \qquad (3)$$

where F_x, F_y are the body forces per unit volume in x and y directions.

Let Z = potential of body forces, so that

$$\left.\begin{aligned} F_x &= -\frac{\partial Z}{\partial x} \\ F_y &= -\frac{\partial Z}{\partial y} \end{aligned}\right\} \qquad (4)$$

*In all engineering problems, such a potential exists. Cf. R.V. Southwell, Theory of Elasticity, p. 367.

Then the equilibrium equations may be satisfied by substituting

$$\left.\begin{aligned} \sigma_x &= \frac{\partial^2\Phi}{\partial y^2} + Z, \\ \sigma_y &= \frac{\partial^2\Phi}{\partial x^2} + Z, \\ \tau_{xy} &= -\frac{\partial^2\Phi}{\partial x \partial y}, \end{aligned}\right\} \quad (5)$$

where Φ is the Airy stress function.

Substituting into (3)

$$\left(\frac{\partial^2}{\partial x^2} + \frac{\partial^2}{\partial y^2}\right)\left(\frac{\partial^2\Phi}{\partial x^2} + \frac{\partial^2\Phi}{\partial y^2} + 2Z\right) - (1+\nu)\left(\frac{\partial^2 Z}{\partial x^2} + \frac{\partial^2 Z}{\partial y^2}\right) = 0$$

or

$$\left(\frac{\partial^2}{\partial x^2} + \frac{\partial^2}{\partial y^2}\right)\left(\frac{\partial^2\Phi}{\partial x^2} + \frac{\partial^2\Phi}{\partial y^2}\right) + (1-\nu)\left(\frac{\partial^2 Z}{\partial x^2} + \frac{\partial^2 Z}{\partial y^2}\right) = 0 \quad (6)$$

In the end block problem, as in most engineering problems, the only body force present is the gravity force. If w represents the unit weight of the material, then

$$F_x = 0, \quad F_y = -w$$

and $Z = wy$.

Substituting into (6), and expanding,

$$\frac{\partial^4\Phi}{\partial x^4} + 2\frac{\partial^4\Phi}{\partial x^2 \partial y^2} + \frac{\partial^4\Phi}{\partial y^4} = 0. \quad (7)$$

Needless to say, Φ must also satisfy certain given conditions along the boundary.

Loading Conditions

Only the "full load" condition was used in the analytical solution. As previously stated in Chapter II, emphasis was placed upon this one loading condition, although five different conditions were used in the experiment. Also, the analytical solution was used only for a comparison with the experimental results, and as a guide for the estimation of transverse stress distributions. The large amount of time and labor necessary for the solution of all these loading conditions were therefore considered unjustified, and only condition V was considered.

Under this loading condition, the forces acting on the end block were as shown in Figure 3.1. Due to the complexity of the force system, it was resolved into the several systems as follows:

1. Force system A, as shown in Figure 3.2a. This was the primary system and will be discussed fully later.
2. Force system B, as shown in Figure 3.2b. This transposes the uniform load of 23.48 lbs. per in. on top edge of system A into the gravity forces. This system was solved by

   $$\Phi = -\frac{1}{6} wy^3$$

   and $\sigma_x = 0$, $\sigma_y = + wy$, $\tau_{xy} = 0$.

   For the concrete used, w = 153.8 pounds per cubic foot or 0.089 pounds per cubic inch.
3. Force system C, as shown in Figure 3.2c. This considers the vertical pressures from the draped cables as a uniform

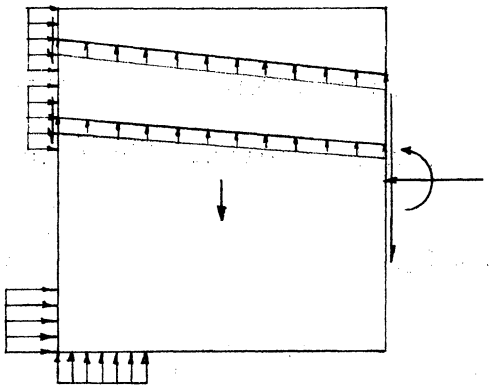

Figure 3.1. Forces on End Block.

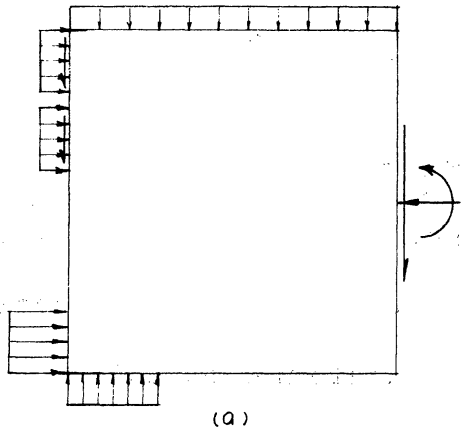

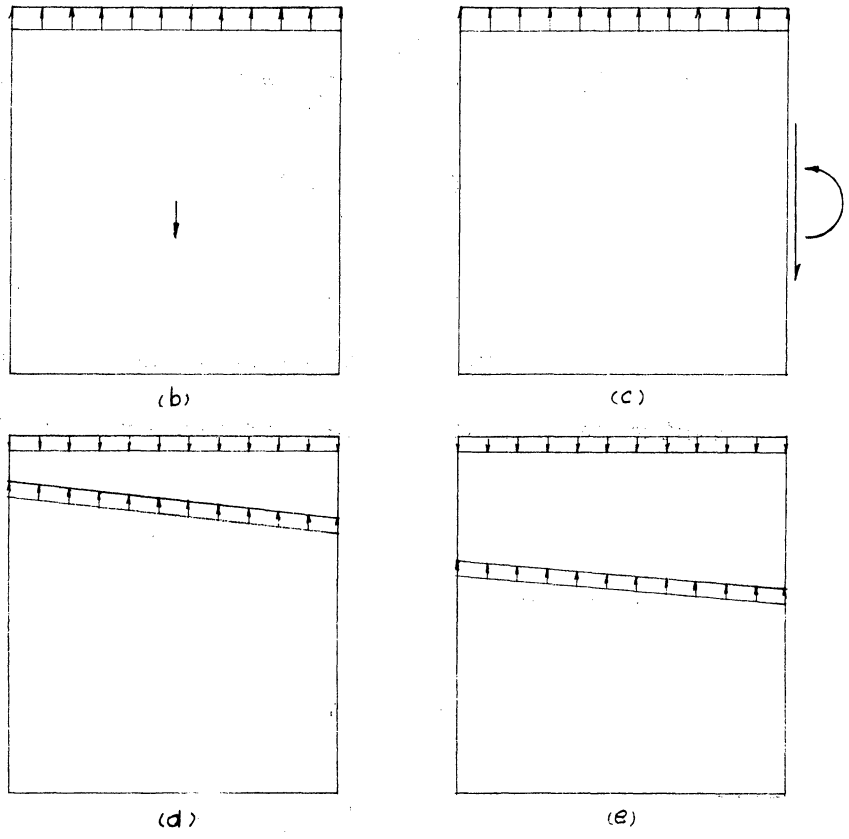

Figure 3.2. Component Force Systems.

load on top of beam, and supported by shear and moment at the juncture plane. The solution of this system is

$$\Phi = - K[x^2(y^3 - \tfrac{3}{2} dy^2) - \tfrac{1}{10} y^2(2y^3 - 5dy^2 + 4d^2y - d^3)]*,$$

where $K = \dfrac{q_T + q_M}{bd^3}$.

Hence $\sigma_x = - K [3x^2(2y - d) - (4y^3 - 6y^2d + \tfrac{12}{5} yd^2 - \tfrac{1}{5} d^3)]$,

$$\sigma_y = - K(2y^3 - 3dy^2),$$

$$\tau_{xy} = - 6K xy(d - y).$$

Force system D, as shown in Figure 3.2d. This system transposes q_T to its actual position. The effect of this system is uniform compression between the top cable and the top, or

$$\sigma_x = 0, \quad \sigma_y = - \frac{q_T}{b}, \quad \tau_{xy} = 0 \qquad y_T \leq y \leq d$$

$$\sigma_x = 0, \quad \sigma_y = 0, \quad \tau_{xy} = 0 \qquad 0 \leq y \leq y_T$$

5. Force system E, as shown in Figure 3.2e. This system transposes q_M to its actual position. The effect of this system is uniform compression between the middle cable and the top, or

$$\sigma_x = 0, \quad \sigma_y = - \frac{q_M}{b}, \quad \tau_{xy} = 0 \qquad y_M \leq y \leq d$$

$$\sigma_x = 0, \quad \sigma_y = 0, \quad \tau_{xy} = 0 \qquad 0 \leq y \leq y_M$$

*R. V. Southwell, Theory of Elasticity, p. 379.

As the forces w, q_T and q_M were all very small compared with the prestressing forces and the concentrated load at center, it was obvious that the stresses due to force systems B through E were small as compared with those from force system A. And, for the degree of accuracy usually desired for engineering problems, these systems may be neglected. Unless otherwise indicated, the discussion hereafter will be limited to the primary force system A.

Boundary Conditions

Along the top, bottom and left (end) boundaries, the conditions of stresses were relatively easy to establish. The forces from the cables and the reaction to the beam were all assumed to be uniformly distributed over the corresponding bearing areas. On the juncture section, the total thrust, shear and bending moment could be determined from the static equilibrium of the entire block, but their distribution was unknown. Various authorities, such as Magnel and Guyon, have been using over the beam section a linear distribution of direct stresses and a parabolic distribution of shearing stress, as by conventional formulae. In view of the unusual depth to span ratio of the model beam, and the closeness of the section in question to the concentrations of external forces, these assumptions were examined before adoption. A similar, but simpler, beam, as shown in Figure 3.3, was first analyzed by the methods of plane stress; the stresses over a section "d" distance away from the end were computed, and compared with the results obtained with conventional beam formulae. This simple

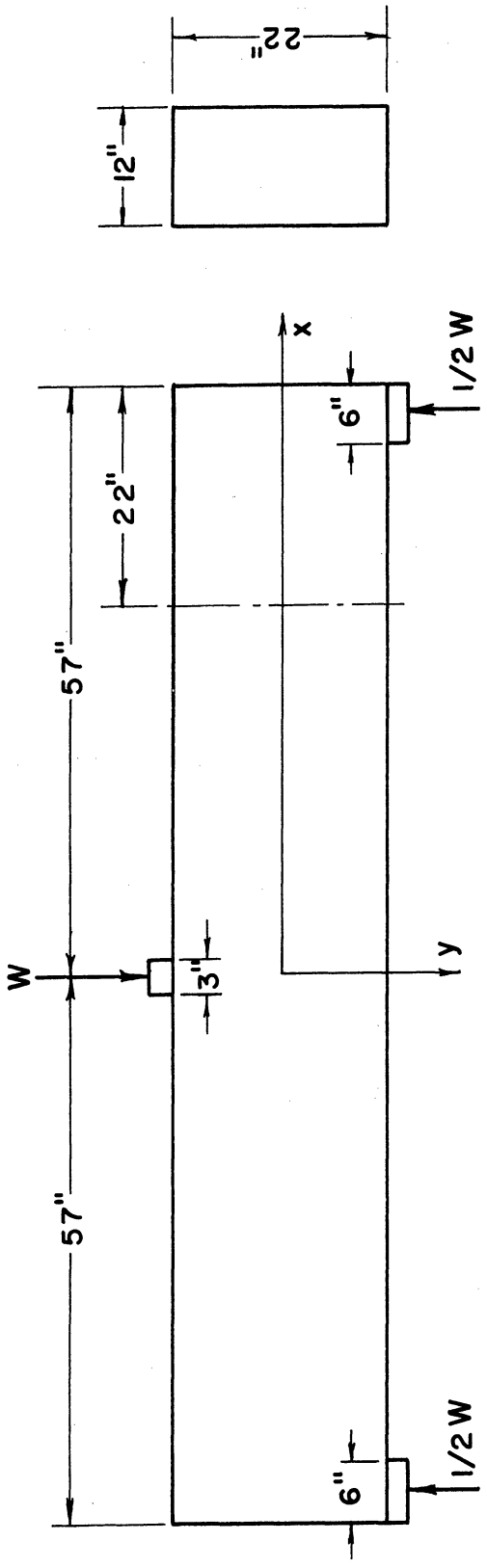

Figure 3.3. Simplified Beam.

beam had the same overall dimensions and the same vertical loadings as the model beam; but the longitudinal loadings from prestressing were omitted, and the beam section was kept uniform. With the coordinate axes as shown, the stress in this beam was solved by Filon[12] to be

$$\sigma_x = \frac{3W\ell}{2c^3\pi^2}\, y \sum_{m=1}^{\infty} \frac{1}{m^2}\left\{\frac{\mathrm{Sin}\alpha b}{\alpha b} - (-1)^m \frac{\mathrm{Sin}\alpha a}{\alpha a}\right\}$$

$$- \frac{W}{\ell}\sum_{m=1}^{\infty} \frac{(\mathrm{Sinh}\alpha c - \alpha c\ \mathrm{Cosh}\alpha c)\mathrm{Cosh}\alpha y + \alpha y\ \mathrm{Sinh}\alpha c\ \mathrm{Sinh}\alpha y}{\mathrm{Sinh}\ 2\alpha c + 2\alpha c}\left\{\frac{\mathrm{Sin}\alpha a}{\alpha a} + (-1)^m \frac{\mathrm{Sin}\alpha b}{\alpha b}\right\}\mathrm{Cos}\alpha x$$

$$+ \frac{W}{\ell}\sum_{m=1}^{\infty} \frac{(\mathrm{Cosh}\alpha c - \alpha c\ \mathrm{Sinh}\alpha c)\mathrm{Sinh}\alpha y + \alpha y\ \mathrm{Cosh}\alpha c\ \mathrm{Cosh}\alpha y}{\mathrm{Sinh}\ 2\alpha c - 2\alpha c}\left\{\frac{\mathrm{Sin}\alpha a}{\alpha a} - (-1)^m \frac{\mathrm{Sin}\alpha b}{\alpha b}\right\}\mathrm{Cos}\alpha x,$$

$$\sigma_y = -\frac{W}{2\ell} - \frac{W}{\ell}\sum_{m=1}^{\infty} \frac{(\mathrm{Sinh}\alpha c + \alpha c\ \mathrm{Cosh}\alpha c)\mathrm{Cosh}\alpha y - \alpha y\ \mathrm{Sinh}\alpha c\ \mathrm{Sinh}\alpha y}{\mathrm{Sinh}\ 2\alpha c + 2\alpha c}\left\{\frac{\mathrm{Sin}\alpha a}{\alpha a} + (-1)^m \frac{\mathrm{Sin}\alpha b}{\alpha b}\right\}\mathrm{Cos}\alpha x$$

$$+ \frac{W}{\ell}\sum_{m=1}^{\infty} \frac{(\mathrm{Cosh}\alpha c + \alpha c\ \mathrm{Sinh}\alpha c)\mathrm{Sinh}\alpha y - \alpha y\ \mathrm{Cosh}\alpha c\ \mathrm{Cosh}\alpha y}{\mathrm{Sinh}\ 2\alpha c - 2\alpha c}\left\{\frac{\mathrm{Sin}\alpha a}{\alpha a} - (-1)^m \frac{\mathrm{Sin}\alpha b}{\alpha b}\right\}\mathrm{Cos}\alpha x,$$

$$\tau_{xy} = -\frac{W}{\ell}\sum_{m=1}^{\infty} \frac{-\alpha c\mathrm{Cosh}\alpha c\ \mathrm{Sinh}\alpha y + \alpha y\ \mathrm{Sinh}\alpha c\ \mathrm{Cosh}\alpha y}{\mathrm{Sinh}\ 2\alpha c + 2\alpha c}\left\{\frac{\mathrm{Sin}\alpha a}{\alpha a} + (-1)^m \frac{\mathrm{Sin}\alpha b}{\alpha b}\right\}\mathrm{Sin}\alpha x$$

$$+ \frac{W}{\ell}\sum_{m=1}^{\infty} \frac{-\alpha c\ \mathrm{Sinh}\alpha c\ \mathrm{Cosh}\alpha y + \alpha y\ \mathrm{Cosh}\alpha c\ \mathrm{Sinh}\alpha y}{\mathrm{Sinh}\ 2\alpha c - 2\alpha c}\left\{\frac{\mathrm{Sin}\alpha a}{\alpha a} - (-1)^m \frac{\mathrm{Sin}\alpha b}{\alpha b}\right\}\mathrm{Sin}\alpha x,$$

where

$\alpha = \frac{m\pi}{\ell}$,

a = half length of the loading plate,

b = length of each bearing plate,

c = half depth of beam,

ℓ = half length of beam,

W = total concentrated load at center per unit width of beam.

In the above analysis, the central load and each of the reactions were assumed to be uniformly distributed over the lengths 2a, and b, respectively.

In the present problem, a = 1.5 inches, b = 6 inches, c = 11 inches, and ℓ = 57 inches. At the section "d" from the right end, x = 35". Stresses at several points at this section were computed by using a sufficient number of terms of the series given above. The results, together with those obtained by the conventional formulae, are shown in Table 3.1.

TABLE 3.1

STRESSES AT x = 35" OF SIMPLIFIED BEAM

Point	Normal Stress		Shear Stress	
	By Series	By Conventional Formula	By Series	By Conventional Formula
y = - c	- 0.11618 W	- 0.11775 W	0 W	0 W
$-\frac{1}{2}c$	- 0.05768	- 0.05888	- 0.02476	- 0.02557
0	- 0.00123	0	- 0.03419	- 0.03409
$\frac{1}{2}c$	+ 0.05734	+ 0.05888	- 0.02619	- 0.02557
c	+ 0.11955	+ 0.11775	0	0

It is thus seen that for the present problem, the conventional formulae for normal and shear stresses were accurate to within 3% of the values obtained by employing series. Hence, the common assumption of linear

variation of normal stress and parabolic variation of shear stress at the juncture were used. This assumption also neglected any effect the non-rectangular section of the beam body might have on the distribution of stresses. However, at the beginning of this chapter, assumption was made that all stresses were independent of z. This assumption, in effect, meant that the average stresses across the width, instead of those at individual points, were being considered. In view of this, the neglecting of the effect of the I-section seemed justifiable.

Based on the above assumptions, the boundary conditions for the short end blocks can be written as follows:

Along $y = 0$: $\sigma_y = -123.63$ psi., $\tau_{xy} = 0$ $\quad 0 \leq x \leq 6$

$\sigma_y = 0$, $\tau_{xy} = 0$ $\quad 6 \leq x \leq 22$

Along $x = 0$: $\sigma_x = -1{,}281.25$ psi., $\tau_{xy} = 0$ $\quad 0 \leq y \leq 4$

$\sigma_x = 0$, $\tau_{xy} = 0$ $\quad 4 \leq y \leq 13$

$\sigma_x = -638.27$ psi., $\tau_{xy} = +54.78$ psi. $\quad 13 \leq y \leq 17$

$\sigma_x = 0$, $\tau_{xy} = 0$ $\quad 17 \leq y \leq 18$

$\sigma_x = -637.05$ psi., $\tau_{xy} = +67.28$ psi. $\quad 18 \leq y \leq 22$

Along $y = 22$: $\sigma_y = -1.958$ psi., $\tau_{xy} = 0$ $\quad 0 \leq x \leq 22$

Along $x = 22$: $\sigma_x = (-111.123 + 1.9321y)t$

$\tau_{xy} = -0.031173\ B$ $\quad \Big\} 0 \leq y \leq 22$

where t = thickness of section (in z direction)

B = moment about centroidal axis of the portion of area of the beam section above the point under consideration $= \int_y^{\bar{y}t} ty\,dy$

For the long end block, the boundary conditions are

Along y = 0: $\sigma_y = -124.74$ psi., $\tau_{xy} = 0$ $\quad 0 \leq x \leq 6$

$\sigma_y = 0$, $\tau_{xy} = 0$ $\quad 6 \leq x \leq 33$

Along x = 0: Same as for short end block.

Along y = 22: $\sigma_y = -1.958$ psi., $\tau_{xy} = 0$ $\quad 0 \leq x \leq 33$

Along x = 33: $\sigma_x = (-107.116 + 1.5772y)t$ $\quad 0 \leq y \leq 22$

$\tau_{xy} = -0.028970\ B$

The boundary conditions for the two end blocks are shown in Figure 3.4 and Figure 3.5.

Method of Numerical Solution

In view of the complexity of the boundary conditions, the stress functions for these end blocks were solved, not by an algebraic method, but by a numerical method involving finite difference equations. Let h be the "grid" dimension; the fourth derivatives of Φ can be approximated by the following finite differences:

$$\frac{\partial^4 \Phi}{\partial x^4} = \frac{1}{h^4} (\Phi_{WW} - 4\Phi_W + 6\Phi_o - 4\Phi_E + \Phi_{EE})$$

$$\frac{\partial^4 \Phi}{\partial y^4} = \frac{1}{h^4} (\Phi_{SS} - 4\Phi_S + 6\Phi_o - 4\Phi_N + \Phi_{NN})$$

$$\frac{\partial^4 \Phi}{\partial x^2 \partial y^2} = \frac{1}{h^4} [(\Phi_{NE} + \Phi_{NW} + \Phi_{SE} + \Phi_{SW}) - 2 (\Phi_N + \Phi_S + \Phi_E + \Phi_W) + 4\Phi_o]$$

Substituting these expressions into Equation (7), one obtains

$$20\Phi_o - 8(\Phi_N + \Phi_S + \Phi_W + \Phi_E) + 2(\Phi_{NE} + \Phi_{NW} + \Phi_{SE} + \Phi_{SW}) + (\Phi_{NN} + \Phi_{SS} + \Phi_{WW} + \Phi_{EE}) = 0. \qquad (8)$$

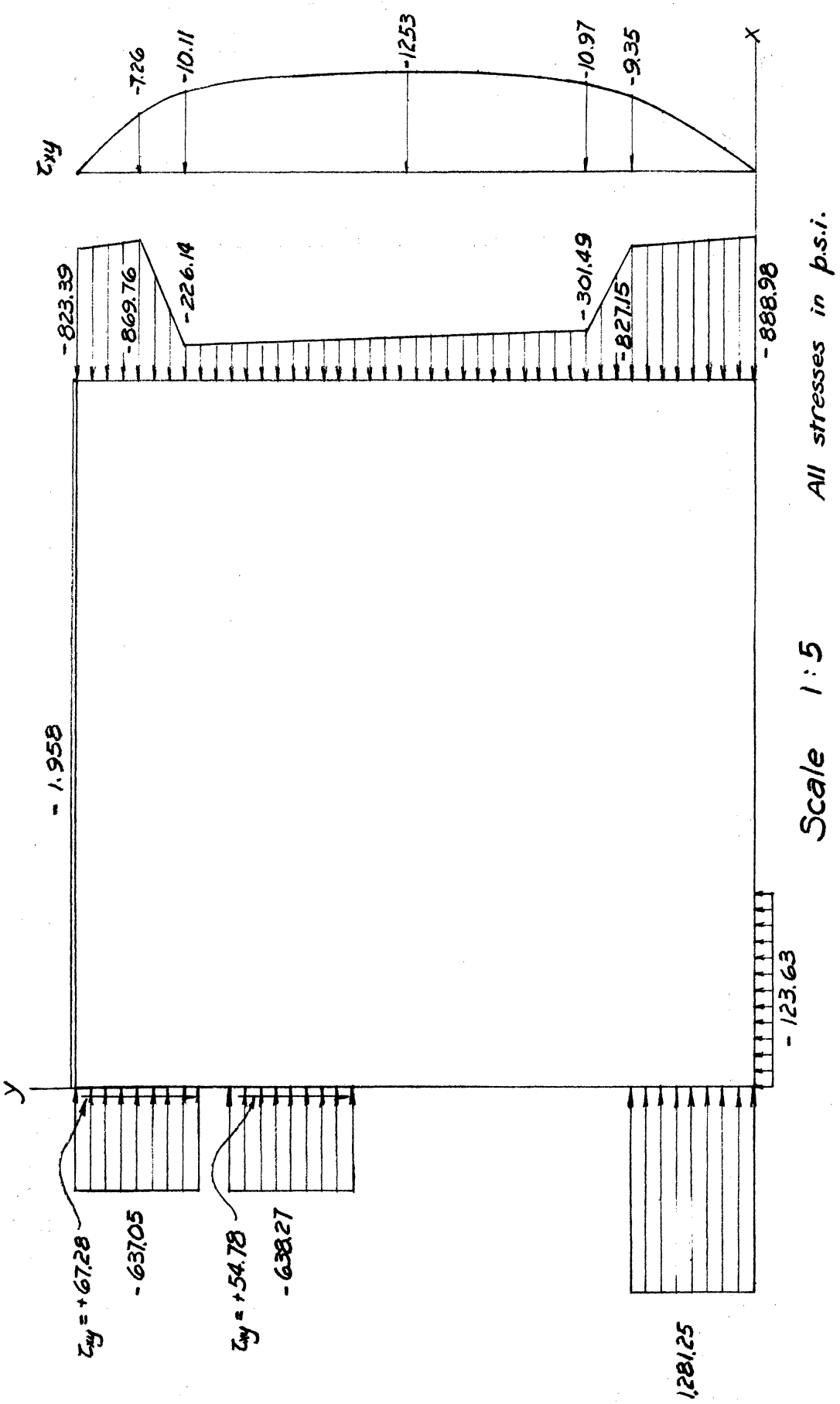

Figure 3.4. Boundary Conditions, Short End.

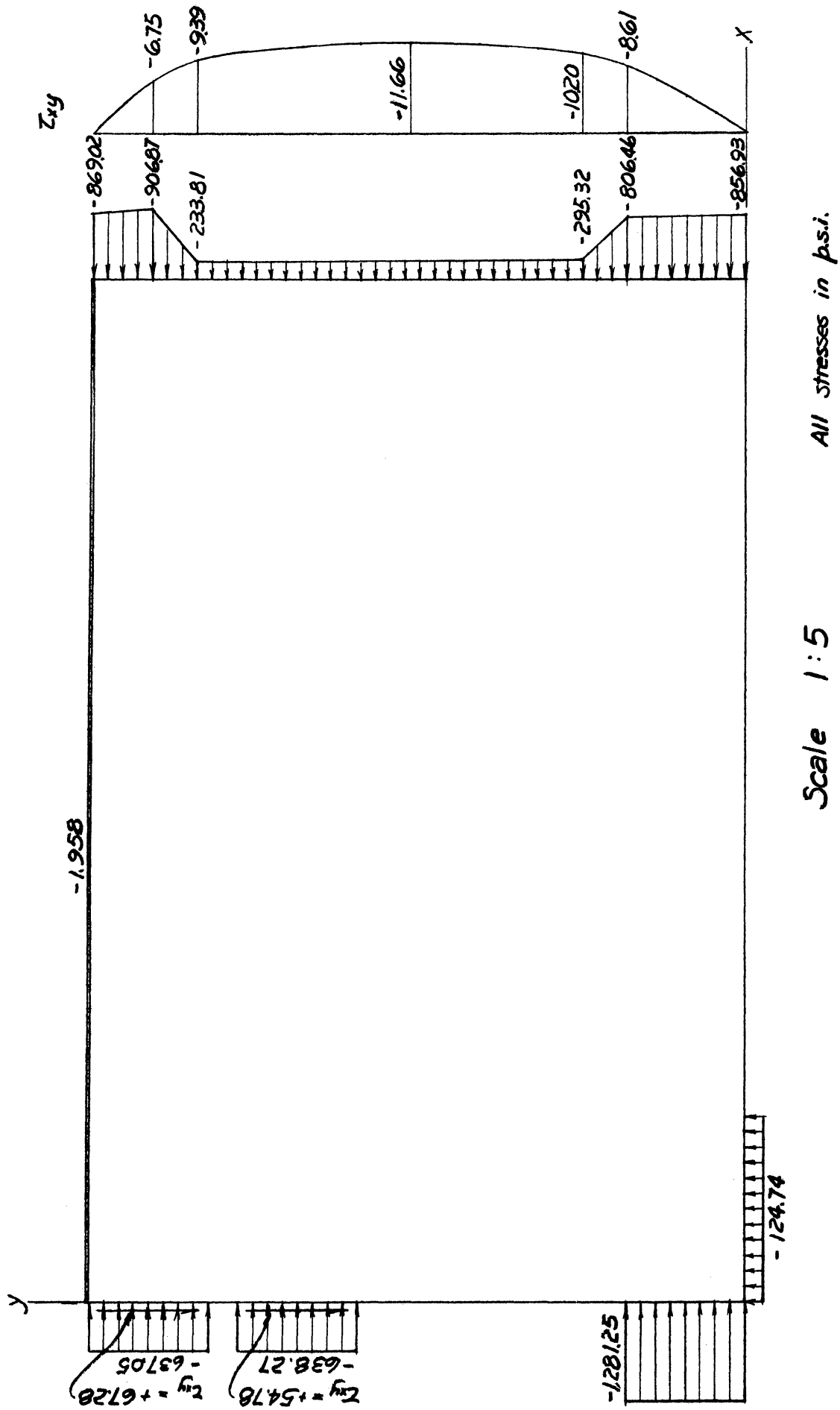

Figure 3.5. Boundary Conditions, Long End.

In the above expressions, the subscript o indicates the point at which the derivatives were being evaluated; N and S indicate the points adjacent to point o in the y-direction (as North and South); E and W indicate the points adjacant to point o in the x-direction; and the double subscripts indicate the points adjacent to the point with the first subscript in the direction as suggested by the second one, thus SW is the point W of S.

Equation (8), though linear, still contains as many as thirteen terms. To simplify the computations further, the "two level" method was used. This method was once suggested by Conwell,[10] and later amplified by Geer.[13] Equation (6) may be transformed into two partial differential equations of second order by introducing a new function

$$\psi = \frac{\partial^2 \Phi}{\partial x^2} + \frac{\partial^2 \Phi}{\partial y^2}, \tag{9}$$

then

$$\frac{\partial^2 \psi}{\partial x^2} + \frac{\partial^2 \psi}{\partial y^2} = 0. \tag{10}$$

The corresponding difference equations are

$$(\Phi_N + \Phi_S + \Phi_W + \Phi_E) - 4\Phi_o = \psi_o h^2, \tag{11}$$

and

$$(\psi_N + \psi_S + \psi_W + \psi_E) - 4\psi_o = 0.$$

Consequently

$$\psi_o = \frac{1}{4} (\psi_N + \psi_S + \psi_E + \psi_W), \tag{12}$$

$$\Phi_o = \frac{1}{4} (\Phi_N + \Phi_S + \Phi_E + \Phi_W - h^2 \psi_o).$$

Let

$$\phi = \frac{1}{h^2} \Phi, \tag{13}$$

then

$$\phi = \frac{1}{4} (\phi_N + \phi_S + \phi_E + \phi_W - \psi_o). \tag{14}$$

Note that in problems where no body forces are present, ψ has the physical meaning of the sum of the principal stresses.

The Equations (12) and (14), each containing no more than six terms, with most of the coefficients one, are very convenient to handle with any calculator. Using these equations, with the boundary values of ϕ known, the value of ϕ at any interior point may be computed to the desired degree of precision by using a fine enough grid, or a small enough h. In this study, the value of h adopted was one-eighth of the depth of the beam, or 2.75 inches. The computation was carried out on successively finer grids, mainly following the method of Dr. Geer. The procedure was as follows:

1. From the known values of boundary stresses, i.e., the second derivatives of Φ, the values of ϕ at all boundary grid points were computed by integration. The constants of integration were so chosen that all ϕ's would be positive. The values of ψ at the four corners were also computed from the known stresses.

2. In the process of computing boundary ϕ's, the values of their derivatives were obtained. The derivatives in the direction normal to the boundary were multiplied by h, and designated as ϕ':

$$\phi' = h \frac{\partial \phi}{\partial n} = \frac{1}{h} \frac{\partial \Phi}{\partial n}.$$

where n was the outward normal. In the subsequent computation, whenever ϕ at an external point E was needed, it was evaluated from that at an interior point I by

$$\phi_E = \phi_I + 2\ m\ \phi'_B, \tag{15}$$

where E, B and I were adjacent points along a grid line normal to the boundary, B being the boundary point; and m was the ratio of the grid size to h.

3. Starting with a very coarse net with grid size 4h, ϕ at a few interior points were computed directly by applying Equation (8) at each of these points and solving simultaneously. Note that Equation (8) could be written in terms of ϕ without any change; and that at this stage, m in Equation (15) was 4. For the short end block, only one interior point was involved at this stage. For the long end block, there were two.

4. ψ's at all grid points were then computed by (14), or, rewritten,

$$\psi_o = \phi_N + \phi_S + \phi_E + \phi_W - 4\phi_o \tag{14a}$$

For points on the boundary, this was further simplified. As the values of ϕ at the boundary points were known, and that at an external point was related to that at the corresponding interior point, Equation (14a) was reduced

to the form

$$\psi_B = \text{Constant} + 2\phi_I \qquad (16)$$

This completed the solution on the coarse net.

5. The values of ϕ were then transposed to the intermediate net with size 2h. The ψ's were first divided by 4 $(= \frac{4^2}{2^2})$. and then transposed. ψ at the four corners at this stage were those obtained in Step 1 multiplied by $4(= \frac{2^2}{1^2})$. At this stage, ϕ was known at all boundary points (and exactly); ψ at alternate boundary points; and in the interior, both were known at those points which were also grid points in the coarser net.

6. The ψ's at the other interior points were computed by Equation (12). This equation was first applied diagonally, as

$$\psi_o = \frac{1}{4} (\psi_{NE} + \psi_{NW} + \psi_{SE} + \psi_{SW}) \qquad (12a)$$

for several points, and later normally for the rest.

7. The values of ϕ at these interior points were computed by using Equation (14), first diagonally and then normally. Note that when applied diagonally, this equation should be modified as:

$$\phi_o = \frac{1}{4} (\phi_{NE} + \phi_{NW} + \phi_{SE} + \phi_{SW} - 2\psi_o) \qquad (14b)$$

8. The boundary values of ψ (except those at the corners) were recomputed by Equation (16).

9. All values of ψ and the interior values of ϕ were then improved by an iterative process:

   a. Interior ψ's were computed by Equation (12).

   b. Interior ϕ's were computed by Equation (14).

   c. Boundary ψ's were computed by Equation (16).

10. The iteration process was continued until the result was judged satisfactory. Then the work was transposed to the fine net with grid size h, and the steps from 4 to 9 were repeated.

It was noted that almost all ψ's (except a few boundary values) were negative, which further simplified the arithmetic in applying Equation (14), as subtraction was actually not needed.

For the coarse net, the solution was exact. For the intermediate net, the iteration was carried only a few cycles, as the results from this were to be used only as initial values in the fine net, and great accuracy was not needed. For the fine net, the work was carried on until correct answers were reasonably assured.

The convergence of the values of ϕ by the iteration process was very slow, partly due to the size of the system, and partly due to the presence of the coefficient 2 in Equation (16). At a number of points, the ϕ values actually showed a tendency to oscillate within a considerably large range, and a half-period of about 10 cycles.

Fortunately, the values of ψ, being numerically much smaller than ϕ, converged much faster. Noting that the aim of these computations was to find the stresses, or the second derivatives of ϕ, but not the ϕ's themselves, it was decided that iteration process should not be carried too far beyond the convergence of ψ.

For the short end block, iteration was stopped after eighteen cycles. The biharmonic residuals were then computed at each interior point, using the following formula.

$$R_o = 20\phi_o - 8(\phi_N + \phi_S + \phi_E + \phi_W) + 2(\phi_{NE} + \phi_{NW} + \phi_{SE} + \phi_{SW}) + (\phi_{NN} + \phi_{SS} + \phi_{EE} + \phi_{WW}) \qquad (17)$$

The largest residual was found to be only 1.08. Relaxation method was then used to make local corrections, and the residuals were reduced to within $\pm$ 0.25, which was considered small enough. The final values of ϕ, together with the boundary values of ϕ', are shown in Figure 3.6.

The work on the long end block was carried a little further. Biharmonic residuals were computed after 30 cycles of iteration, and the largest residual was only 0.59. The residuals were reduced to within $\pm$ 0.08 by relaxation. The final values of ϕ and the boundary values of ϕ' are shown in Figure 3.7.

Computation of Stresses

From Equations (5), with no body forces acting, the difference equations for stresses are:

$$\sigma_x|_o = \frac{1}{h^2}(\Phi_E - 2\Phi_o + \Phi_W),$$

$$\sigma_y|_o = \frac{1}{h^2}(\Phi_N - 2\Phi_o + \Phi_S),$$

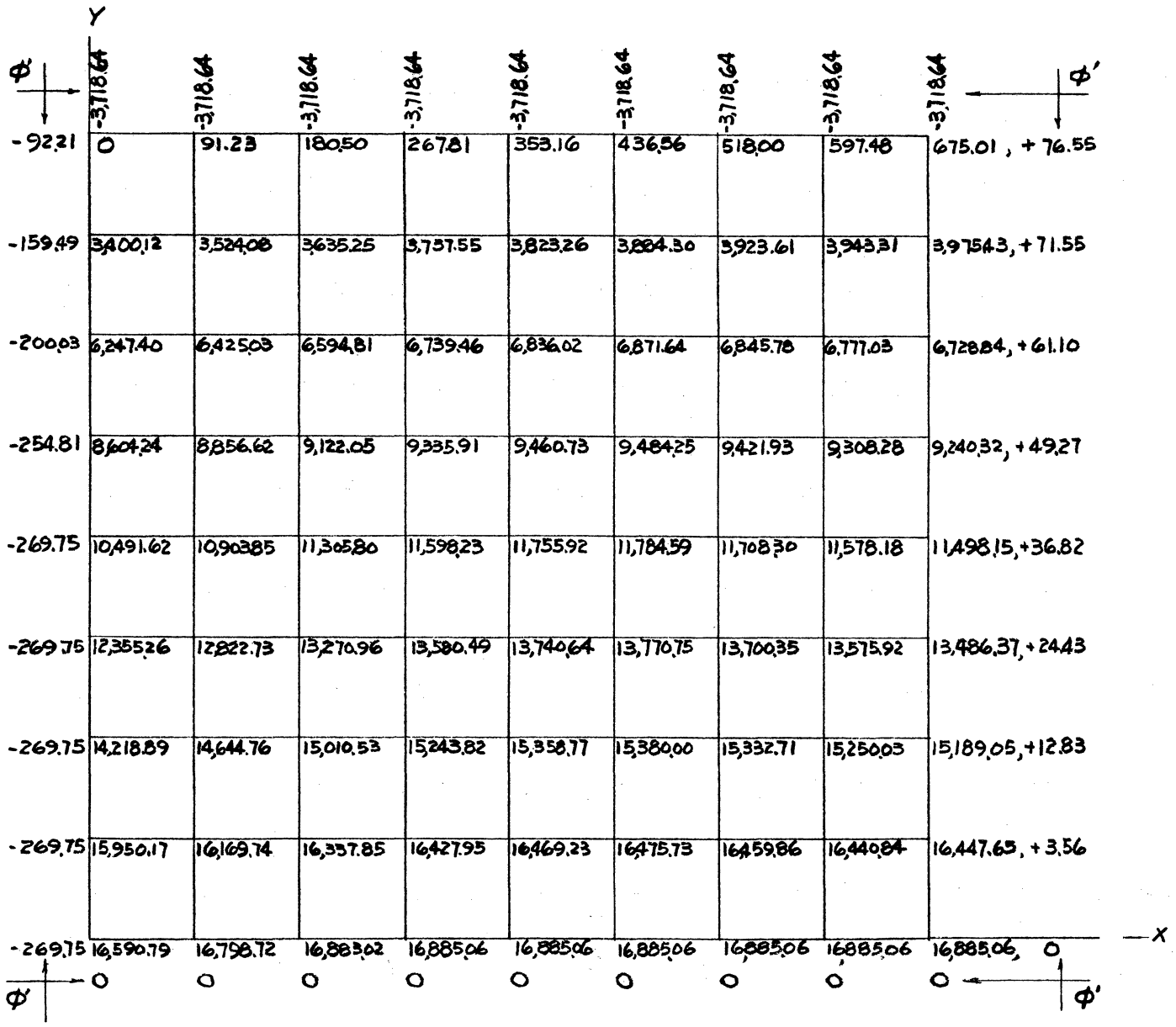

Figure 3.6. Final ϕ and ϕ', Short End.

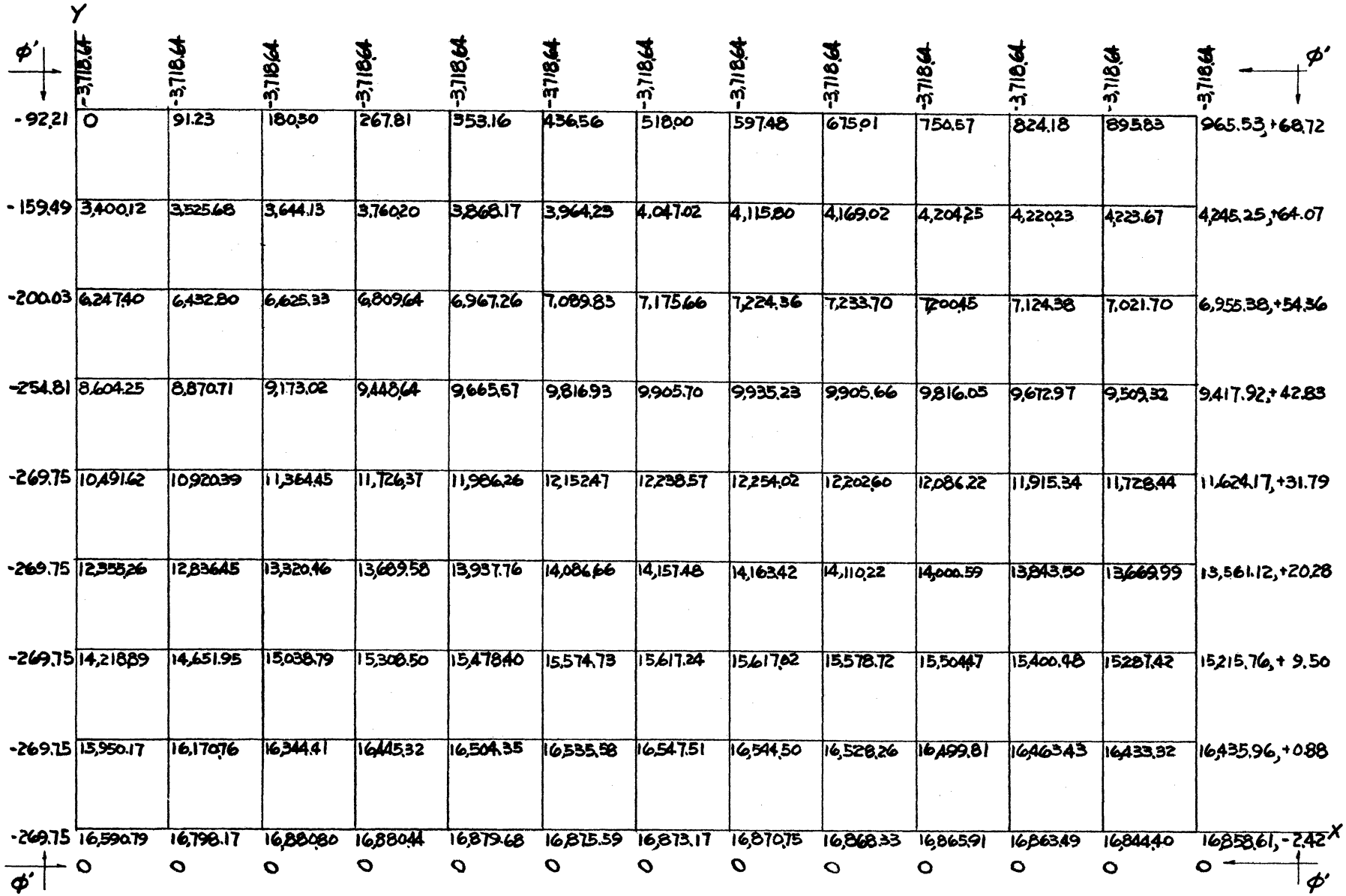

Figure 3.7. Final ϕ and ϕ', Long End.

and

$$\tau_{xy}|_o = \frac{1}{4h^2}(\Phi_{NW} - \Phi_{NE} - \Phi_{SW} + \Phi_{SE}).$$

In terms of ϕ, these may be rewritten:

$$\left.\begin{aligned} \sigma_x|_o &= \phi_E - 2\phi_o + \phi_W \\ \sigma_y|_o &= \phi_N - 2\phi_o + \phi_S \\ \tau_{xy}|_o &= \tfrac{1}{4}(\phi_{NW} - \phi_{NE} - \phi_{SW} + \phi_{SE}) \end{aligned}\right\} \quad (18)$$

These formulae were used to compute all the stresses except τ_{xy} at the corners, where one of the four ϕ's could not be evaluated. These shear stresses were evaluated from the known boundary conditions to be all zero.

The values of the stresses thus obtained were recorded in Figures 3.8 and 3.9. Figures 3.10 and 3.11 show stress contours for σ_y.

It should be mentioned that the stresses thus obtained were actually weighted averages over a length of 2h for normal stresses and over an area of 2h x 2h for shear stresses. This explains why the computed boundary stresses did not agree exactly with the given boundary conditions.

Examination of the Minor Systems

The stresses at various points due to the several minor force systems(B through E) were then examined.

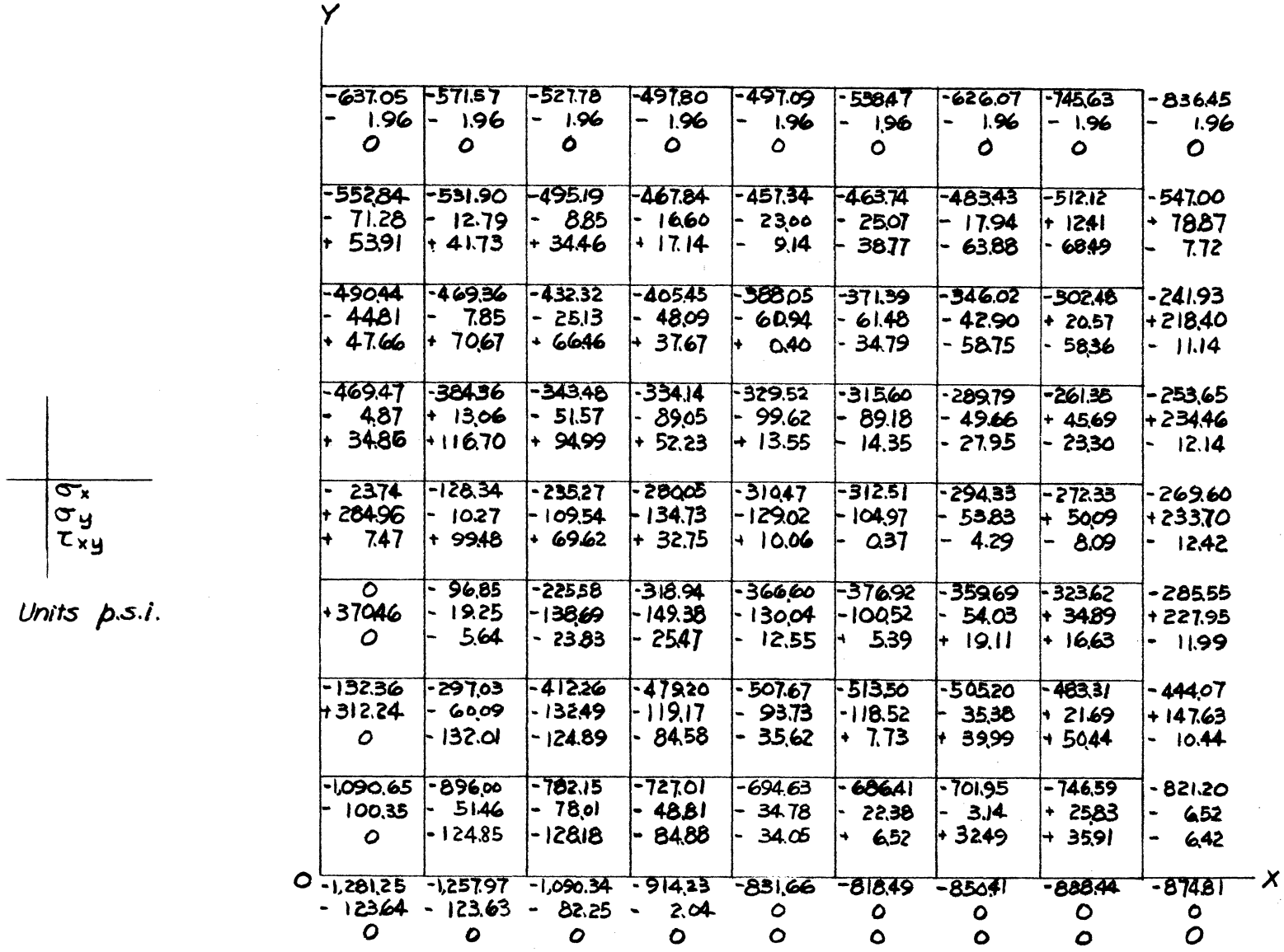

Figure 3.8. Stresses, Short End, Analytical.

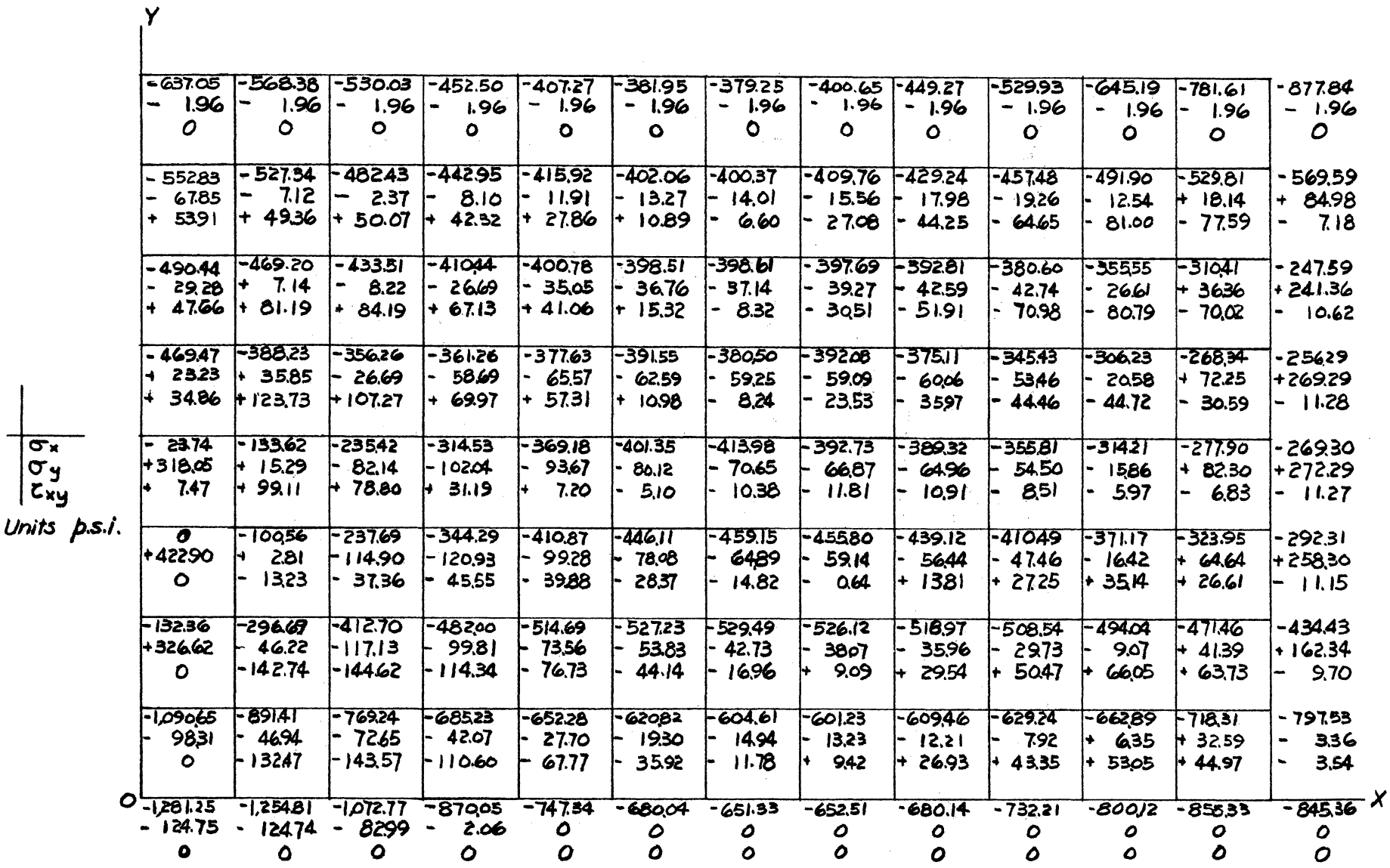

Figure 3.9. Stresses, Long End, Analytical.

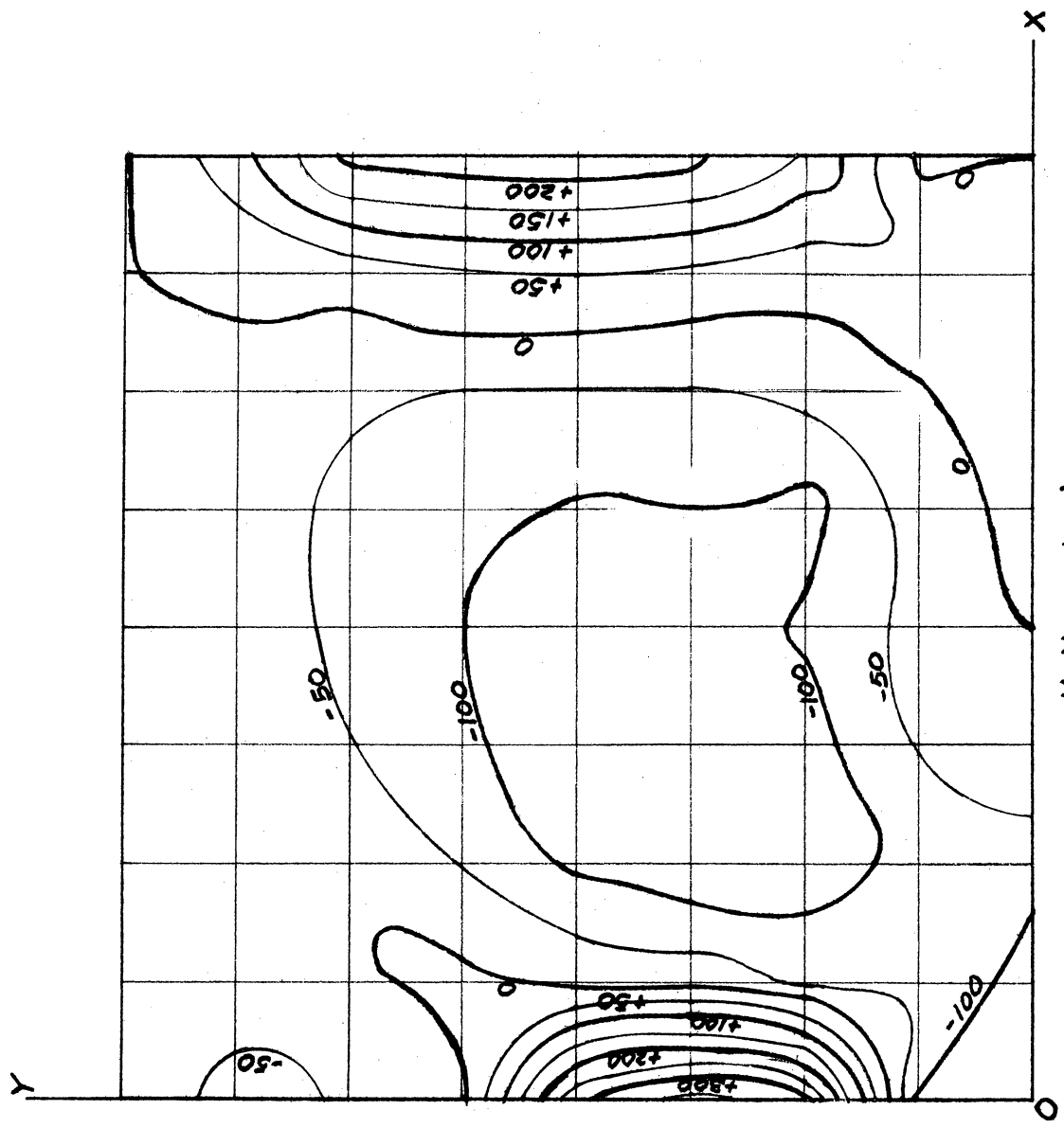

Figure 3.10. Stress Contours of σ_y, Short End.

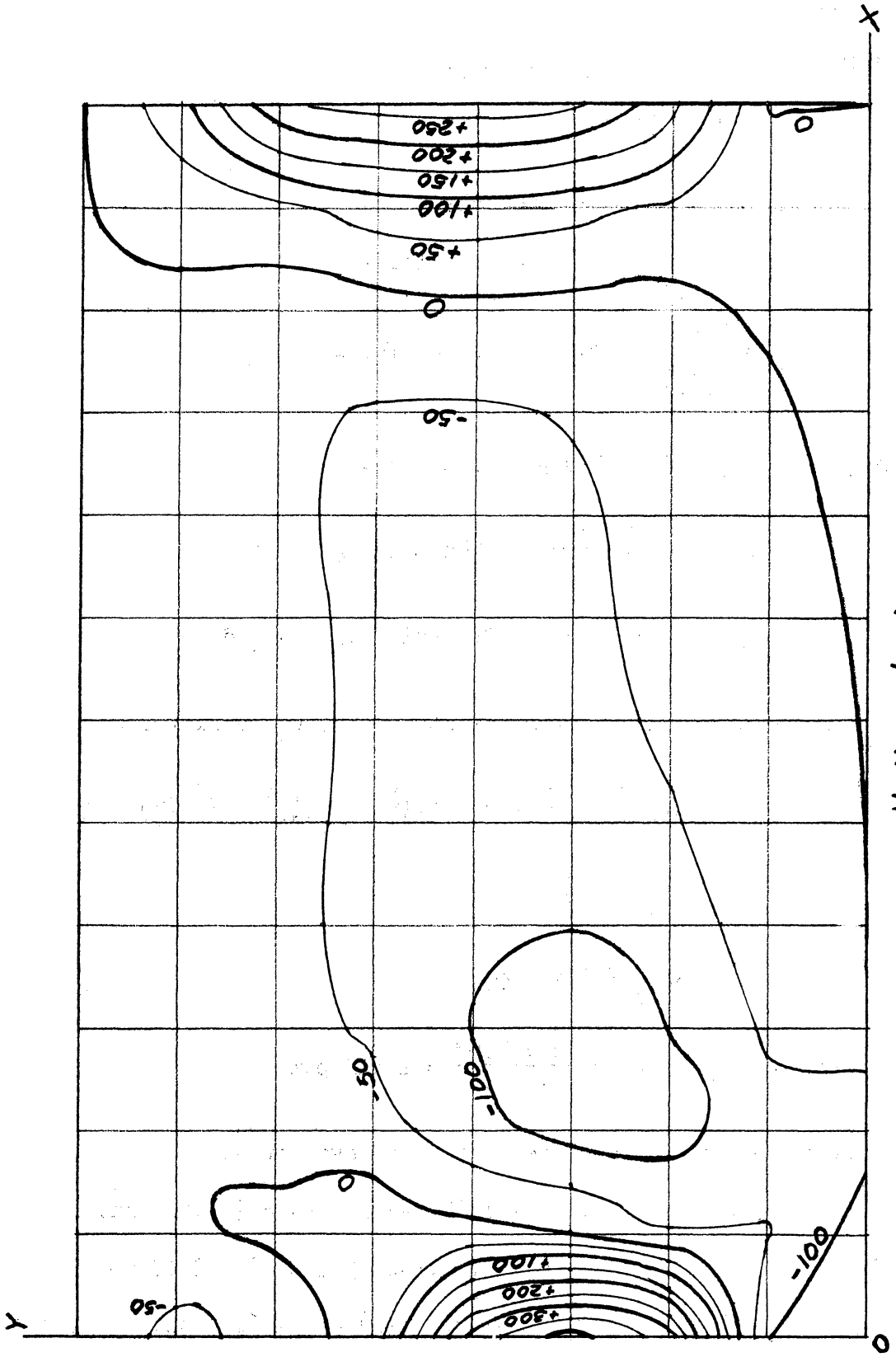

Figure 3.11. Stress Contours of σ_y, Long End.

The force systems B, D and E caused only normal stresses in the vertical direction, σ_y, as indicated above. For the loading condition under consideration

$$w = 153.8 \text{ pcf} = 0.089 \text{ psi}$$

$$q_M = \frac{26}{(303)^2} \times 30{,}750 = 8.68 \text{ lb./in.}$$

$$q_T = \frac{32}{(303)^2} \times 30{,}750 = 10.66 \text{ lb./in.}$$

Therefore, Max. $\sigma_{yB} = 22 \times 0.089 = 1.958$ psi,

$$\sigma_{yD} = -\frac{10.66}{12} = -0.888 \text{ psi} \quad y_T \leq y \leq d,$$

$$\sigma_{yE} = -\frac{8.68}{12} = -0.723 \text{ psi} \quad y_M \leq y \leq d.$$

The stresses due to force system C may be rewritten as follows:

$$\sigma_x = -k\left\{3\left(\frac{x}{d}\right)^2\left(2\,\frac{y}{d} - 1\right) - \left[4\left(\frac{y}{d}\right)^3 - 6\left(\frac{y}{d}\right)^2 + \frac{12}{5}\left(\frac{y}{d}\right) - \frac{1}{5}\right]\right\},$$

$$\sigma_y = -k\left(\frac{y}{d}\right)^2\left(2\,\frac{y}{d} - 3\right),$$

$$\tau_{xy} = -6k\left(\frac{x}{d}\right)\left(\frac{y}{d}\right)\left(1 - \frac{y}{d}\right),$$

where $k = Kd^3 = \dfrac{q_T + q_M}{b} = \dfrac{10.66 + 8.68}{12} = 1.612$ psi.

The extreme values of the stresses were then evaluated:

At $x = d$, $y = 0, d$. $\quad \sigma_x = -1.612(\mp 3 \pm 0.2) = \pm 4.51$ psi.

At $x = 1.5d$, $y = 0, d$. $\quad \sigma_x = -1.612(\mp 6.75 \pm 0.2) = \pm 10.56$ psi.

Along $y = d$, $\quad \sigma_y = -1.612\ (-1) = +1.612$ psi.

At $x = d$, $y = 0.5\ d$. $\tau_{xy} = -\ 6(1.612)(0.25) = -\ 2.418$ psi.

At $x = 1.5\ d$, $y = 0.5\ d$. $\tau_{xy} = -\ 6(1.612)(1.5)(0.25) = -\ 3.627$ psi.

All these stresses are very small as compared with those caused by the primary force system A. Therefore, for practical purposes, they may be neglected.

CHAPTER IV

SOLUTIONS BY EXISTING METHODS

Magnel's Method

The method of analyzing end blocks proposed by Magnel was based on the following assumptions:

1. The pressure under the anchorages of the cables disperses at 45° angles. Area outside of these angles is ineffective in resisting σ_x.
2. Over any vertical transverse section through the end block, σ_x varies linearly according to the conventional formula.
3. Over any horizontal section through the end block, σ_y varies according to a cubic parabola; and consequently, τ_{xy} varies according to a parabola of fourth degree.
4. Both σ_y and τ_{xy} are zero at the juncture section.
5. For the computation of σ_y and τ_{xy}, the effective width of the end block is the overall width minus the width of the openings for cables.

Magnel also neglected most vertical forces on the end block. (The reaction of the beam, and the vertical components of prestresses, etc.). The effect of the vertical shear at the juncture was later taken into consideration by superimposing a constant shear stress over the entire block.

The end blocks were treated as a deep beam supported horizontally. The stresses were computed from the bending moment and shear force on a horizontal section based on the above mentioned distributions.

According to Magnel, the distribution of stresses at the juncture would be the same regardless of the length of the end block. But the longer end block would be much stronger in resisting σ_y and τ_{xy} than the shorter one.

The stresses in the two end blocks of the model beam under loading condition V were computed by Magnel's method with results as shown in Figure 4.1 and Figure 4.2.

Modified Magnel's Method

In their book, Evans and Bennett[11] presented a modified version of Magnel's method. On any horizontal section through the end block, a vertical force was added to maintain static equilibrium, and the adjustment of shear stress by the vertical shear force at the juncture was not used. The assumptions on the distribution of stresses remained the same.

According to this method, the stresses in the end blocks under loading condition V were recorded as in Figure 4.3 and Figure 4.4.

Guyon's Method

Guyon's method of end block analysis was based on the following assumptions:

1. For the basic case of a single normal force acting at mid-depth of the beam, the length of the "lead-in" zone equals the depth; and the distribution of σ_x is uniform over the interior end of this lead-in zone.
2. The knowledge of the maximum value of σ_y in tension is sufficient for the purpose of design. This maximum σ_y occurs on the axis of the basic block, usually at a distance from the end of from $\frac{1}{4}$ to $\frac{1}{2}$ of the length of the lead-in zone.

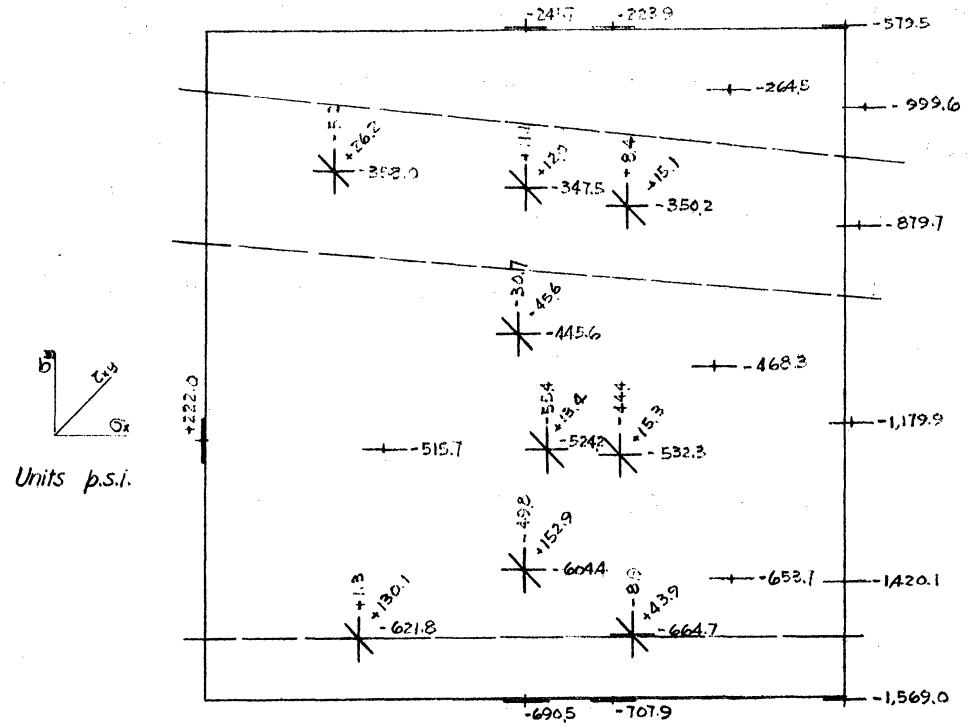

Figure 4.1. Stresses, Short End, Magnel.

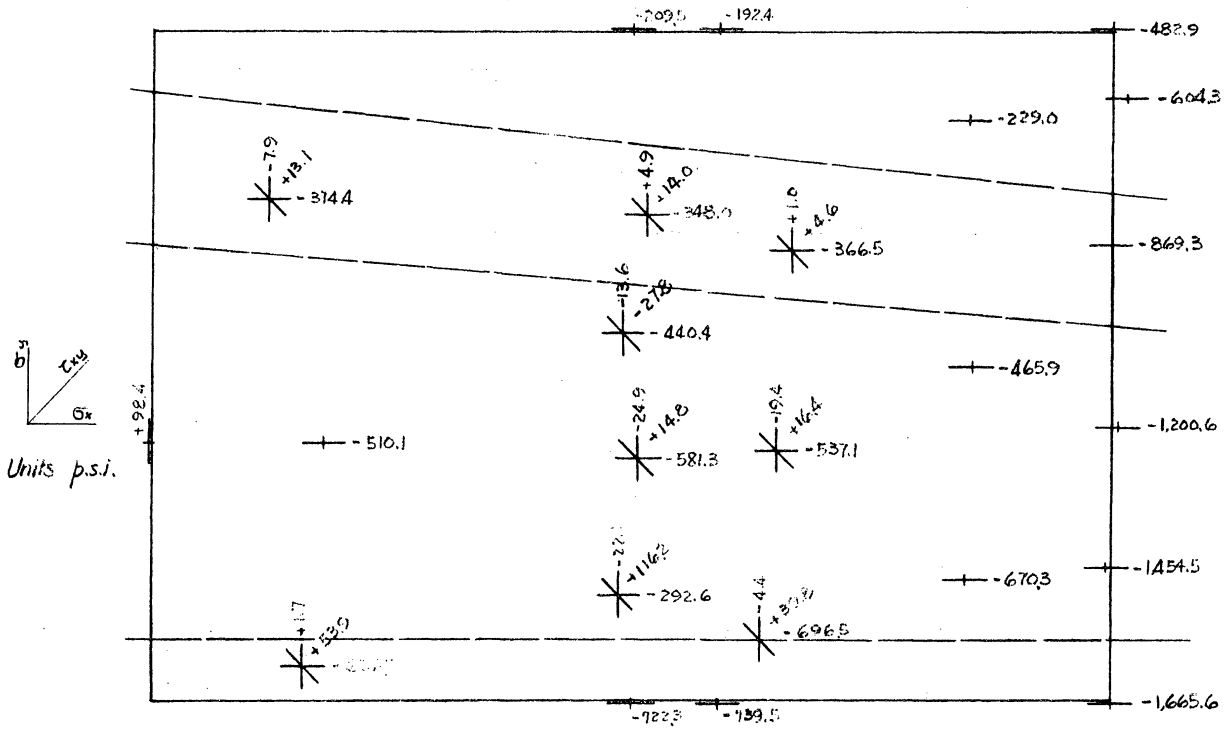

Figure 4.2. Stresses, Long End, Magnel.

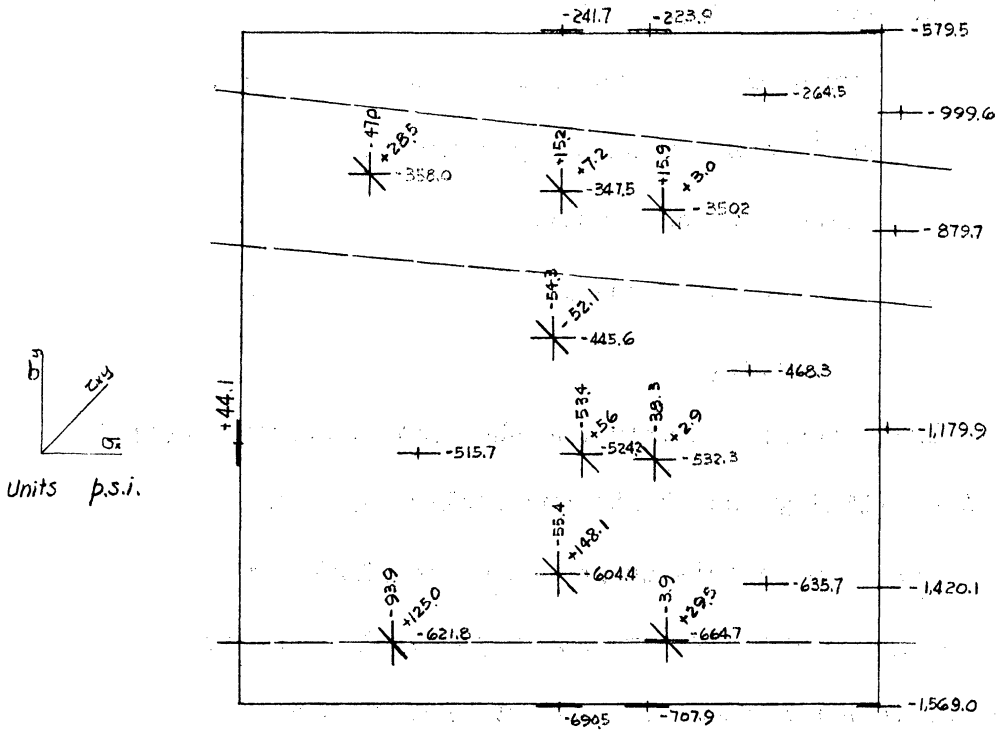

Figure 4.3. Stresses, Short End, Magnel Modified.

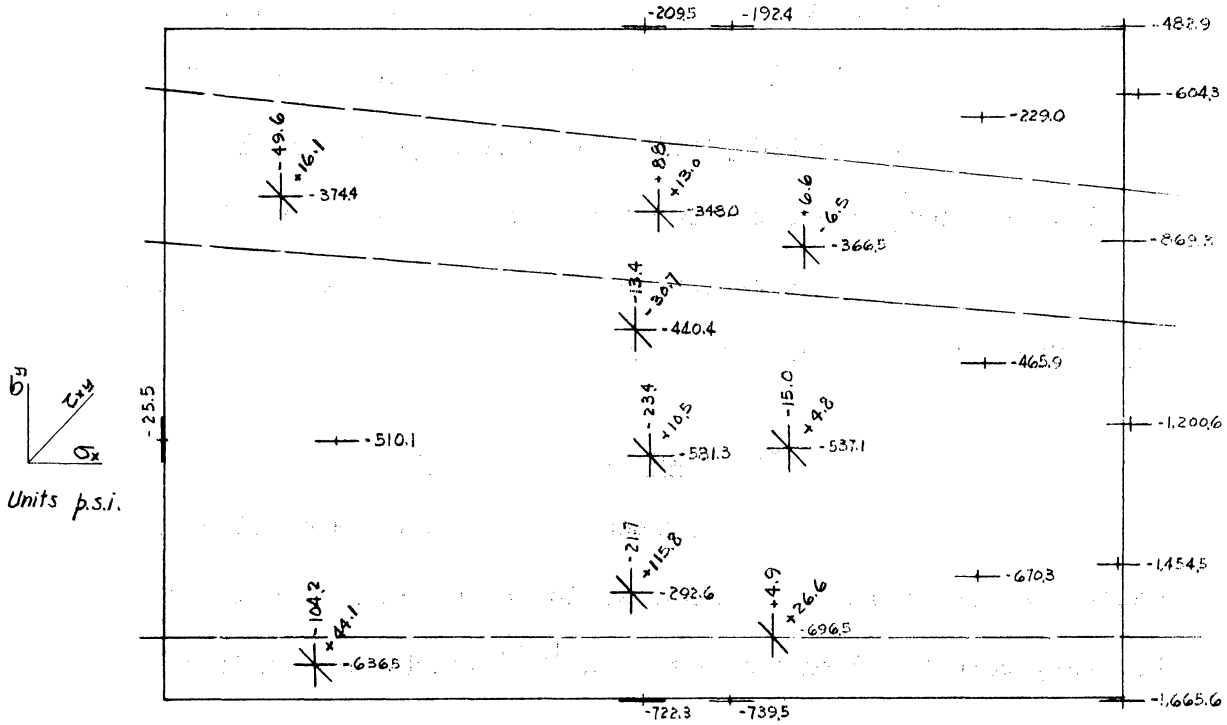

Figure 4.4. Stresses, Long End, Magnel Modified.

3. For the purpose of design, end blocks with any other arrangement of end forces may be reduced to a number of basic case problems by means of "partitioning", "symmetrical prism" or "successive resultant".

4. The effect of the inclination of prestresses may be neglected.

The stresses on axis for the basic case were computed by theory of elasticity and charts and tables were available.

Based on Guyon's method, the end blocks of the model beam under loading condition V were reanalyzed. The maximum tensions for the successive symmetrical prisms were found to be:

σ_y = + 765 psi At x = 0, y = 9.75"

σ_y = + 970 psi At x = 0, y = 17.50"

σ_y = + 670 psi At x = 0.83", y = 2"

Guyon suggested placing the end support of the beam outside the lead-in zone, hence the reaction was not considered in the computation. Also, the extra length of the long end block did not have any effect on the stress according to the method.

The Influence Line Method

Evans and Bennett proposed to use influence lines for the determination of maximum σ_y stress in end blocks. The influence lines, however, were based on Guyon's data,[15] which were derived from a two-dimensional solution of the problem. The solution was first made

by means of Fourier series, and then corrective terms were added to satisfy all of the boundary conditions. The influence lines given by Evans and Bennett were limited to the range of $0.10d \leq x \leq 0.75d$, and $\frac{1}{4}d \leq y \leq \frac{3}{4}d$. It must be noted that, in general, if the cables were located near the top and bottom edges of the beam, maximum vertical tension would not occur within this range. Applying these influence lines to the model beam under loading condition V, the results were as follows:

$y = \frac{3}{4}d$	No tension	
$y = \frac{5}{8}d$	$\sigma_y = +159.4$ psi	at $x = 0.10d$
$y = \frac{1}{2}d$	$\sigma_y = +99$ psi	"
$y = \frac{3}{8}d$	$\sigma_y = +200$ psi	"
$y = \frac{1}{4}d$	No tension	

Obviously, the maximum σ_y found here would be smaller than those found by Guyon's method, as the influence lines for the critical points for this problem were not available. If the influence lines were extended to include $x = 0$, the maximum tension was found to be approximately 600 psi at $y = \frac{3}{8}d$.

CHAPTER V

DISCUSSION

General Discussion of the Experiment

It should be mentioned at the very beginning of discussion that since only one model beam was tested during this investigation, the findings derived from this investigation may very possibly be special to this beam but not common to end blocks in general.

It is obvious that a large number of factors affect the stress distributions in end blocks. The most important ones probably are the length-depth ratio of the end block, the location of pre-stressing cables, the shape of the beam and the position of the end support. Of these four items, only one was actually considered in the present investigation, that is the length-depth ratio. The other three were all fixed, and the effects of them were therefore not detected. Further investigations with a much broader scope are necessary to evaluate all these effects and to furnish a thorough knowledge of the end block problem.

Interpretation of Experimental Results

It was unfortunate that several interior gages were lost during the test, and it was particularly so since a number of rosettes were involved. As a consequence, very little information on principal stresses was obtained and it was difficult to draw any conclusion from these scattered data.

It also should be mentioned that the method of computing experimental stresses at the single gage points involved some error. As stated in Chapter II, under "Computations of Strains and Stresses", these stresses were obtained by simply multiplying the corresponding strains by the modulus of elasticity of concrete. This would be correct only if the other two normal stresses both vanished, which was the exceptional, rather than normal case. As σ_y and σ_z were in most places tensile, the compressive stress σ_x thus obtained was generally larger than its true value.

Surface gages were exposed to the least amount of disturbance, after their mounting. Also, these gages were free from the "drifting" phenomenon, as mentioned in Chapter II, under "Testing of Model Beam". It was thus apparent that the information obtained from these gages was more reliable.

Examination of Figures 2.11 through 2.30 at the end of Chapter II reveals several interesting points.

First, only one region of substantial vertical tension was detected in each end block. This region was located near the exterior end and between the middle and bottom cables. Along the cables, and 3 to 6 inches from the end, where the "bursting zones" were supposed to be, the tensile stresses were rather small (in general less than 10% of the horizontal compression). The outside "spalling zones" did not exist as the cables were placed close to the top and bottom faces. The maximum tensile stress in the above mentioned region, as measured

by surface gage No. 1, differed only slightly in the two end blocks, indicating its virtual independence of the length-depth ratio. The magnitude of this stress was in the neighborhood of 80% of the average pressure over the end block, or 40% of the average pressure over the I-section area. According to Guyon, these ratios should be considerably higher.

Second, the surface gages No. 6 and No. 8 on both end blocks registered very low strains under all loading conditions. Comparison of stresses at the interior gage points at this location revealed that the stress was highest at the plane of symmetry, and gradually reduced toward the side surfaces. As this location was rather close to the juncture and was opposite the web of the beam, the manner of distribution was obviously due to the tendency of the pressure to "re-concentrate" toward the middle plane. This tendency of concentration was observed to be stronger in the short end block than in the long one.

Perhaps the most peculiar findings were the high surface stresses under surface gages No. 5 and No. 7 at both ends. In the long end block, the lateral distribution of σ_x stresses at this points was in the approximate shape of a parabola, with the minimum stress at the plane of symmetry. In the short end block, the distribution was in the shape of the letter W, with peaks at the plane of symmetry and the side surfaces, and the low points in between. These distributions were difficult to explain, particularly that in the short end. Usually,

a drop-off of stresses toward the side surfaces, or an approximately uniform distribution across the member would be expected. But here, the distribution was entirely different. The non-homogeneous and non-uniform character of concrete and the presence of cable duct openings in the end blocks may be partially responsible. However, further investigations are necessary before any positive statement may be made.

In Figure 5.1, the solid lines indicate the variation of horizontal fiber stresses at the juncture, along the line of symmetry. The dashed lines indicate the theoretical distribution by the conventional formula. There seems to be a static inequilibrium of the end block in the longitudinal direction, but that is of course impossible. The author believes that this apparent inequilibrium was actually due to the lateral distribution of the fiber stresses. It should be pointed out that the theoretical stresses were actually the average across the width of the member, and that the "experimental" stresses were measured on the plane of symmetry. It seems reasonable to assume a parabolic distribution of σ_x across the width of the member. Then the static equilibrium of the end blocks can be realized. If lines representing 60% of the theoretical average stresses are drawn, as shown by the long-and-short-dash lines in Figure 5.1, it is interesting to find that these lines agree remarkably well with the experimental results, with the exception of interior gage S8 which registered very high strains under all loading conditions. Accepting the figure of 60% at the mid-plane, a parabolic distribution of σ_x will result in a surface stress

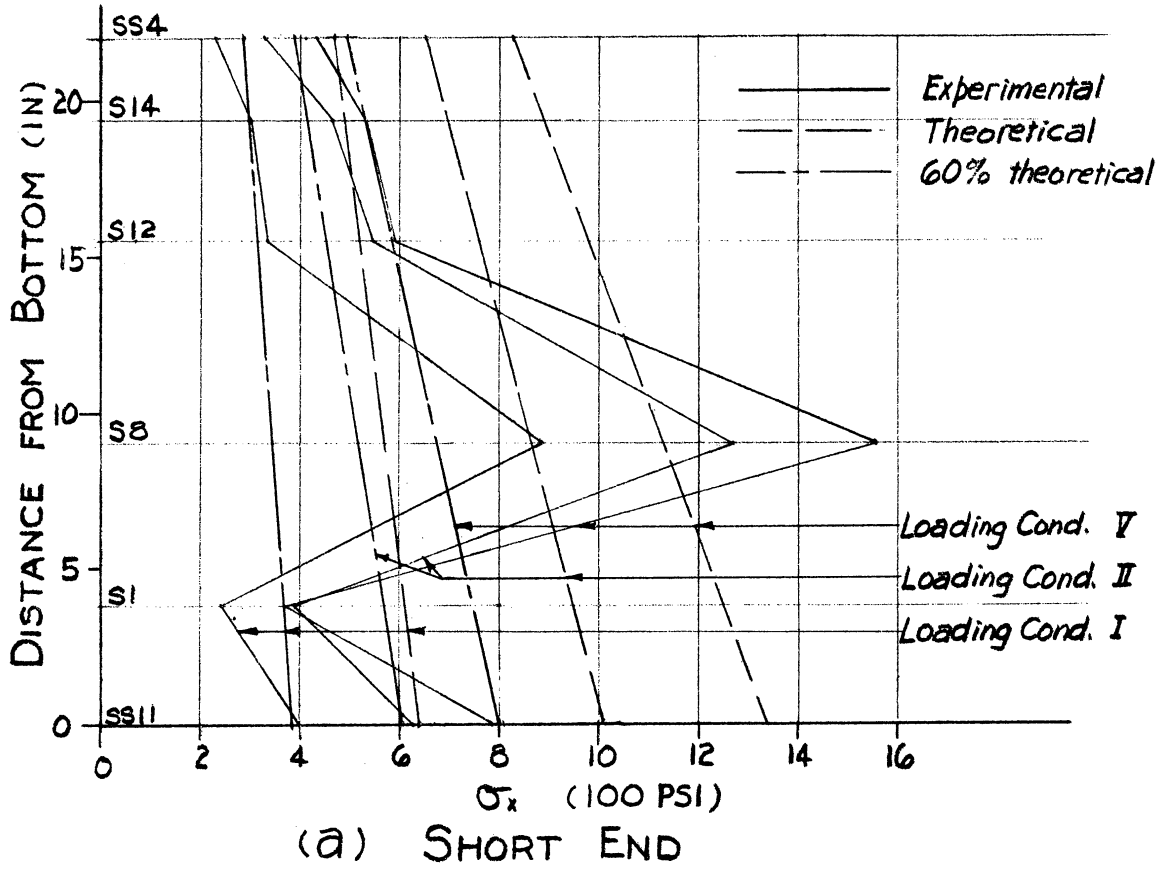

(a) SHORT END

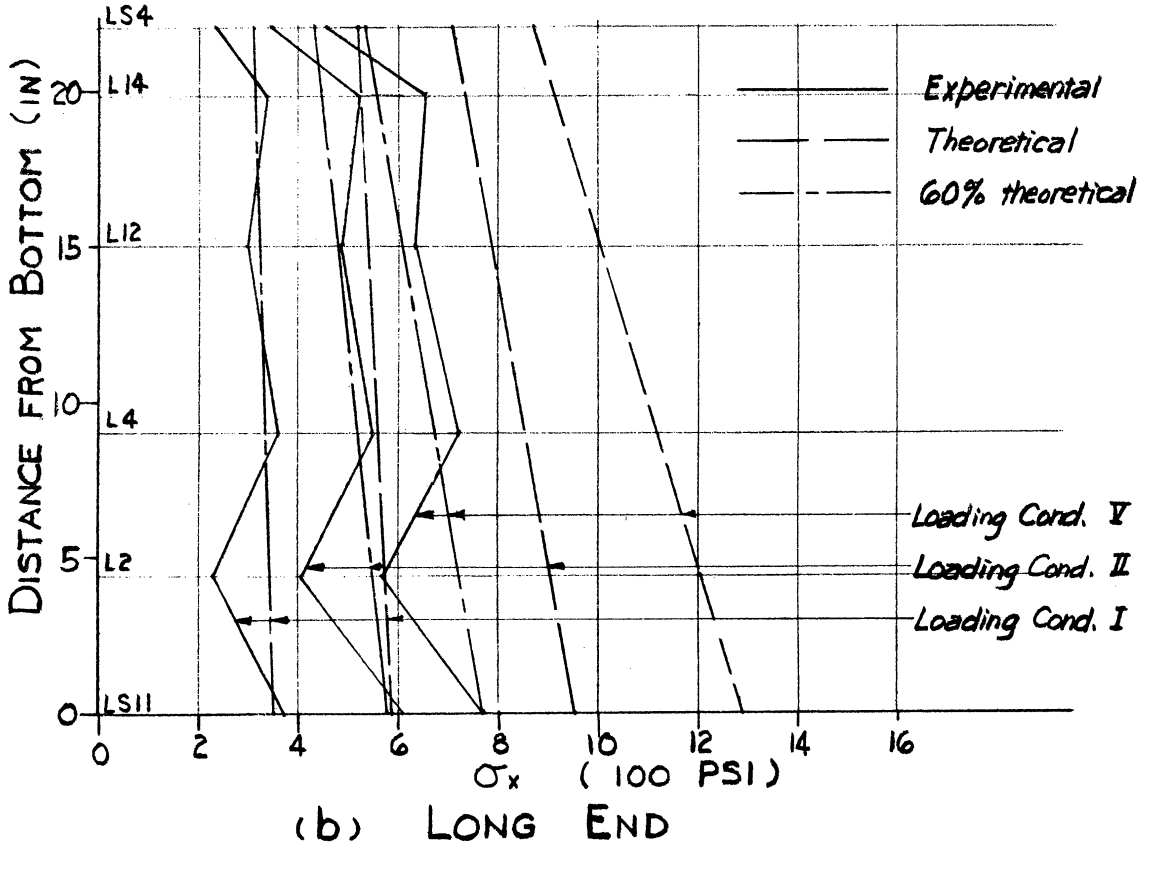

(b) LONG END

Figure 5.1. Fiber Stresses at Juncture.

of 180% of the average value as shown in Figure 5.2.

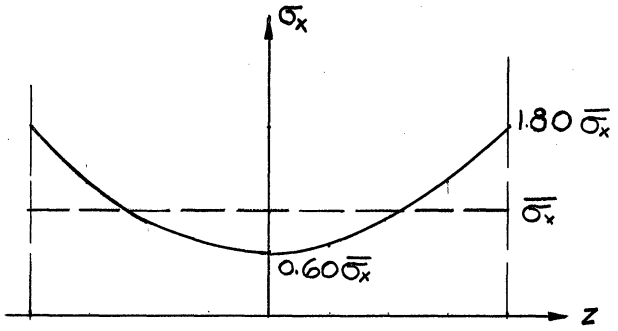

Figure 5.2. Lateral Distribution of σ_x

The stress concentration factor at the juncture was therefore apparently 1.80. However, as mentioned before, the effects of σ_y and σ_z were ignored in computing the stresses at the single gages. As σ_z was undoubtedly compressive at the juncture, and σ_y was comparatively small, the actual value of σ_x was larger than that appeared, and consequently the stress concentration factor based on parabolic distribution was in fact lower than 1.80 computed above.

This parabolic lateral distribution of σ_x also helps explain the apparent dropping off of top fiber stress at the juncture. Since the beam section was much smaller than that of the end block, and the bending moment due to vertical loads increased toward the middle of the span, it was expected that surface gage No. 4 would record higher stress than surface gage No. 3. However, the reverse actually happened. As both gages were on the plane of symmetry, the different ways of lateral distribution at these points give a partial explanation. (It is reasonable to assume uniform lateral distribution at gage No. 3 which

was away from the discontinuity at juncture.) Also, it should be remembered that the eccentricity of total prestress changed between these two sections under discussion, and the change of bending moment caused by this change of eccentricity more than compensated that due to vertical loadings.

In closing it should be mentioned that much better understanding of the state of stress would have been possible if more surface gages were used, particularly at the juncture, where the lateral distribution of stresses was non-uniform.

Interpretation of the Analytical Results

The size of the final network used in the numerical solution of the end block stresses in Chapter III was admittedly not very fine, hence the results obtained can only be a rough approximation. By using the finite difference Equations (18) for the evaluation of stresses, the values obtained were actually weighted averages over a length of 2h in the case of normal stresses, and over a 2h by 2h square in the case of shear stresses. Furthermore, the fact that the problem was solved in two dimensions implied that the results obtained were in fact averages across the width of the beam.

Examination of Figures 3.8 and 3.9 shows that there were two tension zones (where σ_y was tensile) in each end block. The one near the exterior end was the same as found in the experiment. The other one was located at the middle portion of the juncture, opposite the web of the beam. It is obvious that the tensile stress here actually did not spread over the entire width, but was concentrated

outside the web. In the web, the vertical stress was conceivably very small, but remained compressive. This serves to explain why this tensile zone was not detected in the experiment, as most of the strain gages were located on the plane of symmetry. It should be noted that the average tensile stress here was of about the same magnitude as that on the exterior end, but the extent of this zone was much larger. Consequently, this region is actually more critical than the one near the exterior end so far as cracking due to vertical tensile stress is concerned. And if vertical reinforcements are to be used in an end block, this region should be reinforced first.

Outside of the two tension regions just mentioned, σ_y was compressive everywhere in both end blocks. Guyon's "bursting zones" did not appear at all. Again, this does not mean the non-existence of these tension regions. In fact, σ_y was found to be generally tensile on the plane of symmetry by the experiment. However, it has been pointed out before that the magnitude of σ_y was relatively small over these regions. It now seems reasonable to assume that such tensile stresses existed only within a rather restricted region surrounding each cable, outside of which σ_y became compressive.

A comparison of the stresses in the two end blocks showed that contrary to Magnel's postulation, the vertical tensile stresses in the long end block were actually slightly higher than in the short end block. (According to Magnel's method, it should be only 4/9 as much.) Thus the length-depth ratio of one is seen to be more economical than the ratio of 1.5.

It was also noticed that at the mid-length of the long end block, the distribution of σ_x in the vertical direction was almost linear. In the short end, however, the pressure was definitely lower in the region near the centroidal axis. It was therefore apparent that, in the process of transmitting the prestress forces from the anchorage plates to the I-beam section, the stage of spreading out had not been completed in the short end block before the stage of re-concentrating started to take effect. It may thus be claimed that the middle portion of the two side surfaces never did get developed in the short end; consequently, those portions of concrete rendered no service and could be removed. Thus, the use of long horizontal tapers of the end block toward the web of the I-section seems advisable.

Study of Principal Stresses and Trajectories

Figures 5.3 through 5.6 give the experimental principal stresses under loading condition V. Figures 5.7 and 5.8 show the principal stress trajectories based on the analytical results. It was seen that the directions of experimental principal stresses agreed fairly well with the trajectories.

Examination of Figures 5.7 and 5.8 showed that the horizontal plane at $y = \frac{3}{8}d$ (approximately midway between the bottom and the middle cables) might be considered as a "plane of separation". Above this plane, the pressure of the two upper cables was transmitted into the upper part of the I-beam; and below, the pressure from the two bottom cables went into the lower flange. High tensile stress existed across

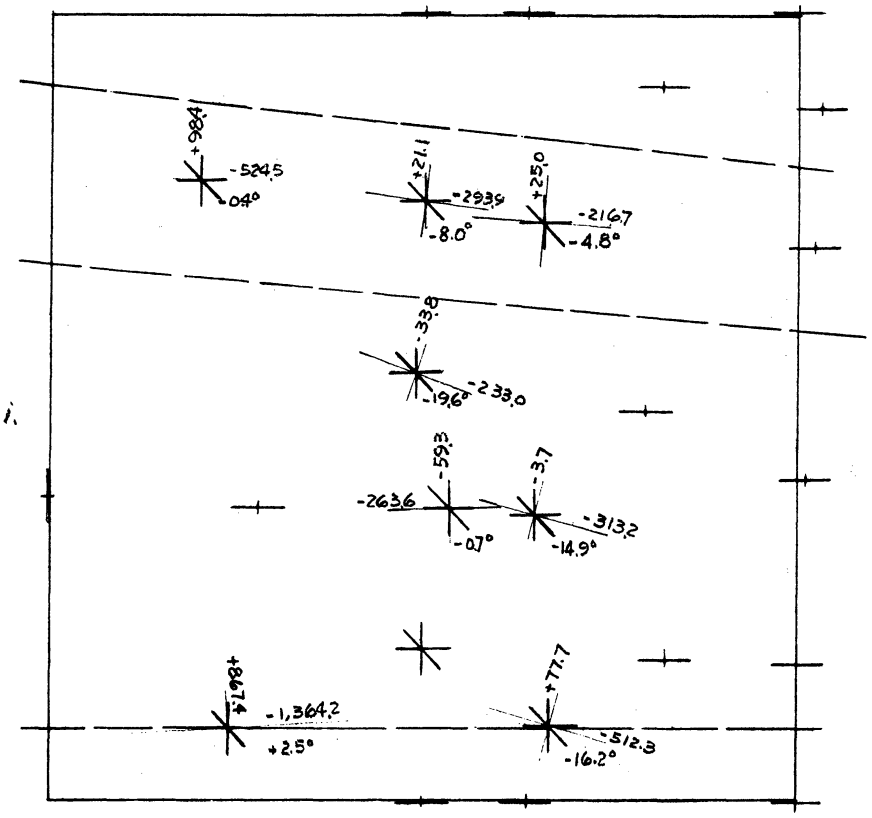

Figure 5.3. Principal Stresses, Short End, Experimental, Loading Condition V, P.L. + D.L. + L.L.

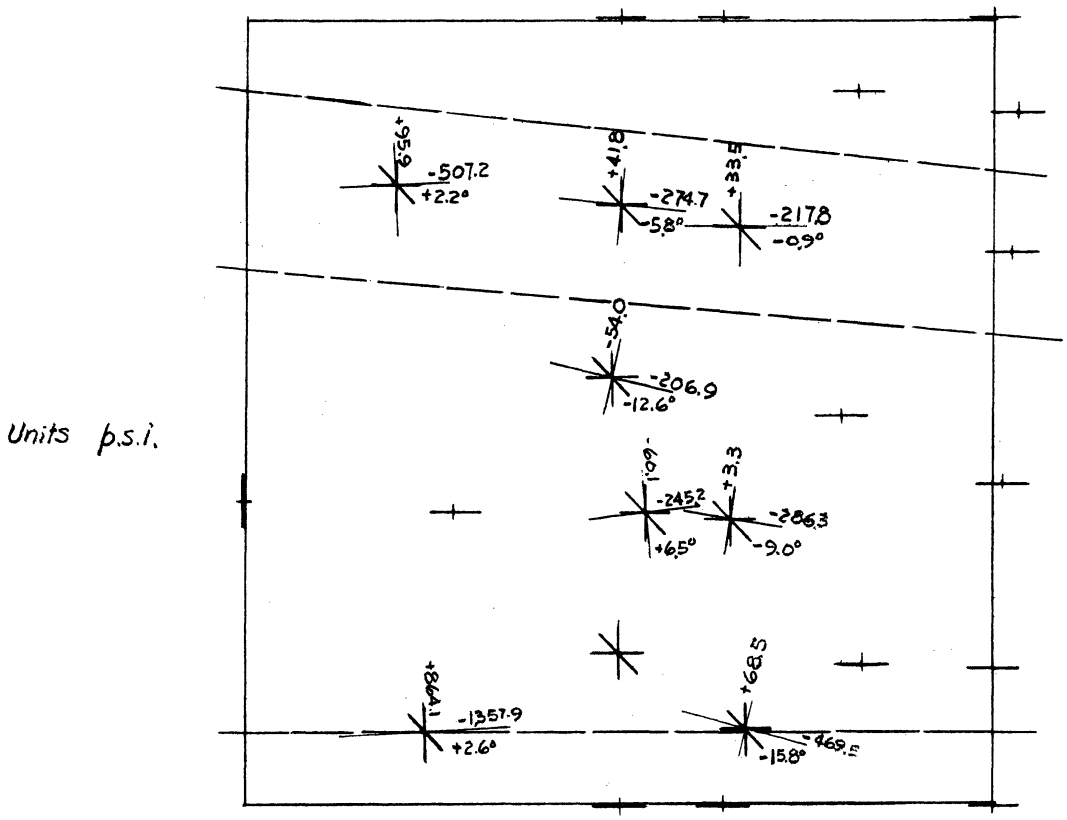

Figure 5.4. Principal Stresses, Short End, Experimental, Loading Condition V, P.L. + D.L. + L.L.

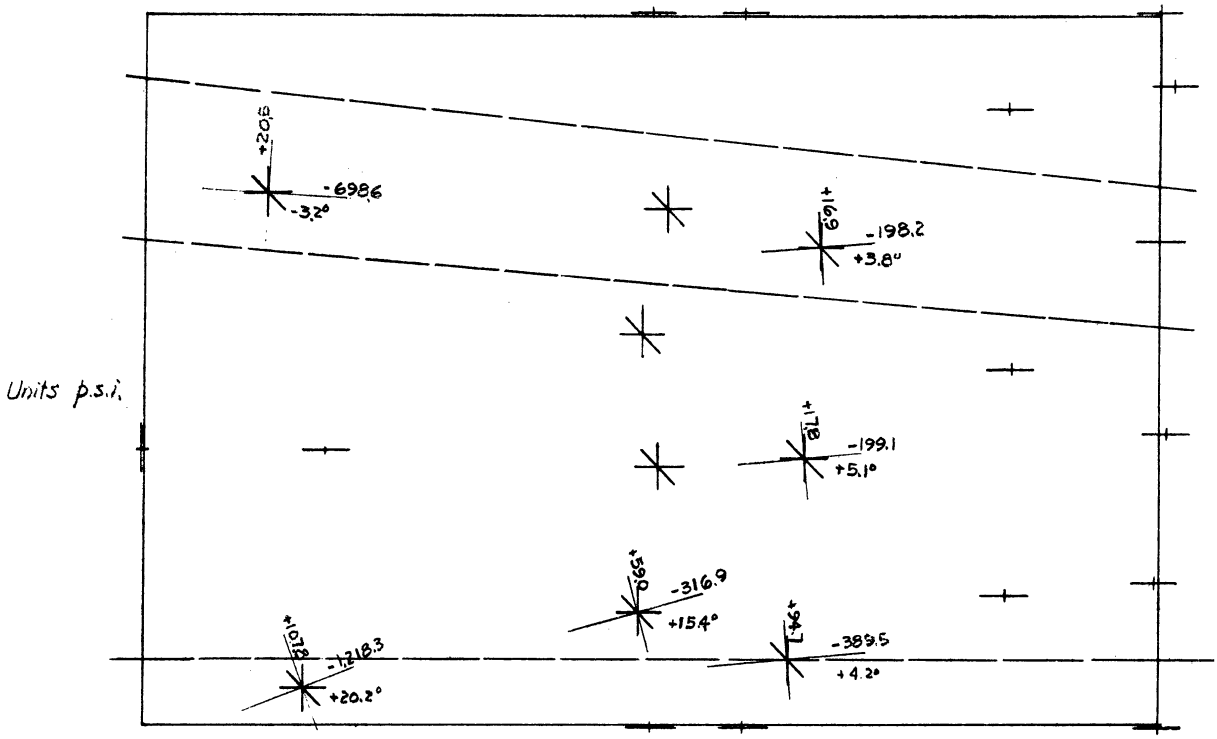

Figure 5.5. Principal Stresses, Long End, Experimental, Loading Condition V, P.L. + D.L.

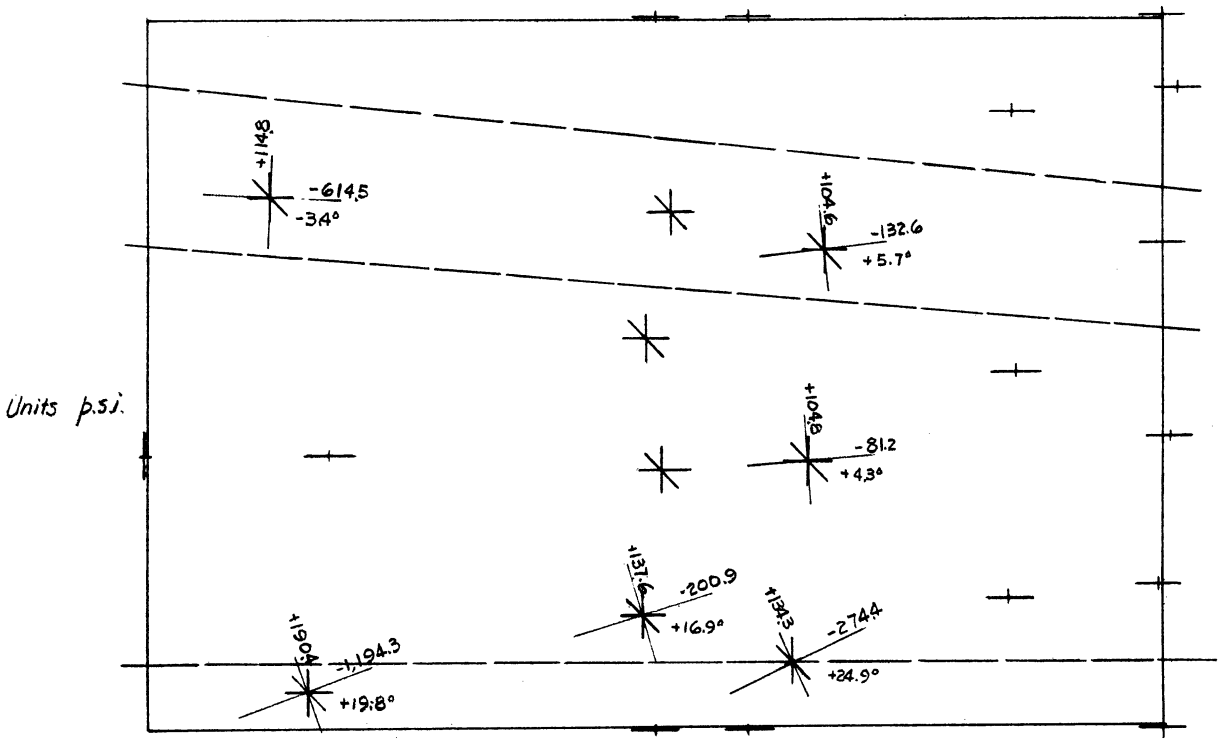

Figure 5.6. Principal Stresses, Long End, Experimental, Loading Condition V, P.L. + D.L. + L.L.

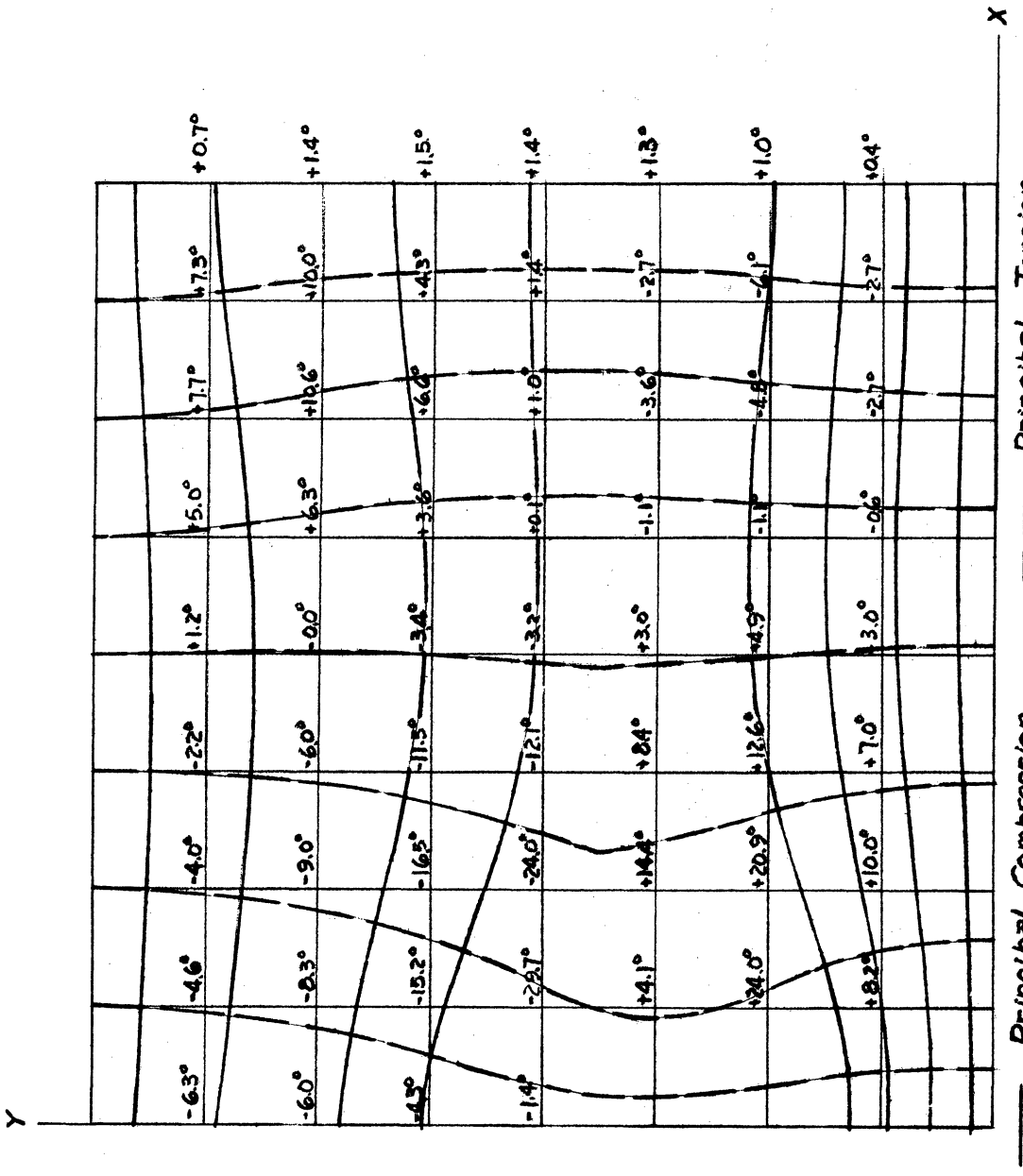

Figure 5.7. Stress Trajectories, Short End.

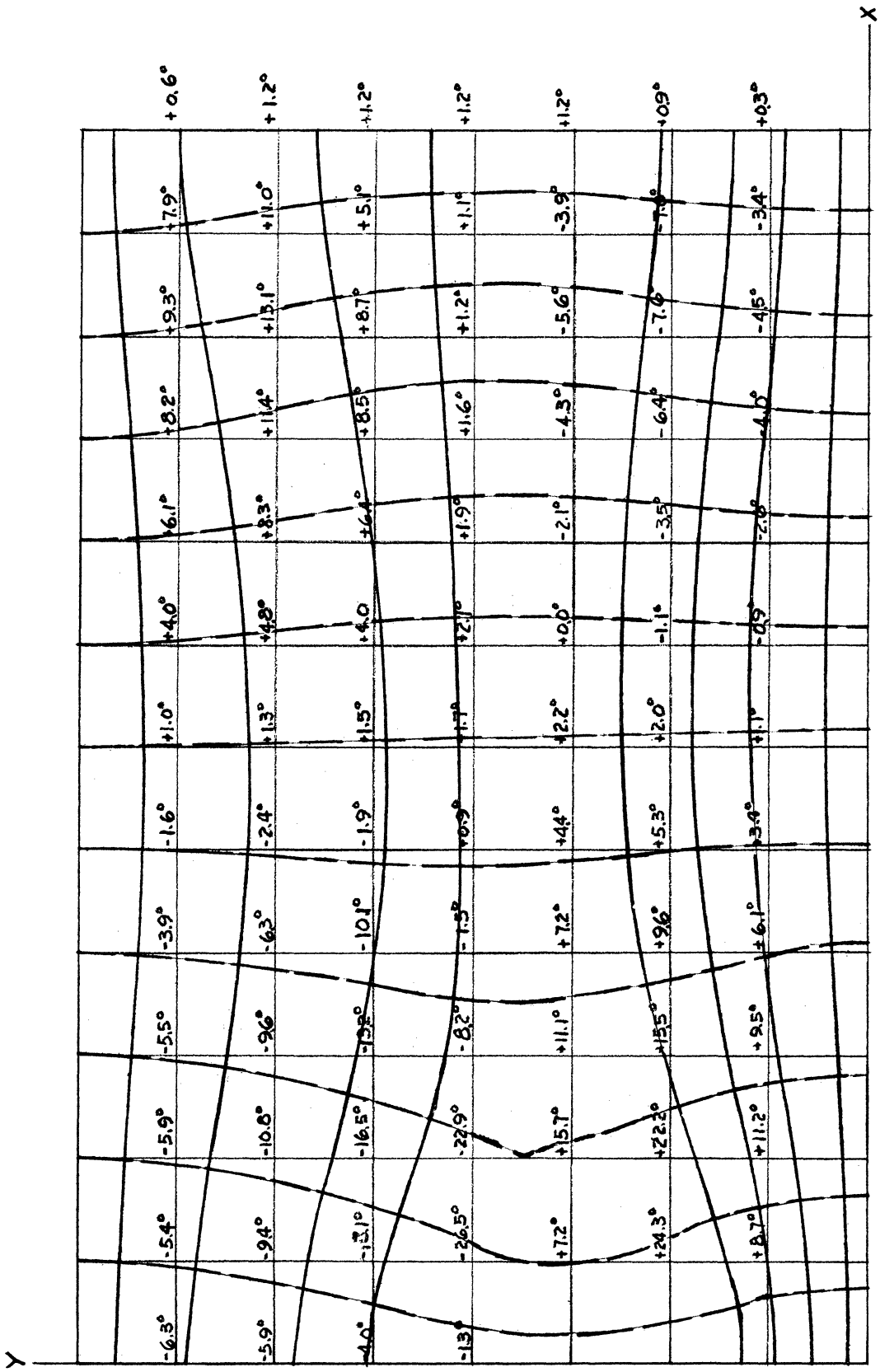

Figure 5.8. Stress Trajectories, Long End.

this plane, particularly at the two ends where the two major tensile zones were located. Potentially, this plane should be the plane of failure. Also, comparison of Figures 5.3 and 5.5 with 5.4 and 5.6 indicated that the directions of principal stresses were not appreciably affected by the application of Q_L. Both of these observations agreed with previous investigators' results.(27)

By comparing Figures 2.20 and 2.30 with 3.8 and 3.9, it was seen that, in general, experimental surface stresses were higher than analytical results, while for interior points, the analytical stresses were higher. Once again, the non-uniform or even non-linear character of lateral distribution of stresses was indicated.

Comparison of Results Obtained by Existing Methods

All of the existing methods treat the end block problems as two dimensional. Consequently, the results obtained by their application must be regarded as averages across the width of the beam. Also, all of the existing methods neglect the forces in the vertical direction, of which the most important one is the reaction R. Thus, an unreal boundary condition on the end blocks was obtained. That in turn affects the accuracy of the resulting stresses.

In particular, Magnel's method resulted in very low vertical stresses, as shown in Figures 4.1 and 4.2. The tensile zone at juncture could not be detected by this method, because one of his basic assumptions was that $\sigma_y = 0$ at the juncture. According to this method, the tensile stresses in the long end block would be much lower than those in the short end block. However, it has been shown before that the tensile

stresses in the long end block were actually higher, though not by much. This method bases all computation on the moment and shear on any horizontal plane. It is interesting to note that the sign of the moment could be reversed by the inclusion of the vertical reaction to the force system. By working on a two-dimensional basis, hence averaging across the width, Magnel's method also overestimates σ_x on the plane of symmetry. This, combined with the underestimated tensile stress σ_y results in principal tensile stresses much less than their true values.

Guyon's method resulted in a very high tensile stress at the exterior end between the bearing plates of middle and top cables. This tension zone was not detected by either the experimental or the numerical solution. However, it must be remembered that the network used in the numerical solution was rather coarse, and no strain gage was placed at this location in the test. The existence of this tensile zone was understandable, although the total tensile force here was undoubtedly small because of the very limited extent of the zone. Other than this, Guyon's method resulted in a tension of 765 psi near the location of surface gage No. 1, and that was considerably higher than the experimental value. Guyon also neglected to consider the state of stresses near the juncture, hence ignored the more critical tension zone there. The influence line method suggested by Evans and Bennett was essentially the same as Guyon's method, and yielded a slightly lower tensile stress.

Of the several existing methods, the modified Magnel's method as presented by Evans and Bennett in their book[11] is the only

one which takes into consideration the vertical reaction from the end support. The inclusion of a vertical force in the computation seemingly should make this method more correct than the others. However, comparison of Figures 4.3 and 4.4 with Figures 4.1 and 4.2 reveals that by this inclusion, the vertical tensile stresses were substantially reduced. The vertical force directly caused some compression all over the end block. And indirectly, the inclusion of the end reaction effectively reversed the sense of the bending moment on the horizontal section. This also contributed to the reduction of tensile stress. At least for the particular problem under investigation, this modified method gave the worst "approximation" of all.

CHAPTER VI

CONCLUSION

The distribution of stresses inside the end blocks of a post-tensioned prestressed concrete beam has been studied. Experimental study was made on one model beam with two end blocks of different lengths, using embedded and surface-mounted strain gages. An analytical solution of these end blocks has been made by means of a numerical procedure. Different existing methods of end block design have also been examined.

It was found that the existing methods gave results quite different from the experimental and analytical results. However, as only one model beam has been tested, no attempt was made to draw general conclusions applicable to all end block problems. Further investigations, particularly experimental, are needed for the establishment of any sound and practical design methods for end blocks.

From the limited amount of information acquired in this study, the following conclusions may be drawn:

1. It is not advisable to use end blocks with length-depth ratio much greater than unity, as such blocks would suffer severe vertical tensile stresses. On the other hand, it is apparent that the end blocks should not be made too short. The optimum length-depth ratio is probably close to one.

2. For beams of I, T or box shape, a tension zone exists near the juncture. The intensity of tensile stress here is similar to that in the exterior end tension zone, but the extent of the former is larger. To prevent failure, vertical and horizontal reinforcements should be used in this region, covering probably $\frac{1}{4}$ of the length of the end block.

3. The fiber stress σ_x at the juncture may be assumed to follow a linear vertical distribution with sufficient accuracy, but laterally, its distribution is better approximated by a parabola. At the plane of symmetry, σ_x is a minimum and is about 60% of the average across the width of the beam.

4. The effects of the weight of the end block, the applied load and the pressure from the curved cables on the stresses in an end block are in general small and for practical purposes may be neglected. But the reaction from end support and the vertical shear at the juncture should be considered.

5. In end blocks with length equal to depth, the portion near the two side faces opposite the web of the beam was largely ineffective. Thus, long horizontal tapers may be used both for economy and for efficiency.

In concluding this paper, it seems appropriate to mention the several things which the author feels advisable to do in future

investigations of this problem.

1. In order to establish the lateral distribution of stresses, more surface gages should be used, particularly at the section of juncture.
2. Several strain gages should be used on the prestressing cables, or some other means should be used to determine the amount of prestress in each cable at any time. In this test, the prestress was controlled solely by the pull bar in the jack. And after the jack was released after anchoring, it was always uncertain whether the anchorage nuts had been turned exactly to the right tightness.
3. Several gages in the I-beam section beyond the juncture would be very helpful.
4. The technique of installation of interior gage capsules still needs improvements, particularly the water-proofing and the placing. Also, thin metal plates may be considered to replace the celluloid plates used for capsules, on account of the troublesome drifting phenomenon which was believed related to the property of celluloid.

BIBLIOGRAPHY

1. Allen, D. N. de G. Relaxation Methods. New York: McGraw-Hill Book Company, Inc., 1954.

2. Ban, Shizuo; Muguruma, Hiroshi; and Ogaki, Zenichi. "Anchorage Zone Stress Distribution in Post-Tensioned Concrete Members." Proceedings of World Conference of Prestressed Concrete, San Francisco, California, (July, 1957), 16-1 - 16-14.

3. Billig, Kurt. Prestressed Concrete. London: MacMillan & Co., Ltd., 1952.

4. Bleich, Freidrich. "Der Gerade Stab mit Rechteckquerschnitt als Ebenes Problem." Der Bauingenieur, 4, (1923), 255-59, 304-07 and 327-31.

5. Chaikes, S. "Calcul des Abouts des Poutres en Béton Précontraint." International Congress of Prestressed Concrete, Ghent, (Sept. 8-13, 1951), 565-91.

6. Christodoulides, S. P. "Two-Dimensional Investigation of the End Anchorages of Post-Tensioned Concrete Beams." The Structural Engineers (London), 33, No. 4, (April, 1955), 120-33.

7. Christodoulides, S. P. "Photoelastic Investigation of Prestressed Concrete Anchorages." Civil Engineering and Public Works Review (London), 51, No. 603, (Sept., 1956), 994-97.

8. Christodoulides, S. P. "The Distribution of Stresses Around the End Anchorages of Prestressed Concrete Beams, Comparison of Results Obtained Photoelastically with Strain Gauge Measurements and Theoretical Solutions." Publications, International Association for Bridge and Structural Engineering, 16, (1956), 55-70.

9. Christodoulides, S. P. "Three Dimensional Investigation of the Stresses in the End Anchorage Blocks of a Prestressed Concrete Gantry Beam." The Structural Engineers (London), 35, No. 9, (Sept., 1957), 349-56.

10. Conwell, William A. Discussion of a paper by Li Chow, Henry D. Conway and George Winter, Proceedings, ASCE, 79, Separate No. D-127, (Feb., 1953), Transactions, ASCE, 118, (1953), 704-07.

11. Evans, R. H., and Bennett, E. W. Prestressed Concrete, Theory and Design. New York: John Wiley & Sons, Inc., 1958.

12. Filon, L. N. G. "On an Approximate Solution for the Bending of a Beam of Rectangular Cross-Section Under any System of Load." Philosophical Transactions, Royal Society of London, Series A, 201, (1903), 63-155.

13. Geer, Elihu. Stresses in Very Deep Beams with Applications to End Blocks of Prestressed Concrete Beams. Ph.D. Thesis, University of Michigan, Ann Arbor, Michigan, 1953.

14. Grinter, L. E. (ed). Numerical Methods of Analysis in Engineering (Successive Corrections). New York: The MacMillan Company, 1949.

15. Guyon, Yves. "Constraintes dans les Pièces Prismatiques Soumises à des Forces Appliquées sur Leurs Bases, au Voisinage de Ces Bases." Publications, International Association for Bridge and Structural Engineering, 11, (1951), 165-226.

16. Guyon, Yves. Prestressed Concrete. Johns, W. M. (ed.). New York: John Wiley and Sons, Inc., 1953.

17. Lin, T. Y. Design of Prestressed Concrete Structures. New York: John Wiley and Sons, Inc., 1955.

18. Magnel, Gustave. "Béton Précontraint, Pratique du Calcul des Pièces Isostatiques Soumises à la Flexion Simple." Annales Travaux Publics de Belgique, 47, (1946), 155-88 and 299-333.

19. Magnel, Gustave. "Design of Ends of Prestressed Concrete Beams." Concrete and Constructional Engineering (London), 44, No. 5, (May, 1949), 141-48.

20. Magnel, Gustave. Prestressed Concrete. 3d edition; New York: McGraw-Hill Book Company, Inc., 1954.

21. Pirson, E. "Considérations sur les Abouts de Poutres en Béton Précontraintes, Exposé dune Méthode de Calcul Basée sur L'étude des Trajectoires de Efforts." Annales des Travaux Publics de Belgique, 54, No. 3, (June, 1953), 401-36.

22. Ramaswamy, G. S., and Goel, Harish. "Stresses in End Blocks of Prestressed Beams by Lattice Analogy." Proceedings of World Conference on Prestressed Concrete, San Francisco, California, (July, 1957), 23-1 - 23-4.

23. Sievers, Hans. "Die Berechnung von Auflagerbänken und Auflagerquadern von Brückenpfeilern." Der Bauingenieur, 27, No. 6, (June, 1952), 209-13.

24. Sievers, Hans. "Über den Spannungszustand im Bereich der Ankerplatten von Spanngliedern Vorgespannter Stahlbetonkonstrukionen." Der Bauingenieur, 31, No. 4, (April, 1956), 134-135.

25. Southwell, R. V. An Introduction to the Theory of Elasticity for Engineers and Physicists, The Oxford Engineering Science Series, London, Oxford University Press, 1936.

26. Southwell, R. V. Relaxation Methods in Theoretical Physics, The Oxford Engineering Science Series, London, Oxford University Press, 1946.

27. Steel, R. K., and Libby, J. R. "Preliminary Tests of Prestressed Concrete at the U. S. Naval Civil Engineering Research and Evaluation Lab., Port Hueneme, California." Proceedings of the First United States Conference on Prestressed Concrete, Cambridge, Mass., (August, 14-16, 1951), 231-40.

28. Tesař, V. "Détermination Expérimentale des Tensions dans les Extrémités des Pièces Prismatiques Munies dùne Semi-Articulation." Publications, International Association for Bridge and Structural Engineering, 1, (1932), 497-506.

29. Timoshenko, S., and Goodier, J. N. Theory of Elasticity. 2d Edition, New York: Engineering Societies Monographs, McGraw-Hill Book Co., Inc., 1951.

30. Walley, Francis. Prestressed Concrete, Design and Construction. London: The Ministry of Works (by H. B. M. Stationery Office), 1953.